Study of ambient air quality at Preston New Road 23 August 2017 – 11 September 2020

Chief Scientist's Group research report

November 2022

We are the Environment Agency. We protect and improve the environment.

We help people and wildlife adapt to climate change and reduce its impacts, including flooding, drought, sea level rise and coastal erosion.

We improve the quality of our water, land, and air by tackling pollution. We work with businesses to help them comply with environmental regulations. A healthy and diverse environment enhances people's lives and contributes to economic growth.

We can't do this alone. We work as part of the Defra group (Department for Environment, Food & Rural Affairs), with the rest of government, local councils, businesses, civil society groups and local communities to create a better place for people and wildlife.

Published by:

Environment Agency
Horizon House, Deanery Road,
Bristol BS1 5AH

www.gov.uk/environment-agency

Further copies of this report are available from our publications catalogue: www.gov.uk/government/publications or our National Customer Contact Centre: 03708 506 506

Email: research@environment-agency.gov.uk

Author(s):
Victoria Sheppard

Keywords:
ambient air quality monitoring, Preston New Road, exploratory well site, well pad, oxides of nitrogen, particulate matter, methane, volatile organic compounds

Research contractor:
Environment Agency – Ambient Air Monitoring Team.
Environment Agency's Project Manager:
Roger Timmis

Project number:
SC190008

Citation:
Environment Agency (2022) Study of ambient air quality at Preston New Road. Environment Agency, Bristol.

Research at the Environment Agency

Scientific research and analysis underpin everything the Environment Agency does. It helps us to understand and manage the environment effectively. Our own experts work with leading scientific organisations, universities, and other parts of the Defra group to bring the best knowledge to bear on the environmental problems that we face now and in the future. Our scientific work is published as summaries and reports, freely available to all.

This report is the result of research commissioned by the Environment Agency's Chief Scientist's Group.

You can find out more about our current science programmes at https://www.gov.uk/government/organisations/environment-agency/about/research

If you have any comments or questions about this report or the Environment Agency's other scientific work, please contact research@environment-agency.gov.uk.

Dr Robert Bradburne
Chief Scientist

Contents

Executive summary

This report provides the results from a study of ambient air quality in the vicinity of the Cuadrilla exploratory well site at Preston New Road (PNR), near Little Plumpton, which has been regulated by the Environment Agency. The Environment Agency's Ambient Air Monitoring Team (AAM Team) carried out the study on behalf of the Environment Agency's Onshore Oil and Gas subgroup. The monitoring was carried out for just over 3 years.

The reported pollutants are oxides of nitrogen (NO_X, NO, NO_2), particulate matter (PM_{10} and $PM_{2.5}$), methane (CH_4) and volatile organic compounds comprising benzene, toluene, ethylbenzene and m&p-xylene (BTEX). These pollutants were chosen because there is potential for them to be emitted during onshore oil and gas operations and related activities at the well site. Wind speed and wind direction were also measured.

The monitoring site was located on the grounds of the nearest residential community, approximately 0.4km west-south-west of the well pad near Little Plumpton. The well pad was at a bearing of approximately 53° to 70° from the monitoring site. The monitoring site was chosen to complement another air quality monitoring site that was already located approximately 0.4km east of the well pad and was run by the British Geological Survey. By locating the Environment Agency's monitoring site in the closest residential community, it was able to provide information about the potential impact of the well pad and to reassure local residents that their ambient air quality was being routinely monitored and assessed.

The UK Air Quality Strategy (AQS)[1] provides health-based limits for PM_{10} and $PM_{2.5}$ in ambient air. Comparison with the AQS objectives for formal assessment of statutory compliance can only be made at specific Defra monitoring stations. However, a comparison with the AQS objectives has been made in this report so that the air quality data from near the well pad site can be informally assessed for compliance, and because the comparison helps to quantify the environmental impact of the well pad.

The data is also, retrospectively, compared against the Daily Air Quality Index (DAQI)[2]. This index uses air quality forecasts to predict next day air quality levels and to assign an index number (1 = low to 10 = very high), which is then used to assign each day to an air quality band. There are 4 bands (low, moderate, high, and very high) and each band has an associated health advisory message that warns people and informs them how to limit their exposure, for example, by reducing or avoiding exercise outside. PM_{10} and $PM_{2.5}$ are 2 of the 5 pollutants used to assess air quality for the DAQI.

Comparing the collected data from the monitoring at PNR with the AQS objectives showed that the monitoring location was subject to concentrations of PM_{10}, $PM_{2.5}$, NO_2 and benzene that were likely to meet their respective AQS objectives.

Comparison of the data with the Daily Air Quality Index showed that levels during the study remained in the low band of the index for NO_2 throughout the 3-year survey duration.

PM_{10} and $PM_{2.5}$ remained primarily in the low band of the index, with just 4 days in the moderate band for PM_{10} and 9 days in the moderate band for $PM_{2.5}$.

The toluene data was compared with the World Health Organisation (WHO)[3] guidelines. Toluene levels at the monitoring site were found to be within the specified health and odour limits.

The position of the monitoring location was useful for informing residents about ambient air quality during the period of well pad operations. However, it was not possible to carry out a detailed statistical analysis of any well pad impacts here for 2 reasons. Firstly, because winds from the well pad were very infrequent. Secondly, because the A583 lay in the same direction, so that any impacts from the well pad were combined with traffic-derived impacts and were generally too small to be distinguishable from those impacts.

Although the data did not allow a detailed statistical assessment of well pad impacts, pollutant time series and directional plots were inspected visually for any prominent signals from the direction of the well pad. These inspections indicated that there were no substantially elevated levels of air pollution that arrived from the direction of the well pad during periods of hydraulic fracturing.

1. Department for Environment, Food and Rural Affairs. (July 2007) The Air Quality Strategy for England, Scotland, Wales, and Northern Ireland, (HMSO).
2 Department for Environment, Food and Rural Affairs. UK AIR - Air Information Resource, Daily Air Quality Index (DAQI) Daily Air Quality Index - Defra, UK

1 Introduction

In October 2016, planning permission was granted for the exploratory drilling of 2 test wells at a site approximately 500m to the west of Little Plumpton in Lancashire. Site construction started in January 2017 and hydraulic fracturing and gas extraction of the wells took place at well 1 between 15 October and 17 December 2018 and at well 2 between 15 and 26 August 2019.

A moratorium on hydraulic fracturing (known as 'fracking') was introduced in England on 2 November 2019, which suspended any further hydraulic fracturing activities on the grounds that it was not yet possible to accurately predict the probability or magnitude of seismicity due to fracking operations.

This report provides the results of a campaign of ambient air monitoring carried out between 23 August 2017 and 11 September 2020 (1,116 days) in the vicinity of the Cuadrilla exploratory well sites at Preston New Road (PNR), ~1km west of Little Plumpton. The Environment Agency's Ambient Air Monitoring Team (AAM Team) carried out the study on behalf of the Environment Agency's Onshore Oil and Gas subgroup. The monitoring period covers the period of exploratory operations, and not the baseline phase prior to drilling at the well pad. The monitoring period covered the 2 periods of hydraulic fracturing, where air quality impacts from the site were potentially more detectable.

The pollutants reported are particulate matter (PM_{10} & $PM_{2.5}$), oxides of nitrogen (NO and NO_2), methane (CH_4), benzene, toluene, ethylbenzene, and m&p-xylene (BTEX). These pollutants were chosen as there is potential for them to be emitted during onshore oil and gas operations and related activities at the site.

The monitoring site of an independent study by the British Geological Survey (BGS) was located ~0.4km east of the well pad, and it measured air quality during both baseline and operational conditions at the well pad. To complement this monitoring, the Environment Agency monitoring site was located on the grounds of the nearest residential community, ~0.4km (380m) to the west-south-west of the well pad. The position of the monitoring location was useful for informing residents about ambient air quality during the period of well pad operations. It was originally envisaged that the data analysis would focus on any impacts from the well pad. However, it was not possible to carry out a detailed analysis of any well pad impacts here for 2 reasons. Firstly, because winds from the well pad were very infrequent. Secondly, because the A583 lay in the same direction, so that any impacts from the well pad were combined with traffic-derived impacts and were generally too small to be distinguishable from those impacts. For these reasons, the analysis of monitoring focuses on comparisons with air quality standards rather than on a detailed analysis of well pad impacts. As winds from the well pad were rare and had no particularly elevated levels of air pollution, the data from the Environment Agency site was not compared with the data from the BGS site.

2 Location

The Ambient Air Monitoring team deployed its mobile monitoring facility (MMF) on the grounds of the nearest residential community, ~380m to the west-south-west of the well pad near Little Plumpton (Figure 2.1). The well pad subtended a sector between bearings of about 53° to 70° from the monitoring site. However, most of the directional analysis looks at 10° sectors and therefore the bearing range of interest is between 50° to 70°. The A583 runs between the MMF and the well pad. This means that any air pollution contributions from the well pad became mixed with, and were potentially obscured by, contributions from road traffic. Because the well pad and the road traffic were likely to have emitted some of the same pollutants, for example, NO_X and PM, it was difficult to distinguish between the 2 emission sources. Consequently, any concentrations of relevant pollutants from well pad activities would only be discernible if they were substantially higher than local traffic contributions.

The monitoring site was chosen to complement the BGS monitoring site that was already located to the east of the well pad. The location of the MMF was appropriate for comparing its data with Air Quality Strategy (AQS) objectives. These comparisons were used to assess local air quality against health standards, and to provide information relevant to the exposure of residents. The sampling point was at a height of 2 metres above ground level (Figure 2.2).

Figure 2.1: Aerial photograph showing MMF monitoring location

Figure 2.2: Photograph showing the MMF monitoring location

3 Monitoring results

3.1 Meteorology

Wind speed and direction measurements were collected at the MMF site during the study. The sensor was mounted on a mast extending 8m from the top of the MMF trailer, giving an overall height above ground of 10m. Where possible, MMFs are located over 100m from any buildings of greater or comparable height to reduce any influence that surrounding buildings may have on the wind distribution. However, this was not possible at this monitoring location and the nearest building was ~20m north-east of the MMF, in the direction of the well pad. This building, and a bank of trees to the north of the building, are likely to have affected the wind coming from the direction of the well pad.

When setting up the instrument for measuring wind direction, at the beginning of the study, the mast was rotated such that the vane pointed in a known direction, and this was used as a datum from which other directions were determined by the sensor. An uncertainty of ±5° on the wind direction is introduced, which affects all readings by the same amount. To produce rose plots, the wind direction data are resolved into 10° sectors for analysis and interpretation, therefore the uncertainty of each sector is ±5°.

Monitoring continued for 37 months that spanned 4 calendar years. Table 3.1 summarises the dates and data capture for each year, and shows the percentages of the monitoring period in each year with wind from the well pad. The monitoring site was upwind of the well pad with respect to the generally prevailing west/south-west winds (the well pad is at a bearing of about 53° to 70° from the MMF), and the amount of time that the wind blew from the well pad to the MMF was very low. The lack of winds from the direction of the well pad constrained the type of analysis that was possible, and meant that detailed statistical analysis of the well pad signal was not feasible.

Table 3.1: Summary of annual data capture and wind direction (WD)

	Year			
	2017	2018	2019	2020
Date range	23 August – 31 December	1 January – 31 December	1 January – 31 December	1 January – 11 September
Data capture	93%	99%	99%	98%
Percentage of time wind direction coming from the direction of well pad	0.5%	1.8%	1.8%	3.5%

During the first hydraulic fracturing period (15 October to 17 December 2018) the wind came from the direction of the well pad 3% of the time. During the second hydraulic

fracturing period (15 to 26 August 2019) the wind came from the direction of the well pad 0.3% of the time.

The frequency distribution of wind direction for each year between 23 August 2017 and 11 September 2020 is shown in Figure 3.1.

Figure 3.1: Wind roses in 2017 to 2020, showing percentage of time in 7 wind speed bands for 10° sectors

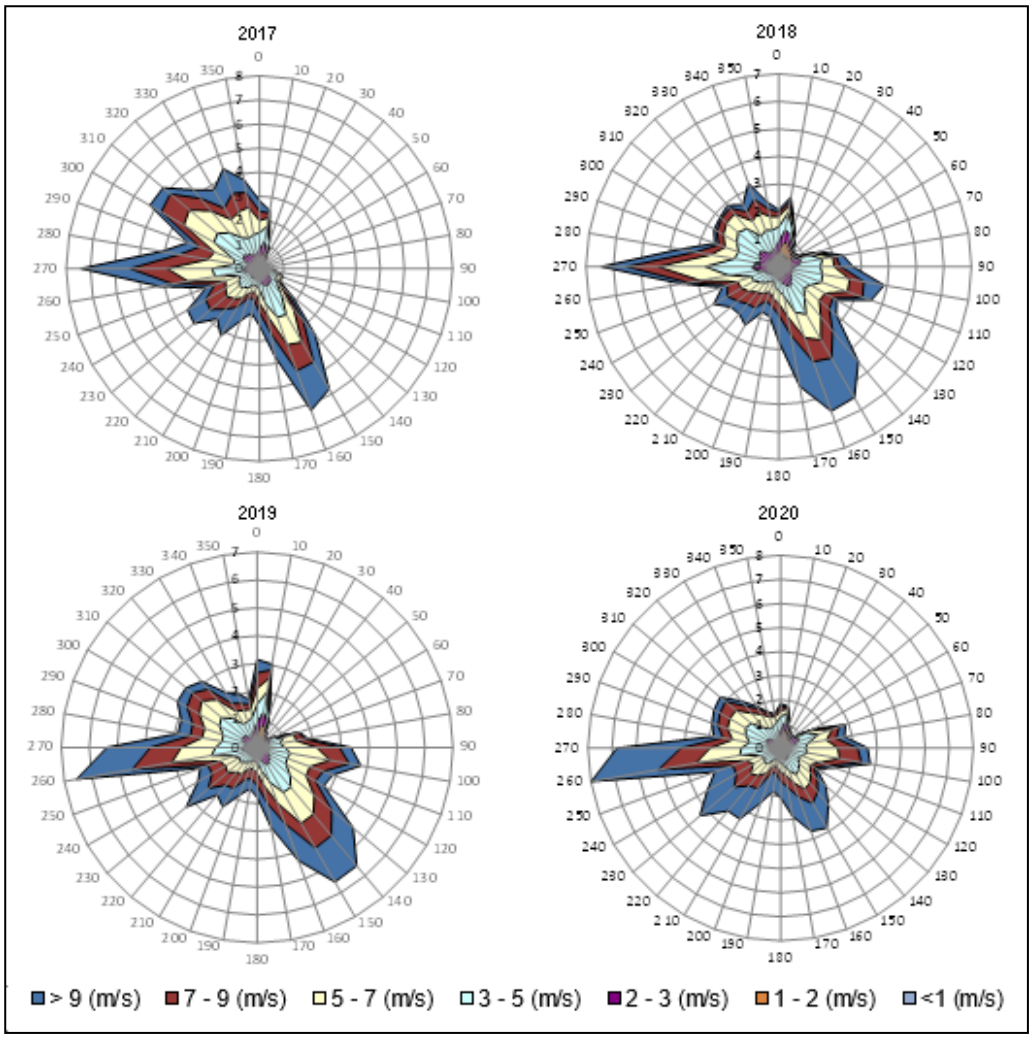

The plot shows that:

- the dominant wind directions in 2017 were from between 140° to 170° and 260° to 350°, with wind coming from these wind sectors 19% and 46% of the time respectively
- the dominant wind directions in 2018 were from between 140° to 170° and 260° to 280°, with wind coming from these wind sectors 20% and 14% of the time respectively
- the dominant wind directions in 2019 were from between 130° to 160° and 260° to 270°, with wind coming from these wind sectors 20% and 12% of the time respectively

- the dominant wind direction in 2020 was from between 260° to 270°, with wind coming from this wind sector 15% of the time

The wind speed frequencies are summarised in Table 3.2.

Table 3.2: Summary of wind speed frequencies

Wind speed (m/s)	2017 Frequency of wind speed	2018 Frequency of wind speed	2019 Frequency of wind speed	2020 Frequency of wind speed
<1	4%	5%	4%	3%
1 - 2	7%	9%	6%	6%
2 - 3	9%	10%	8%	8%
3 - 5	22%	24%	21%	21%
5 - 7	22%	21%	23%	22%
7 - 9	17%	14%	18%	16%
>9	20%	17%	20%	24%
Total	**100.00**	**100.00**	**100.00**	**100.00**

Polar frequency plots showing the frequency of wind speed against wind direction for each year are shown in Figure 3.2. It can be seen that most winds were below 15m/s, and that the most frequent wind condition was a westerly wind at about 5m/s – for example, as shown in 2018.

Figure 3.2: Openair polar plot of wind frequency (colour ramp, 5-minutes/year) and speed (radial axis, m/s)

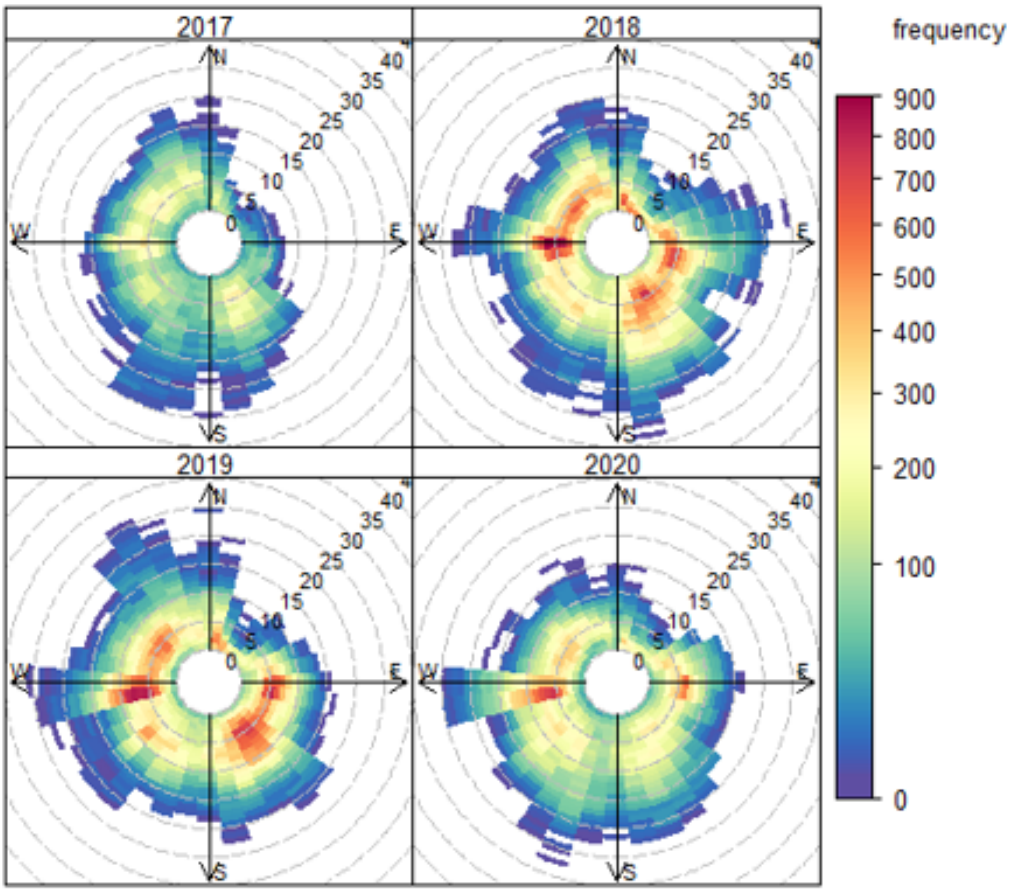

3.2 Particulate matter (PM_{10} & $PM_{2.5}$)

Between 23 August 2017 and 11 September 2020 (1,116 days), airborne PM_{10} (particulate matter less than 10 microns in diameter) and $PM_{2.5}$ (particulate matter less than 2.5 microns in diameter) concentrations were measured at the MMF.

During the period 23 August 2017 to 15 January 2019 measurements were made using a tapered element oscillating microbalance (TEOM) instrument. Details of the instrumentation and methodology are given in Appendix C. PM_{10} data collected using a TEOM instrument must be adjusted using the Defra-approved Volatile Correction Model (VCM) in order to be equivalent to the reference method, and therefore comparable to the standards. The VCM allows a small adjustment to TEOM measurements to be made, to correct for the loss of volatile components of PM_{10}. The VCM uses data from a filter dynamic measuring system (FDMS) TEOM instrument from sites within 130km distance of the MMF in order to adjust the PM_{10} measurements to be comparable with the reference method. There is not currently a validated correction factor for $PM_{2.5}$ TEOM data. However, the patchy availability of FDMS data led to a decision to change the TEOM instruments to a different particulate analyser called a fine dust analyser system (FIDAS), which does not need correcting to be equivalent to the reference method. The exchange took place on 15 January 2019. Details of the instrumentation and methodology are given in Appendix C.

Figures 3.3 and Figure 3.4 show the hourly particulate concentrations at the monitoring site for the TEOM and FIDAS respectively. The vertical green and orange lines on Figure 3.3 mark the start and finish dates of the first hydraulic fracturing period (15 October to 17 December 2018). The vertical green and orange lines on Figure 3.4 mark the start and finish dates of the second hydraulic fracturing period (15 to 26 August 2019).

Hydraulic fracturing during these periods was intermittent and the Environment Agency site officers provided the dates of the 2 periods. There is no evidence of particularly elevated levels of particulate air pollution occurring during the hydraulic fracturing periods, although it should be noted that the wind direction was rarely blowing from the shale well pad to the monitoring site.

Successful data collection for PM_{10} and $PM_{2.5}$ over the period 23 August 2017 to 15 January 2019 was 92%.

Successful data collection for PM_{10} and $PM_{2.5}$ over the period 15 January 2019 to 11 September 2020 was 98%.

Figure 3.3: Time series plot of TEOM PM_{10} (VCM adjusted) and $PM_{2.5}$ 1-hour mean concentrations for August 2017 to January 2019

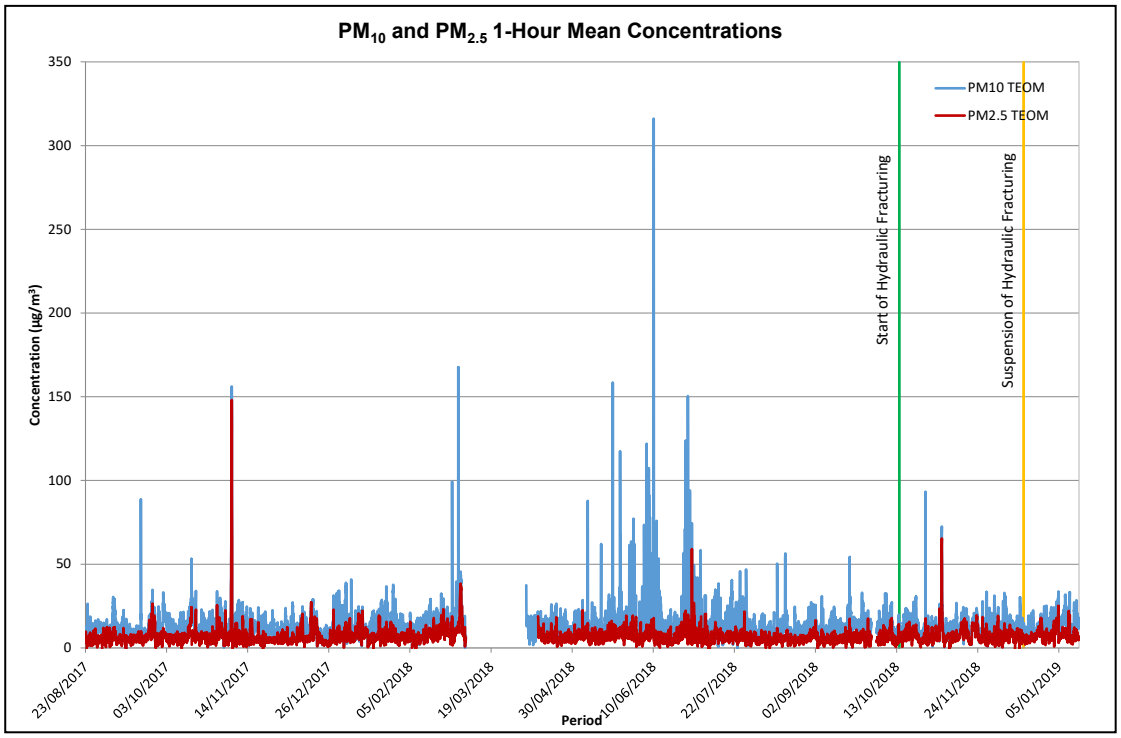

Figure 3.4: Time series plot of FIDAS PM_{10} and $PM_{2.5}$ 1-hour mean concentrations for January 2019 to August 2020

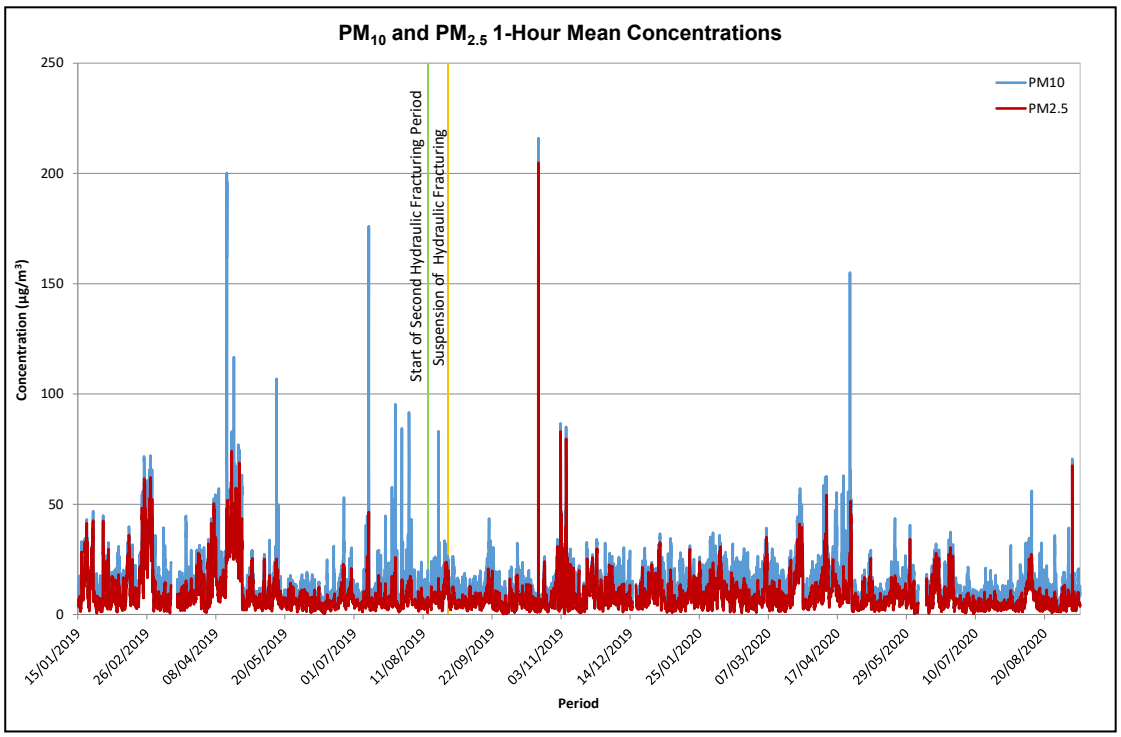

3.2.1 Comparison with standards

3.2.1.1 Comparison with Air Quality Strategy (AQS) objectives

The AQS has 2 objectives for PM_{10}, the first is to limit the annual mean concentration to 40µg/m^3 and the second objective states that the 24-hour mean (midnight to midnight) must not exceed 50µg/m^3 on more than 35 occasions during one year. The AQS objective for $PM_{2.5}$ is an annual mean concentration of 25µg/m^3.

Table 3.3 provides a summary of the annual mean PM_{10} and $PM_{2.5}$ concentrations over the monitoring period. A projected exceedance ratio ≤1 indicates non-exceedance, while a value >1 indicates exceedance. There were only ~4 and ~8 months of data available for 2017 and 2020, respectively, and it is assumed that the concentrations measured in these sub-annual periods were representative of each year.

Table 3.3: PM_{10} and $PM_{2.5}$ annual averages for each year during study

Pollutant	Averaging time	AQS	Standard (A) (µg/m^3)	Measurement (B) (µg/m^3)	Projected exceedance ratio (B/A)
2017 PM_{10}	Year	2000	40	12.5*	0.31
2018 PM_{10}				15.8	0.40
2019 PM_{10}				14.5	0.36
2020 PM_{10}				13.4*	0.34
2017 $PM_{2.5}$		2007	25	6.56*	0.26
2018 $PM_{2.5}$				7.12	0.28
2019 $PM_{2.5}$				9.31	0.37
2020 $PM_{2.5}$				8.05*	0.32

* Extrapolated from effective monitoring period

If the assumption is made that the conditions during 2017 and 2020 (part years) were representative of a typical year, then the results shown in Table 3.3 would indicate that the annual mean concentrations for both PM_{10} and $PM_{2.5}$ were below the limits set out in the AQS objectives at the monitoring site. The highest PM_{10} concentrations were seen in 2018, while the highest $PM_{2.5}$ concentrations were seen in 2019. However, the lower concentrations of $PM_{2.5}$ in 2017 and 2018 may in part be due to the fact that the TEOM measurements for $PM_{2.5}$ could not be corrected for the loss of volatiles.

Table 3.4 provides a comparison of the PM_{10} data against the AQS short-term objective for each year over the monitoring period.

Table 3.4: Impact summary for short-term air quality objectives for PM_{10}

Pollutant	Averaging time	AQS	Standard	Maximum concentration	Permitted exceedance (A)	Measured exceedance	Extrapolated exceedance (B)	Projected exceedance ratio (B/A)
2017 PM_{10}	24-hr (midnight-midnight)	2,000	50µg/m³	54.9µg/m³	35/year	1	3*	0.09
2018 PM_{10}				45.9µg/m³		0	0	0.00
2019 PM_{10}				63.1µg/m³		6	6	0.17
2020 PM_{10}				43.1µg/m³		0	0*	0.00

* Extrapolated from effective monitoring period

Comparing the collected data with the short-term PM_{10} AQS objectives showed that the monitoring location did not exceed the 24-hour AQS objective for PM_{10} during the study period.

Figure 3.5 shows PM_{10} 24-hour (midnight to midnight) mean concentrations for each year during the monitoring period.

Figure 3.5: 24-hour (midnight to midnight) mean PM_{10} concentrations at the monitoring site for each year (the dashed line marks 50µg/m³)

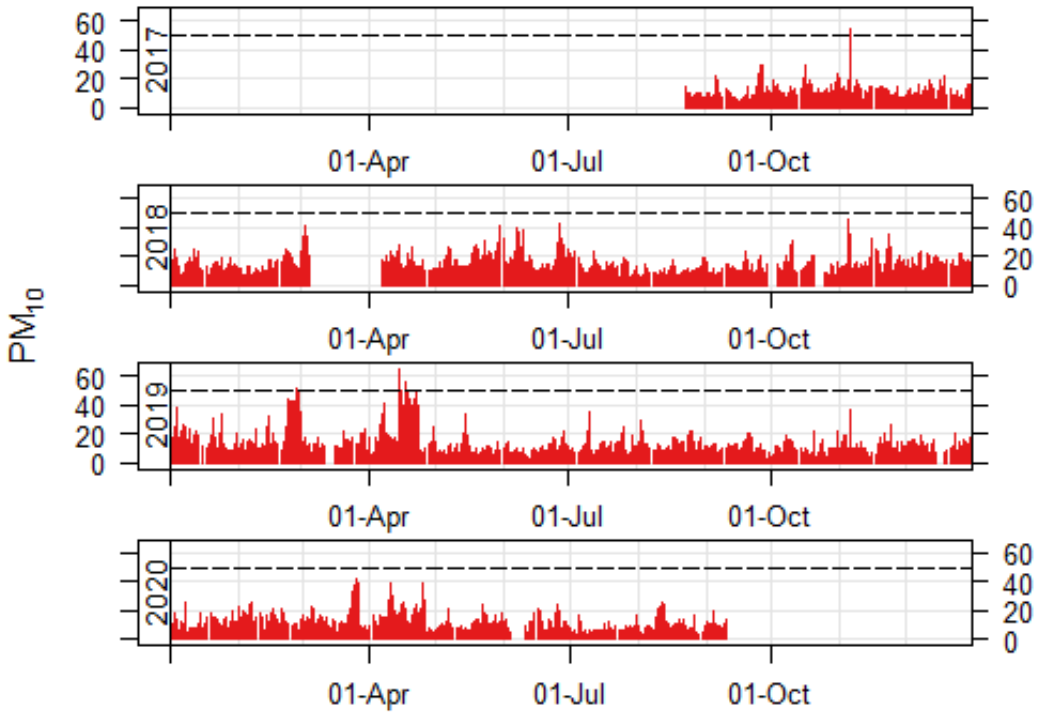

3.2.2 Comparison with Air Quality Index

In the United Kingdom a Daily Air Quality Index (DAQI) has been developed. This index uses air quality forecasts to predict next day air quality levels and to assign an index number (1 = low to 10 = very high) to each day. Index numbers are grouped into 4 different bands (low, moderate, high and very high) and each band has an associated health advisory message, warning people when to limit, or avoid, exercise outside. The index is especially important to those most at risk from air pollution, such as the elderly and adults and children with heart and lung conditions. Although the index is usually used with predicted air quality data, in this study it has been used to assign index numbers and bands retrospectively to the measured air quality data from the monitoring site.

PM_{10} is one of 5 pollutants used to assign index numbers for daily air quality, the others being $PM_{2.5}$, SO_2, NO_2 and O_3, and the highest number is used to set the daily band. Figure 3.6 and Figure 3.7 summarise the daily index numbers for PM_{10} and $PM_{2.5}$ concentrations, respectively, for each year.

Figure 3.6: PM_{10} AQI pie chart for each year

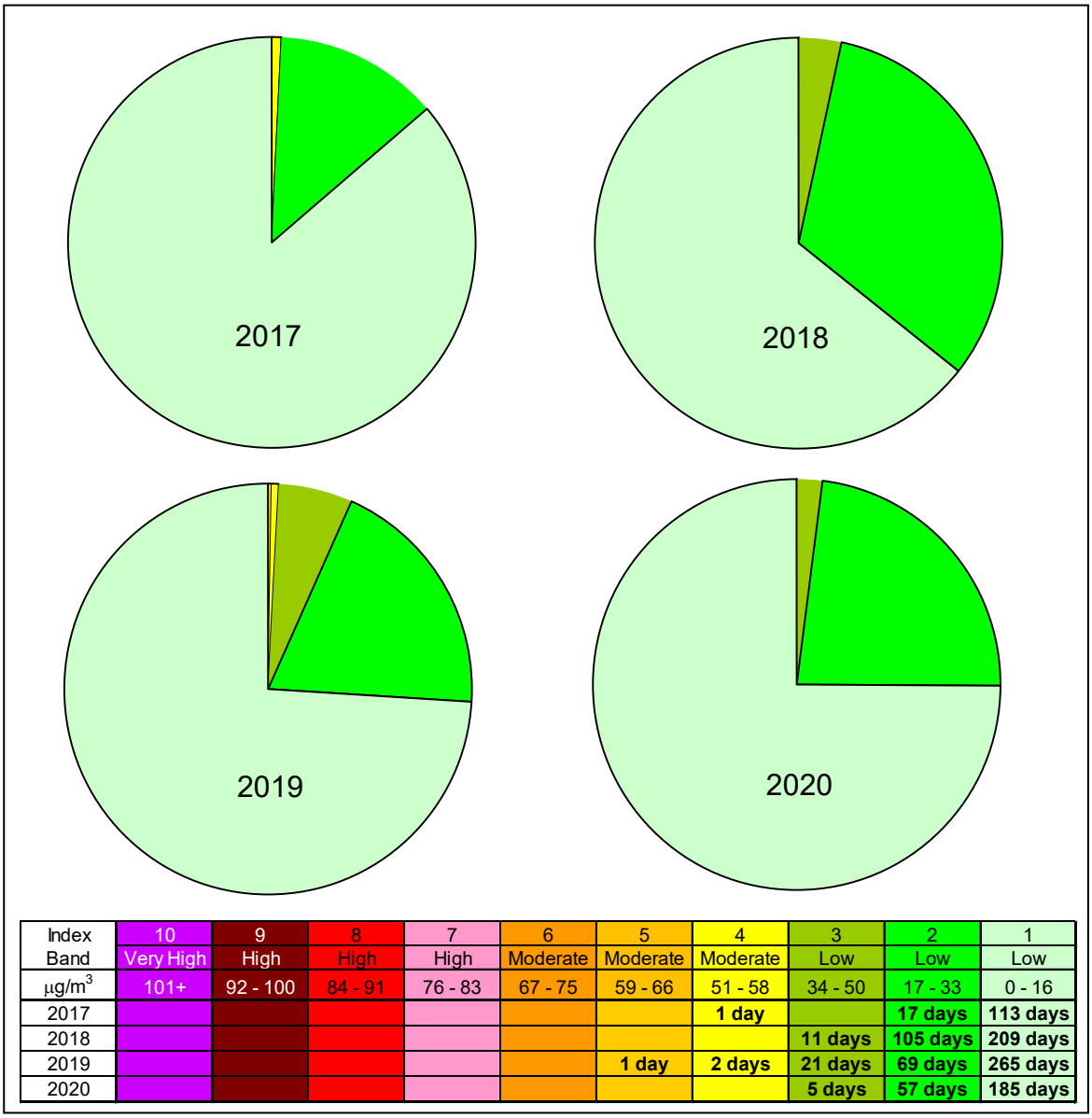

Index	10	9	8	7	6	5	4	3	2	1
Band	Very High	High	High	High	Moderate	Moderate	Moderate	Low	Low	Low
µg/m^3	101+	92 - 100	84 - 91	76 - 83	67 - 75	59 - 66	51 - 58	34 - 50	17 - 33	0 - 16
2017							**1 day**		**17 days**	**113 days**
2018								**11 days**	**105 days**	**209 days**
2019						**1 day**	**2 days**	**21 days**	**69 days**	**265 days**
2020								**5 days**	**57 days**	**185 days**

The plots show that the majority of the PM_{10} 24-hour concentrations at the monitoring site were in the low band (index numbers 1 to 3) of the air quality index. There was just one day in 2017 and 3 days in 2019 when concentrations were in the moderate band (index numbers 4 to 6), when precautions might be required for at risk individuals.

Figure 3.7: Pie charts of $PM_{2.5}$ daily air quality indices for each year 2017 to 2020

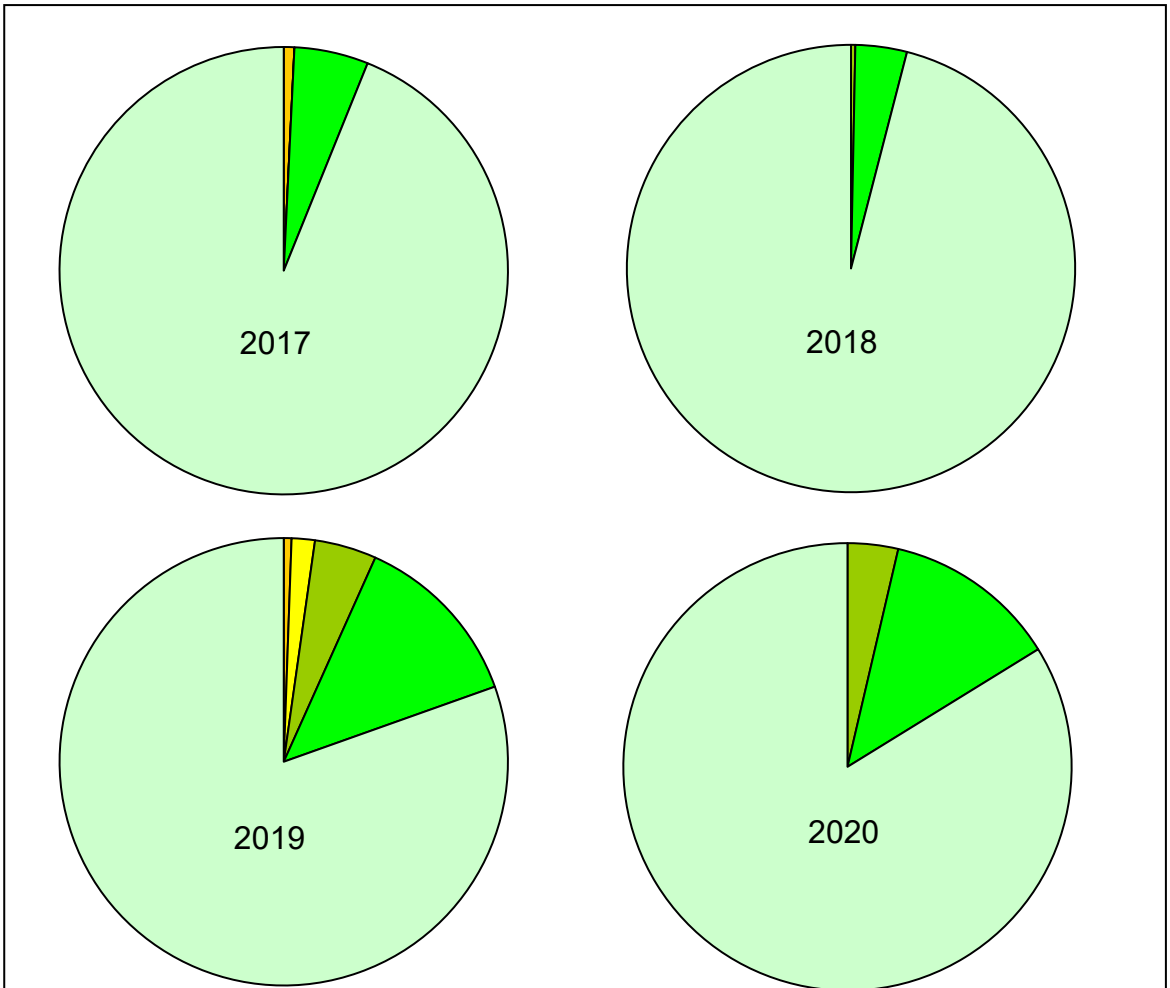

Index Band	10 Very High	9 High	8 High	7 High	6 Moderate	5 Moderate	4 Moderate	3 Low	2 Low	1 Low
µg/m^3	71+	65 - 70	59 - 64	54 - 58	48 - 53	42 - 47	36 - 41	24 - 35	12 - 23	0 - 11
2017						1 day			7 days	123 days
2018								1 day	12 days	310 days
2019						2 days	6 days	16 days	46 days	288 days
2020								9 days	31 days	207 days

The plots show that the majority of the $PM_{2.5}$ 24-hour concentrations at the monitoring site were in the low banding (index numbers 1 to 3) of the air quality index. There was just one day in 2017 and 8 days in 2019 when concentrations were in the moderate banding (index numbers 4 to 6), when precautions might be required for at risk individuals.

3.2.3 Directional analysis

3.2.3.1 Time series plots for 45° sectors

Figure 3.8 shows the 1-hour mean concentrations of PM_{10} and $PM_{2.5}$ for 8, 45° sectors.

Figure 3.8: PM_{10} and $PM_{2.5}$ 1-hour mean time series for each 45° wind sector

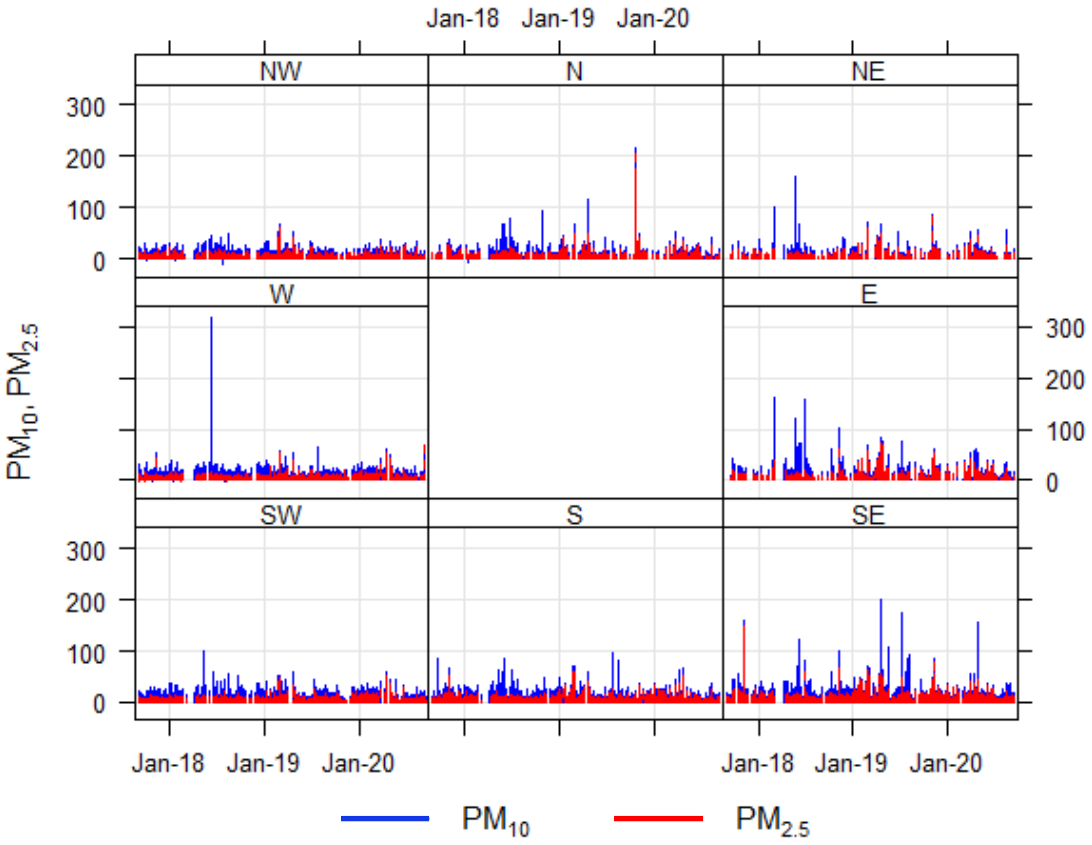

The plot shows that the highest PM_{10} concentration came from the west of the monitoring site in 2018. PM_{10} concentrations are generally higher from the sectors that have easterly components of wind, that is, from the NE, E and SE sectors. There is no evidence of notably elevated concentrations coming from the (NE) 45° sector that contained the well pad during periods of hydraulic fracturing. This sector was not notably elevated in comparison to the other 7 45° sectors during the 4-year monitoring campaign.

3.2.3.2 Radial plots

Radial plots of mean PM_{10} and $PM_{2.5}$ concentrations ($\mu g/m^3$) for each year against wind direction at the MMF site are shown in Figure 3.9 and Figure 3.10 respectively. The highest average PM_{10} and $PM_{2.5}$ concentrations are seen in the 10° wind sectors centred on 70° to 150° for each year. Further observations of relatively high concentrations with winds coming from the sectors centred on 20°, 30° and 50° are seen in certain years.

Figure 3.9: PM_{10} Pollution rose

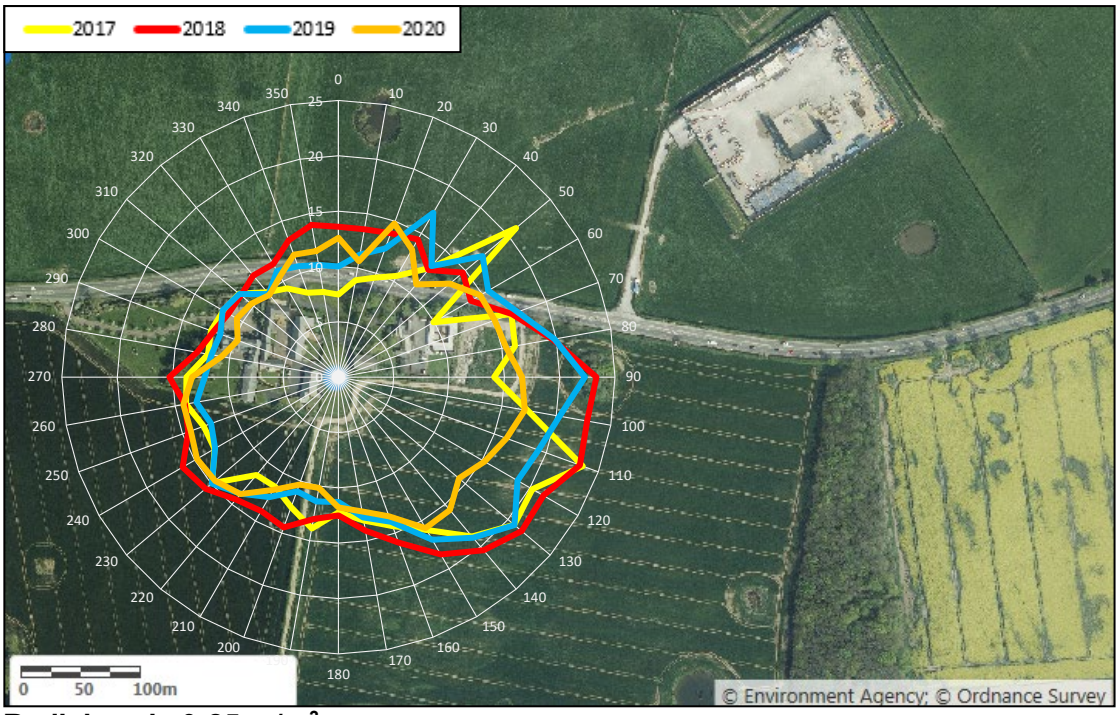

Radial scale 0-25µg/m^3

Figure 3.10: $PM_{2.5}$ Pollution rose

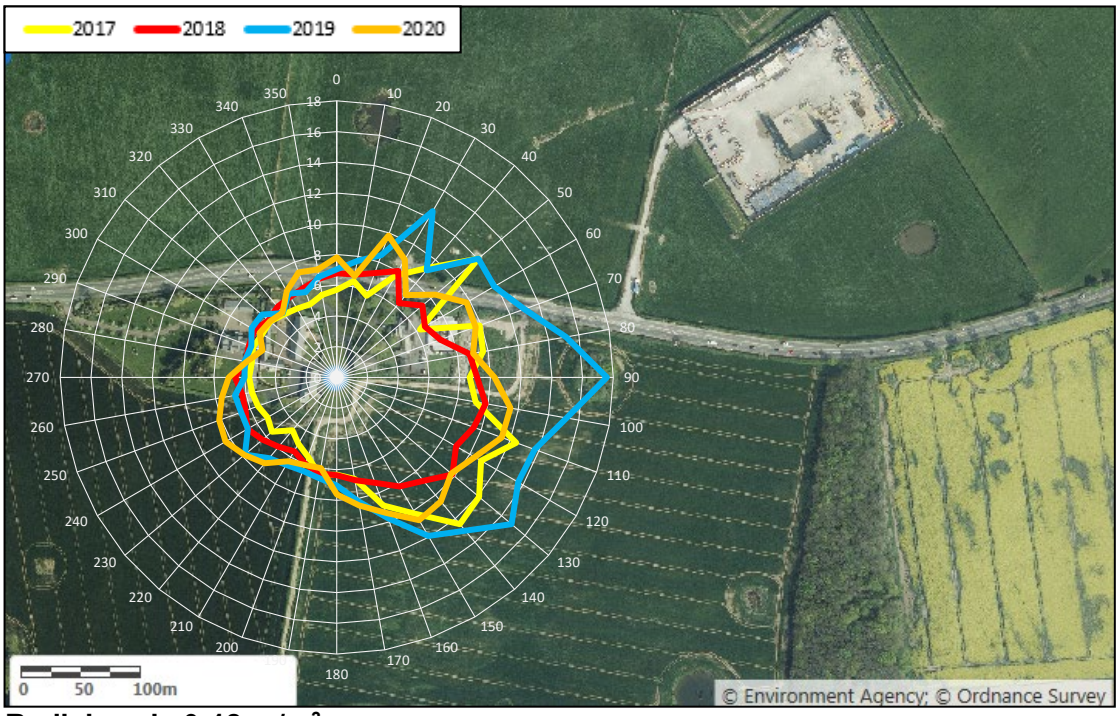

Radial scale 0-18µg/m^3

The average concentration for each 10° wind sector can also be tabulated and colour coded from the lowest (dark green) to the highest (red) average concentration (Table 3.5). This highlights the wind directions with the highest averages for PM_{10} and $PM_{2.5}$, but also emphasises correlations between the 2, showing the wind directions of common sources.

The bearing of the well pad is highlighted in blue. The table demonstrates that the wind directions most associated with higher concentrations of particulate matter in the area are 70° to 150° and this does not vary over the monitoring period.

Table 3.5: Comparison of the mean concentrations for each 10° wind sector

	2017		2018		2019		2020	
Wind direction	**PM_{10}**	**$PM_{2.5}$**	**PM_{10}**	**$PM_{2.5}$**	**PM_{10}**	**$PM_{2.5}$**	**PM_{10}**	**$PM_{2.5}$**
0								
10								
20								
30								
40								
50								
60								
70								
80								
90								
100								
110								
120								
130								
140								
150								
160								
170								
180								
190								
200								
210								
220								
230								
240								
250								
260								
270								
280								
290								
300								
310								
320								
330								
340								
350								

3.2.3.3 Percentile rose plots

Arrays of plots showing directional contributions to PM_{10} and $PM_{2.5}$ concentrations ($\mu g/m^3$) at the MMF site for different percentiles are shown in Figure 3.11 and Figure 3.12 respectively. An explanation of percentile analysis is given in Appendix G.

Figure 3.11: PM_{10} Percentile rose ($\mu g/m^3$)

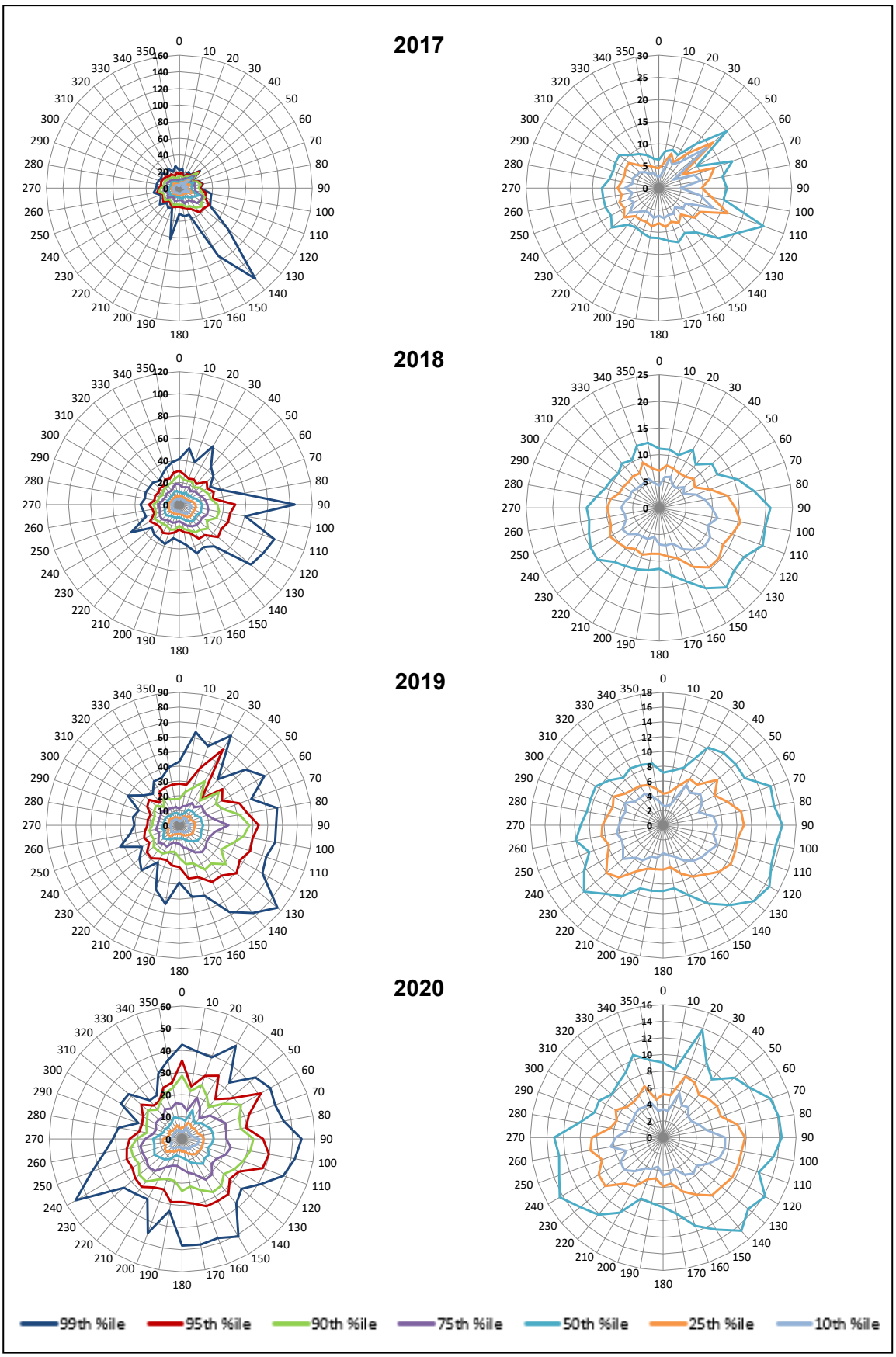

The PM_{10} plots for 2017 show that the contribution from the source(s) between 140° and 150° is more evident in the higher percentiles. This suggests that there is an intermittent source(s) in this wind sector that leads to elevated PM_{10} concentrations at the monitoring site. The plots also show that contributions from source(s) between 50° and 110° are more evident in the lower percentiles, suggesting that the sources in this wind sector are relatively continuous, but do not cause appreciably high concentrations of PM_{10} at the monitoring site.

2018 included a period of hydraulic fracturing. The PM_{10} plots for 2018 show that the contribution from the source(s) between 90° and 130° affects all the percentiles, which indicates that the source(s) is relatively continuous and commonly affects PM_{10} concentrations at the monitoring site. The plots also show that the contributions from the source(s) at 10°, 30° and 240° are more evident in the higher percentiles. This suggests that there are intermittent sources in these wind directions that lead to elevated PM_{10} concentrations at the monitoring site.

2019 included a period of hydraulic fracturing. The PM_{10} plots for 2019 show that the contribution from the source(s) between 30° and 140° affects all the percentiles, which indicates that the source(s) is relatively continuous and commonly affects PM_{10} concentrations at the monitoring site. The plots also show that the contributions from the source(s) at 10° to 20° and 190° are more evident in the higher percentiles. This suggests that there are intermittent sources in these wind directions that lead to elevated PM_{10} concentrations at the monitoring site. The plots also show that contributions from source(s) between 230° and 300° are more evident in the lower percentiles, suggesting that the sources in this wind sector are relatively continuous, but do not cause appreciably high concentrations of PM_{10} at the monitoring site.

The PM_{10} plots for 2020 show that the contributions from the source(s) between 90° and 110° affect all the percentiles, which indicates that the source(s) are relatively continuous and commonly affect PM_{10} concentrations at the monitoring site. The plots also show that the contributions from the source(s) at 150° to 180° and 240° are more evident in the higher percentiles. This suggests that there are intermittent sources in these wind directions that lead to elevated PM_{10} concentrations at the monitoring site.

Figure 3.12: $PM_{2.5}$ Percentile rose (µg/m^3)

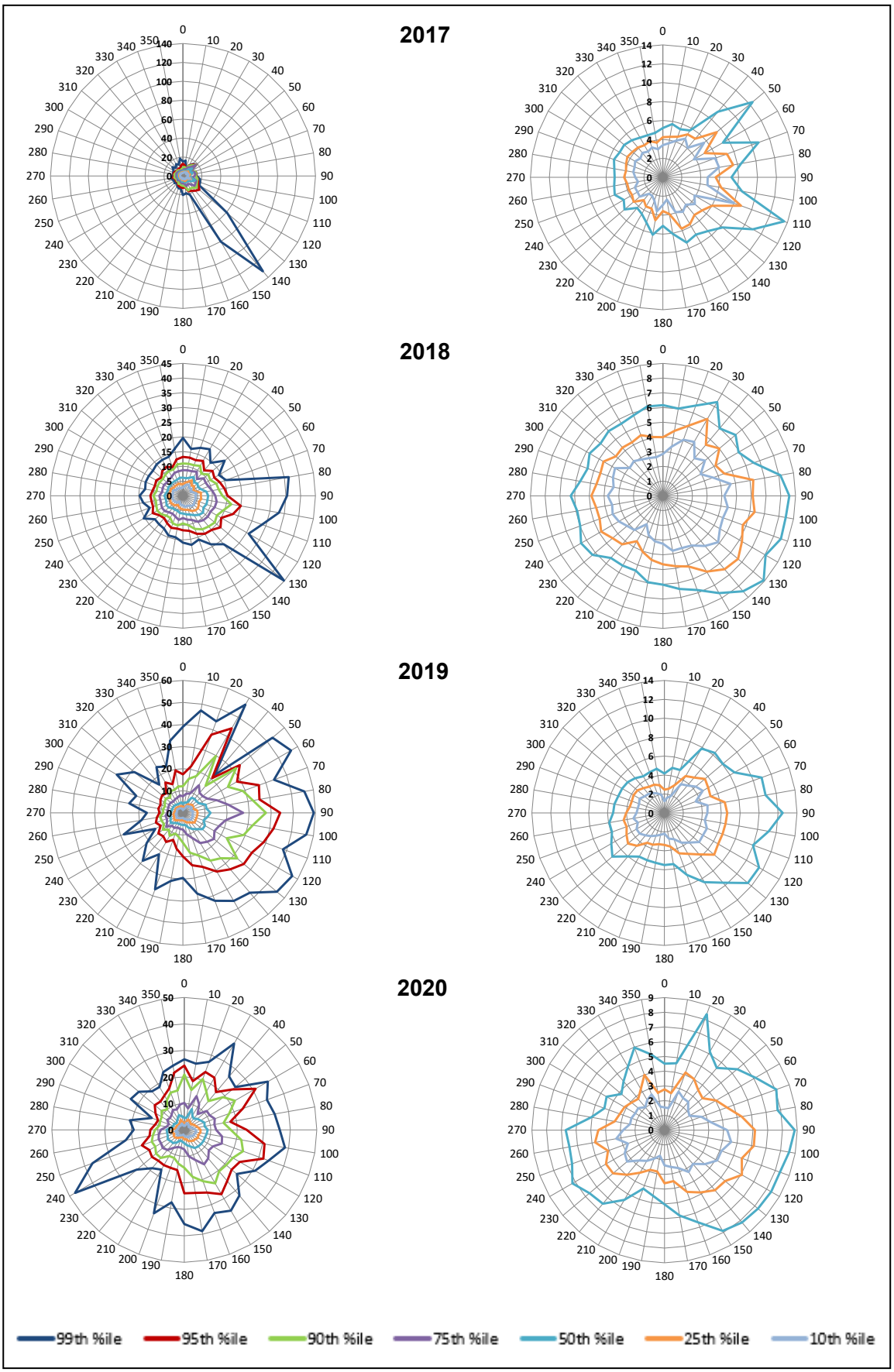

The $PM_{2.5}$ plots for 2017 show that the contribution from the source(s) between 140° and 150° is more evident in the higher percentiles. This suggests that there is an intermittent source(s) in this wind sector that leads to elevated $PM_{2.5}$ concentrations at the monitoring site. The plots also show that the contribution from the sources between 50° and 110° is more evident in the lower percentiles, suggesting that the sources in this wind sector are relatively continuous, but do not cause appreciably high concentrations of $PM_{2.5}$ at the monitoring site.

2018 included a period of hydraulic fracturing. The $PM_{2.5}$ plots for 2018 show that the contribution from the source(s) between 80° and 130° is more evident in the higher percentiles. This suggests that there are intermittent sources in these wind directions that lead to elevated $PM_{2.5}$ concentrations at the monitoring site.

2019 included a period a hydraulic fracturing. The $PM_{2.5}$ plots for 2019 show that the contributions from the source(s) between 20º and 30° and 50° to 130° affect all the percentiles, which indicates that the source(s) are relatively continuous and commonly affect $PM_{2.5}$ concentrations at the monitoring site. The plots also show that the contributions from the sources at 350° to 10° are more evident in the higher percentiles. This suggests that there are intermittent sources in these wind directions that lead to elevated $PM_{2.5}$ concentrations at the monitoring site.

The $PM_{2.5}$ plots for 2020 show that the contributions from the source(s) between 90° and 150° affect all the percentiles, which indicates that the source(s) are relatively continuous and commonly affect $PM_{2.5}$ concentrations at the monitoring site. The plots also show that the contributions from the sources at 150° to 200° and 240° to 250° are more evident in the higher percentiles. This suggests that there are intermittent sources in these wind directions that lead to elevated $PM_{2.5}$ concentrations at the monitoring site. The plots also show that the contribution from the sources between 70° and 150° is more evident in the lower percentiles, suggesting that the sources in this wind sector are relatively continuous, but do not cause appreciably high concentrations of $PM_{2.5}$ at the monitoring site.

3.2.3.4 Conditional probability function plots

Figure 3.13 and Figure 3.14 show conditional probability function (CPF) plots for PM_{10} and $PM_{2.5}$ concentrations above the 90th percentile. The plot calculates the probability that PM_{10} and $PM_{2.5}$ concentrations would be greater than their 90th percentile value (25 and 14µg/m^{-3} respectively over the whole ~3-year monitoring period) for a particular wind speed and wind direction. The scale of a CPF plot ranges from 0 to 1, from lowest to highest probability. Further information about this method can be found in Appendix H.

Figure 3.13 shows that high concentrations of PM_{10} (greater than the 90th percentile of all observations) were most probable in 2019, at wind speeds above 20m/s for the wind sector 215° to 245°. There is no evidence that high concentrations were more likely to occur from the direction of the well pad.

Figure 3.14 shows that high concentrations of $PM_{2.5}$ (greater than the 90th percentile of all observations) were most probable in 2019, at wind speeds above 20m/s for the wind

sector 215° to 245°. There is no evidence that high concentrations were more likely to occur from the direction of the well pad.

Figure 3.13: Openair PM_{10} conditional probability function plots

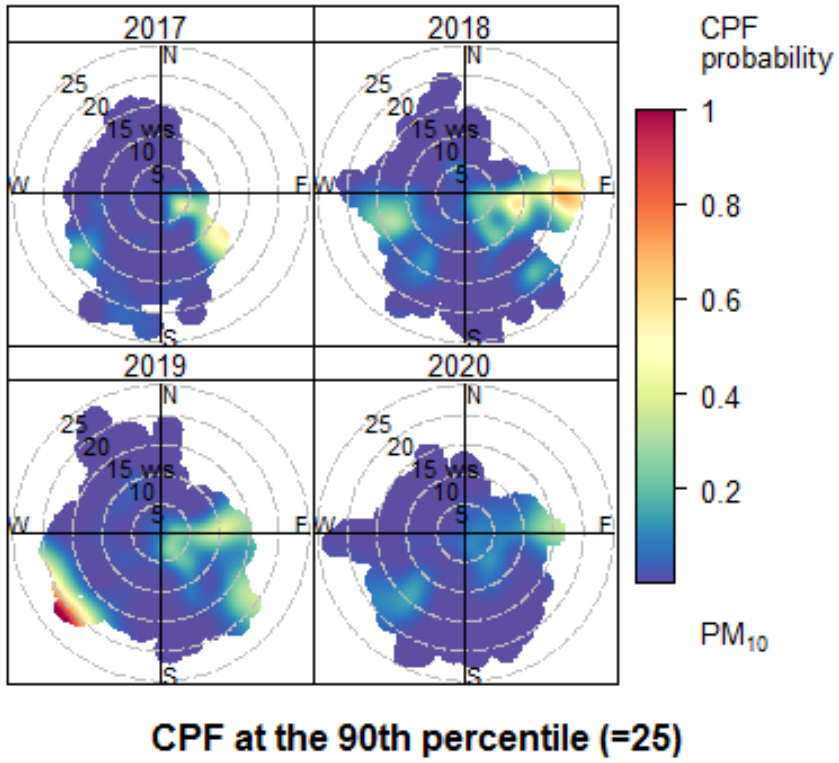

Figure 3.14: Openair $PM_{2.5}$ conditional probability function plots

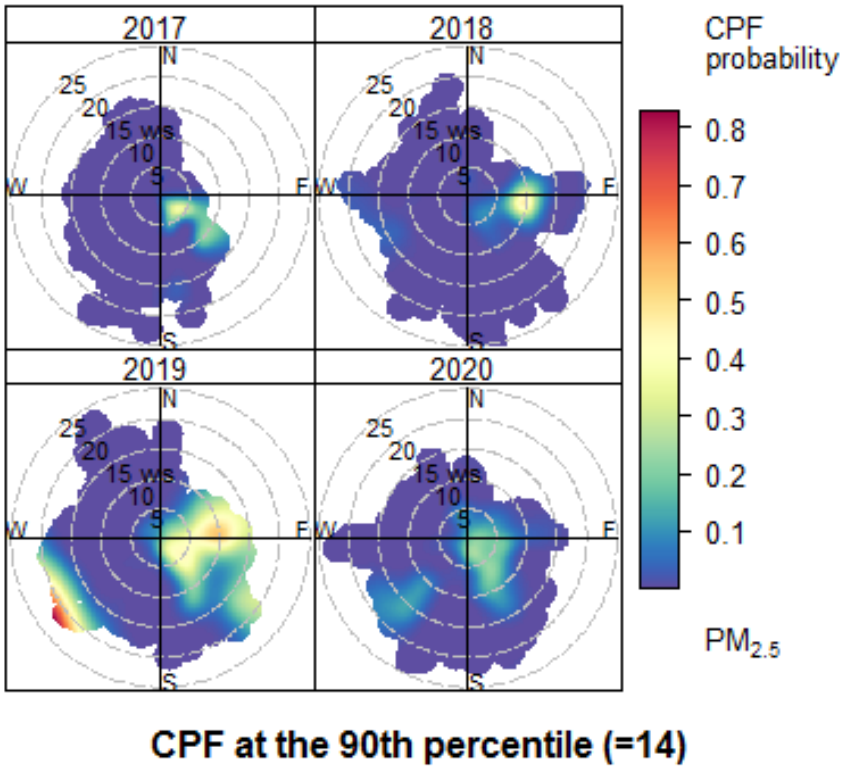

3.2.4 Wind speed variation

Wind speed plays an important role in the dispersion of air pollutants. Higher wind speeds generate more mechanical turbulence, which has the effect of distributing emissions more rapidly through the mixed boundary layer of the atmosphere. Higher wind speeds also have the potential to raise dust from loose surfaces, which can increase emissions and ambient concentrations, but also dilute stack emissions relatively rapidly so that concentrations are reduced. The relative concentrations measured at different wind speeds can provide an insight into the nature of contributing sources.

Figure 3.15 and Figure 3.16 show polar (wind speed dependency) plots for PM_{10} and $PM_{2.5}$ respectively.

Figure 3.15: PM_{10} Openair wind speed dependency plot

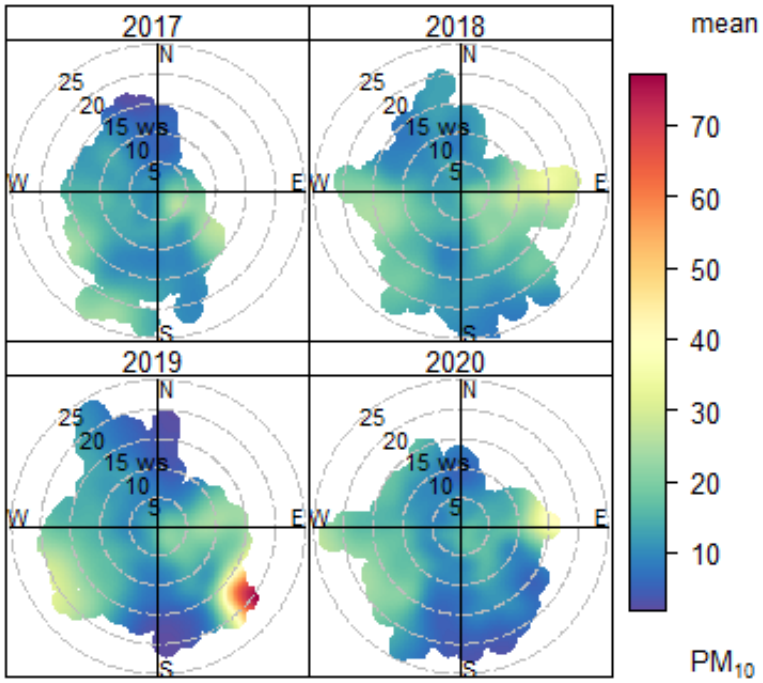

Figure 3.15 suggests that the highest mean PM_{10} concentrations were generated in 2019 at wind speeds >15m/s for wind directions 115° to 135°.This differs from the wind sector of the highest concentrations identified in the CPF plots (Figure 3.13). To understand the difference between the CPF plots and the wind speed dependence plots it must be understood that the latter looked at mean values (for each wind speed and direction), while the CPF looked at values above the 90%ile. The wind speed and direction conditions giving high values in the CPF analysis are the conditions that bring about the highest concentrations at the site. The wind speed dependency plots in Figure 3.15 show the conditions associated with the greatest mean concentrations at the site. The CPF analysis is a better indicator of the conditions that may bring about exceedance events, whereas the plots in Figure 3.15 are more effective at displaying the conditions that affect average concentrations at the site as a whole.

Figure 3.16: $PM_{2.5}$ Openair wind speed dependency plot

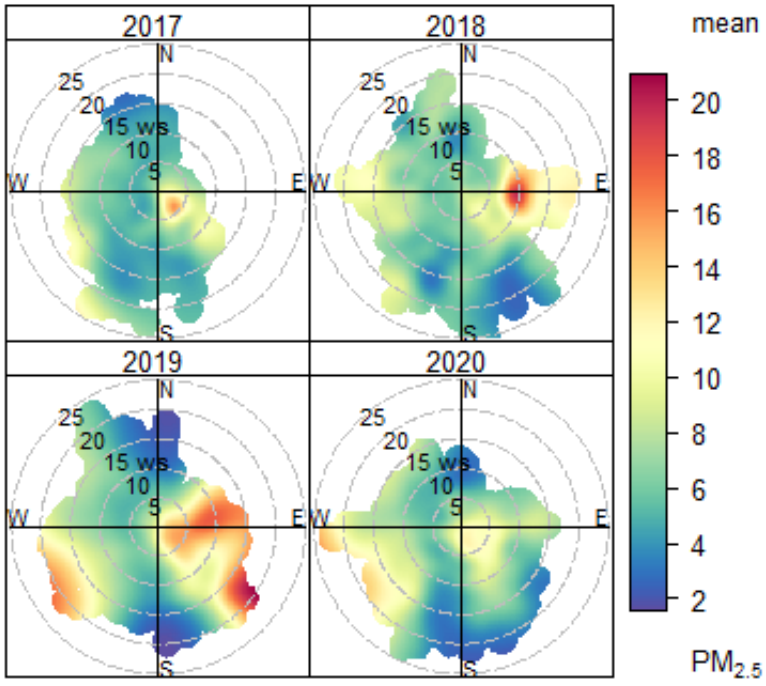

Figure 3.16 suggests that in 2017 the highest mean $PM_{2.5}$ concentrations were associated with winds from the directions 90° to 180° at wind speeds <5m/s.

In 2018, the highest mean $PM_{2.5}$ concentrations were from the wind directions 65° to 115° at wind speeds ~6-13m/s.

In 2019, the highest mean $PM_{2.5}$ concentrations were from the wind directions 220° to 265° at wind speeds >15m/s, and from 60° to 115° at all wind speeds, and from 115° to 140° at wind speeds >15m/s.

In 2020, the highest mean $PM_{2.5}$ concentrations were from the wind directions 225° to 170° at wind speeds >15m/s, and from 90° to 180° at wind speeds <5m/s.

3.2.5 Diurnal analysis

Considering the diurnal distribution of concentration levels can provide further useful information about the sources contributing to the ambient levels in each sector. Pollutants generated from everyday traffic on the roads typically show a double peak pattern, where the peaks correspond to the morning and afternoon/evening rush hours. By contrast, emissions from activities on an industrial process site are usually characterised by a single, broad peak spanning the hours of the working day or operations on site.

Diurnal Openair plots for PM_{10} and $PM_{2.5}$ are shown in Figure 3.17 and Figure 3.18.

Figure 3.17 suggests that in 2017, the highest mean PM_{10} concentrations were seen in the wind directions 90° to 150° during the whole of the day, but that the time of highest concentrations was in the early morning. The area of white in the north-east of the plot indicates that there was no data for this wind direction and time period.

In 2018, the highest mean PM_{10} concentrations were seen in the wind directions 55° to 150° during the whole of the day, but the time of highest concentrations was in the middle of the day.

In 2019, the highest mean PM_{10} concentrations were seen in the wind directions 35° to 150°, with levels highest in the middle of the day between 90° to 150°.

In 2020, the highest mean PM_{10} concentrations were seen in the wind directions 35° to 90°, with high levels in the early morning between 35° and 60° and high levels in the late afternoon between 60° and 90°.

Figure 3.17: PM_{10} Openair diurnal annulus plots

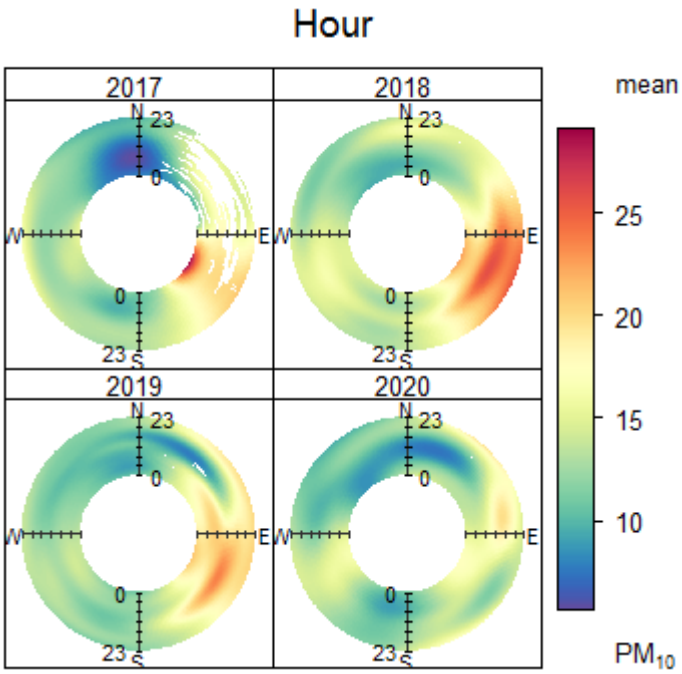

Figure 3.18 suggests that in 2017, the highest mean $PM_{2.5}$ concentrations were seen in the wind directions 90° to 150° during the morning and the evening.

In 2018, the highest mean $PM_{2.5}$ concentrations were seen in the wind directions 90° to 140° during the late evening.

In 2019, the highest mean $PM_{2.5}$ concentrations were seen in the wind directions 15° to 160°, with levels highest in the morning between 50° and 160°.

In 2020, the highest mean $PM_{2.5}$ concentrations were seen in the wind directions 15° to 170°, with high levels in the early morning between 15° and 70° and 140° and 170° and high levels in the morning between 80° and 140°.

Figure 3.18: $PM_{2.5}$ Openair diurnal annulus plots

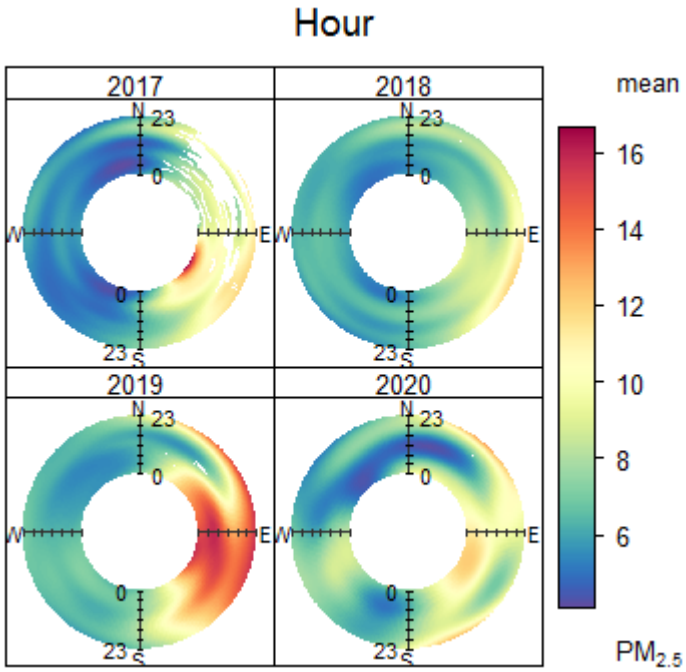

3.2.6 Conclusions

Time series plots

Based on visual inspection of time series plots, there is no evidence of particularly elevated levels of particulate air pollution occurring during the hydraulic fracturing periods, although it should be noted that the wind direction was rarely blowing from the shale well pad to the monitoring site.

Comparison with standards

Comparison of the PM_{10} data with the AQS objective for the 24-hour (midnight to midnight) mean indicated that it was not exceeded at the monitoring site during the monitoring period.

Comparison of the PM_{10} data with the AQS annual mean indicated that it was not exceeded at the monitoring site during the monitoring period.

Comparison of the $PM_{2.5}$ data with the AQS annual mean indicated that it was not exceeded at the monitoring site during the monitoring period.

Comparison with air quality index

The PM_{10} 24-hour concentrations were all in the low banding of the air quality index during 2018 and 2020. During 2017 there was one day in the moderate banding, and during 2019 there were 3 days in the moderate banding.

The $PM_{2.5}$ 24-hour concentrations were all in the low band of the air quality index during 2018 and 2020. During 2017 there was one day in the moderate band, and during 2019 there were 8 days in the moderate band.

Directional analysis

Based on visual inspection of time series plots for 45° sectors, there is no evidence of notably elevated concentrations coming from the (NE) 45° sector that contained the well pad during periods of hydraulic fracturing.

Pollution rose analysis indicates that the main source(s) of particulate in the area was in the wind sector 70° to 150° and this did not vary over the monitoring period.

Percentile rose analysis suggested that the monitoring site was affected by both relatively continuous and intermittent particulate matter emissions.

Conditional probability function (CPF) plots suggested that high concentrations of both PM_{10} and $PM_{2.5}$ (greater than the 90^{th} percentile of all observations) were most probable during 2019, and occurred at wind speeds above 20m/s from the wind sector 215° to 245°. There is no evidence that high concentrations were more likely to occur from the direction of the well pad.

Wind speed variation

Polar wind speed dependency plots suggest that the highest mean PM_{10} concentrations were generated at wind speeds >15m/s for wind directions 115° to 135° in 2019. In 2019, mean $PM_{2.5}$ concentrations were moderately elevated when stronger winds came from the direction of the well pad site (50° to 70°), but not in other years.

Diurnal analysis

Diurnal analysis suggests that the high mean PM_{10} concentrations were seen in 2018 in the wind directions 55° to 150° during the whole of the day, but were highest in the middle of the day.

Diurnal analysis suggests that the high mean $PM_{2.5}$ concentrations were seen in 2019 in the wind directions 15° to 160°, with levels highest in the morning between 50° and 160°.

Summary

There was no evidence of relatively elevated particulate concentrations from the direction of the well pad, except tentatively in 2019 when $PM_{2.5}$ was slightly elevated during higher wind speed conditions. Any contributions from the well pad were not discernible above the contribution from that direction of road traffic on the A583, which was substantially closer to the MMF (~130m distant compared to ~380m).

3.3 Oxides of nitrogen (NO_X)

Between 23 August 2017 and 11 September 2020 (1,116 days) airborne NO_X and NO_2 concentrations were measured at a height of 2m above ground. Details of the instrumentation and methodology are given in Appendix D. Successful data collection at the MMF was 96%.

Considering NO_X in the atmosphere can give a more direct indication of local pollution sources than looking solely at NO_2. Combustion processes generally emit a greater proportion of NO than NO_2, with NO subsequently oxidising to form NO_2 (typically hours-days later, although oxidation can occur more rapidly during ozone episodes). The NO_X signature of an emission is relatively unaffected by such oxidation, compared to the signature of NO_2, so NO_X is more easily attributed to particular sources than NO_2. There is also the advantage that NO_X can be treated as a conserved quantity (that is, a quantity that is not changed by chemical reaction) during short-range, local dispersion.

A time series plot of 1-hour concentrations of NO_X at the monitoring sites is shown in Figure 3.19. Two periods with hydraulic fracturing at the well pad are marked on Figure 3.19, using green and orange lines to show dates of 'start' and 'suspension' respectively. The levels of NO_x during these periods are not particularly elevated; however, it should be noted that, in general, the wind rarely blew from the well pad to the monitoring site (as discussed in section 3.1).

Figure 3.19: NO_X 1-hour mean concentrations ($\mu g/m^3$)

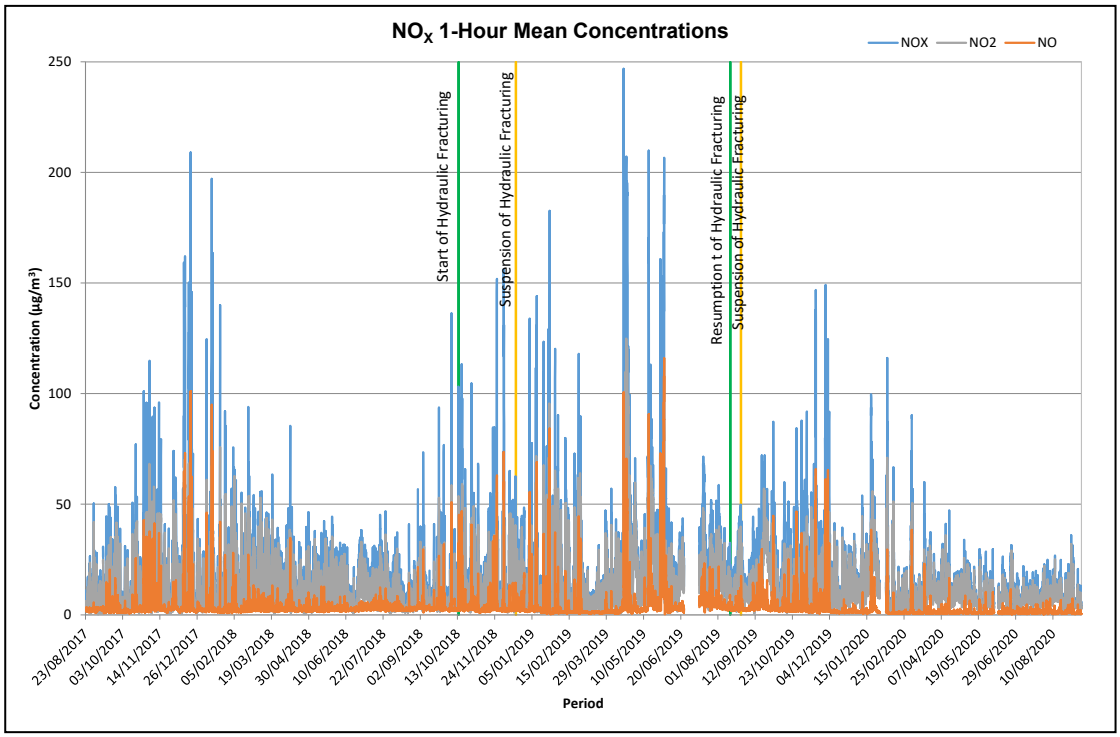

The plot shows that NO_X concentrations remained predominantly below 100µg/$m^{3,}$ with discrete excursions above this level. The period of higher levels during April to June 2019 was investigated in case these might be due to a calibration issue. Although the analyser

appeared to be calibrating correctly during this period, further data analysis suggested the possibility of erroneous values. Specifically, a comparison of NO_X concentrations at the MMF with the Preston Automatic Urban and Rural Network (AURN) site is shown in Figure 3.20. In general, the NOx levels at the MMF are lower than at the Preston AURN, and the levels at both sites vary similarly through the year. The plot shows that the increased levels during April to June 2019 are not seen at the AURN site. This could be down to very local sources near the MMF, but no one source appears to dominate at the monitoring site during this period. However, as the instrument appeared to be performing satisfactorily during this period, the data has not been removed. It is worth noting that the period in question does not occur during a period of hydraulic fracturing.

Figure 3.20: Comparison of NO_X 1-hour mean concentrations (µg/m^3) with the Preston AURN monitoring site

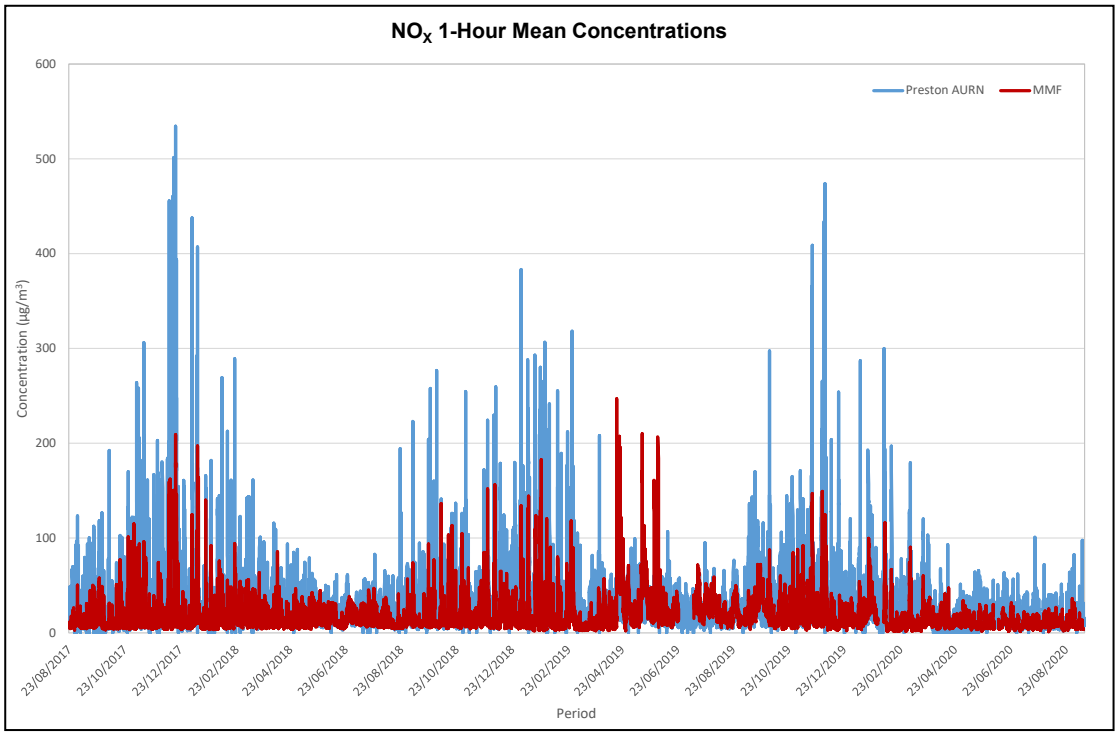

3.3.1 Comparison with standards

3.3.2 Comparison with Air Quality Strategy (AQS) objectives

While considering NO_X levels can be more informative in determining the source of pollution, the level of NO_2 concentration is more important from a human health standpoint. NO_2 is the constituent of NO_X that is harmful to health and there is a national Air Quality Strategy objective for NO_2 levels. NO_2 has therefore been considered, in addition to NO_X, to reflect the public health risk.

The AQS has objectives for 1-hour mean and annual mean NO_2 concentrations. The AQS objectives for the 1-hour mean concentrations state that a value of 200µg/m^3 (105ppb) must not be exceeded on more than 18 occasions during one year.

As these standards are measured over a year, the data has been broken down into the respective years before being compared with the standards.

A time series plot of annual 1-hour concentrations of NO_2 measured at the monitoring site is shown in Figure 3.21, with the dashed line marking 200µg/m^3.

Figure 3.21: NO_2 annual 1-hour mean concentrations (µg/m^3)

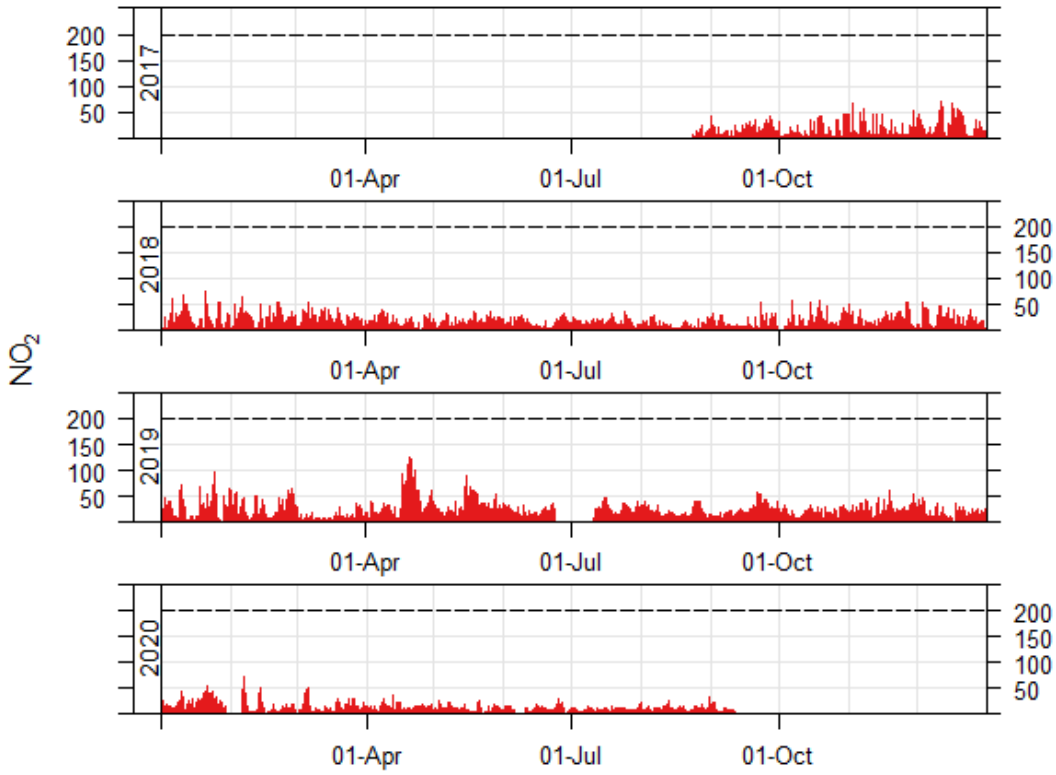

The 1-hour NO_2 concentrations were never greater than 200µg/m^3 during the monitoring period, the maximum concentration being 125µg/m^3 in 2019. Therefore, the AQS for 1-hour mean NO_2 concentrations was not exceeded at the monitoring site.

The NO_2 annual objective states that the annual mean concentration must not exceed 40µg/m^3 (21ppb). Table 3.6 compares the annual average concentrations of NO_2 and NO_X for each year of the monitoring study. Table 3.6 shows that during the monitoring period the annual NO_2 objective was not exceeded at the monitoring site; the highest annual concentration being 16.6µg/m^3 measured in 2019.

The AQS objectives include an annual standard for NO_X of 30µg/m^3, for the protection of vegetation and ecosystems. Table 3.6 shows that during the monitoring period the annual NO_X objective was not exceeded at the monitoring site; the highest annual concentration being 23.3µg/m^3 measured in 2019.

Table 3.6: Comparison of NO_2 and NO_X concentrations with annual-average standards

Pollutant	Averaging time	AQS	Standard (A) ($\mu g/m^3$)	Measurement (B) ($\mu g/m^3$)	Projected exceedance ratio (B/A)
2017 NO_2	Year	2000	40	10.4*	0.26
2018 NO_2				10.8	0.27
2019 NO_2				16.6	0.42
2020 NO_2				9.38*	0.23
2017 NO_X		2000	30	16.3*	0.54
2018 NO_X				15.8	0.53
2019 NO_X				23.3	0.78
2020 NO_X				11.6*	0.39

* Extrapolated from effective monitoring period

3.3.2.1 Comparison with Air Quality Index

In the United Kingdom a daily Air Quality Index has been developed. The system uses an index numbered 1 to 10 (low to high pollution), divided into 4 bands to provide more detail on a daily basis about air pollution levels to the general population and those at higher risk from air pollution.

Figure 3.22 looks retrospectively at the daily NO_2 concentrations for each year at the monitoring site in relation to the Air Quality Index (AQI) band.

The plots show that all the NO_2 1-hour concentrations were in the low band of the air quality index at the monitoring site.

Figure 3.22: Pie charts of daily air quality indices in each year 2017 to 2020

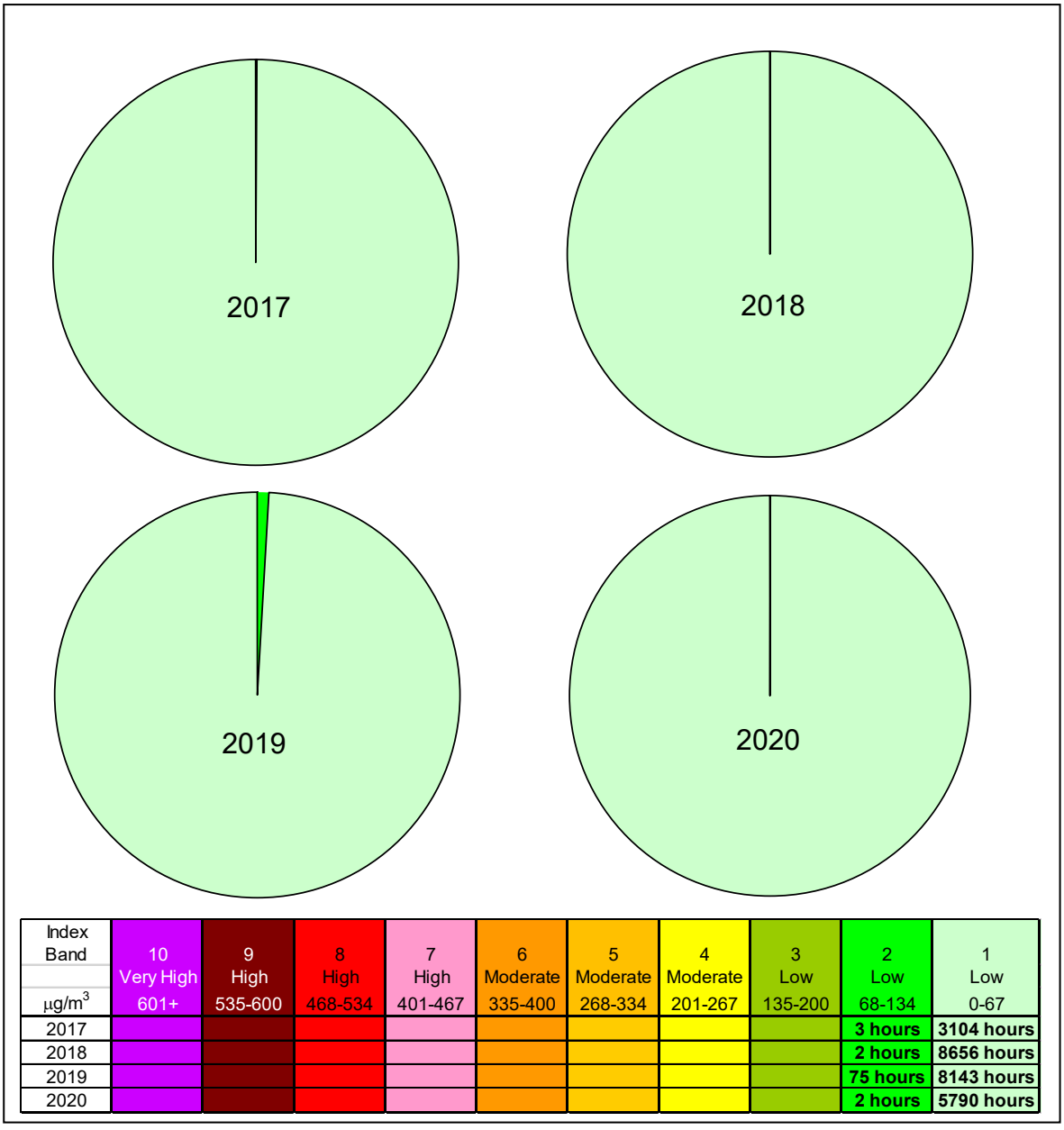

Index Band	10 Very High	9 High	8 High	7 High	6 Moderate	5 Moderate	4 Moderate	3 Low	2 Low	1 Low
µg/m^3	601+	535-600	468-534	401-467	335-400	268-334	201-267	135-200	68-134	0-67
2017									**3 hours**	**3104 hours**
2018									**2 hours**	**8656 hours**
2019									**75 hours**	**8143 hours**
2020									**2 hours**	**5790 hours**

3.3.3 Directional analysis

3.3.3.1 Time series plots for 45° sectors

Figure 3.23 shows the 5-minute mean concentrations of NO_X for all wind directions, grouped into 45° sectors. The plot shows that the NO_X concentrations were fairly uniform, with the highest levels seen from the east in 2019. The levels of NO_x from the NE sector (direction of the well pad) during the hydraulic fracturing periods were not particularly elevated; however, it should be noted that in general the wind rarely blew from the well pad to the monitoring site (as discussed in section 3.1).

Figure 3.23: NO_X 5-minute mean time series for each 45° wind sector

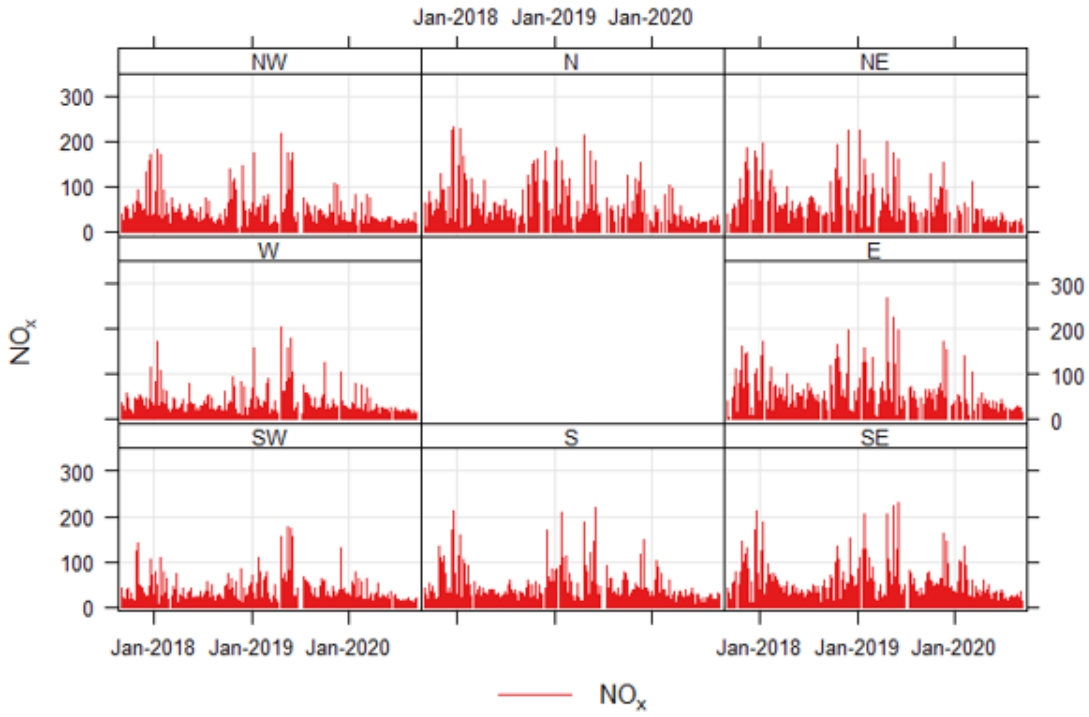

3.3.3.2 Radial plots

A radial plot of mean NO_X concentrations ($\mu g/m^3$) for each year against wind direction is shown in Figure 3.24. The pollution rose for 2019 looks slightly anomalous when compared to the other years as it shows an increase in all directions, including those directions to the west where levels were consistently lower in other years. As has already been mentioned, there is a period of data in April to June 2019 that was investigated because it had unusual values that might have been invalid; if these values are removed, the resulting pollution rose for 2019 appears much more in keeping with the plots for other years.

Periods of hydraulic fracturing occurred in 2018 and 2019. The highest average NO_X concentrations occurred in 2017 and are seen at the 10° sector centred on 60°, which is the direction of the road and the well pad. The rose for 2020, during the period of national Covid-19 lockdown, shows the lowest concentration.

Figure 3.24: NO_X Pollution rose

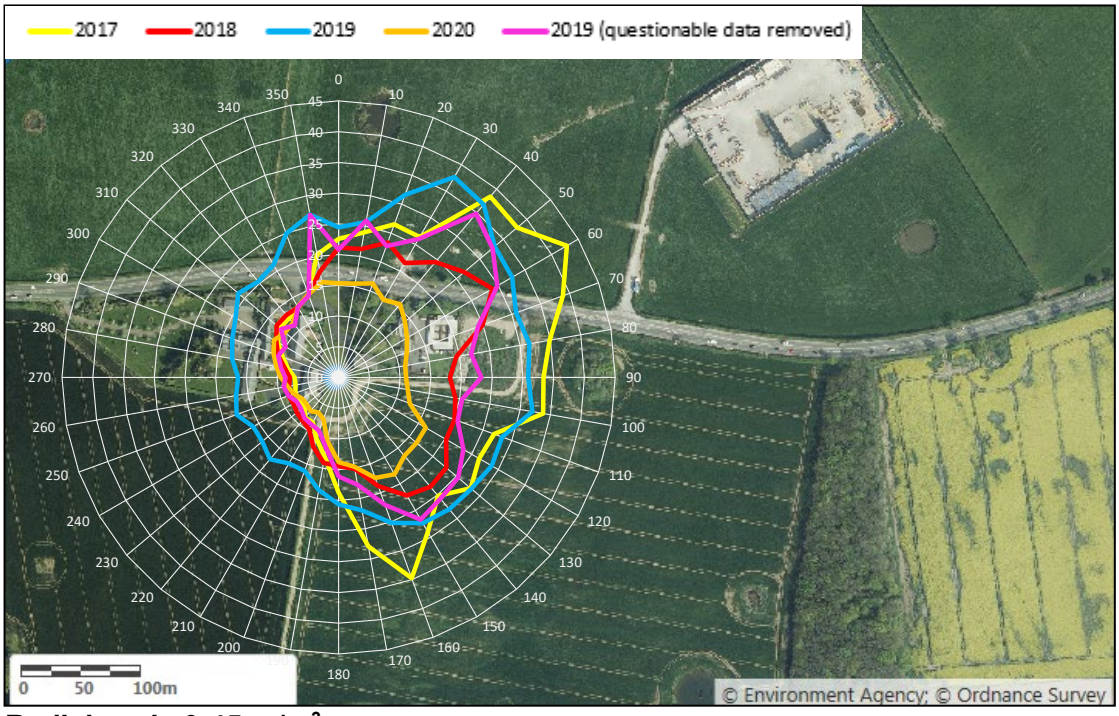

Radial scale 0-45µg/m^3

The average concentration for each 10° wind sector can also be tabulated and colour coded from the lowest (dark green) to the highest (red) average concentration (Table 3.7). This highlights the wind directions with the highest averages for NO_X. The bearing of the well pad is highlighted in blue. The table demonstrates that the wind direction range that is most associated with elevated NO_X is 350° to 160°. This range includes 10° sectors that cover the A583 road, including 3 sectors that partly or wholly cover the well pad as well as the road (that is, those centred on 50°, 60° and 70°). The occurrence of elevated NOx in the range 350° to 160° does not alter over the monitoring period, except in 2020 which may have been affected by changes in emission sources, such as reduced traffic and industrial activity, because of the Covid-19 lockdown.

Table 3.7: Comparison of the mean NO_X concentrations for each 10° wind sector

Wind direction	2017	2018	2019	2019*	2020
0					
10					
20					
30					
40					
50					
60					
70					
80					
90					
100					
110					
120					
130					
140					
150					
160					
170					
180					
190					
200					
210					
220					
230					
240					
250					
260					
270					
280					
290					
300					
310					
320					
330					
340					
350					

*2019 data with questionable data removed

3.3.3.3 Percentile rose plots

An array of plots showing the contribution to NO_X concentrations ($\mu g/m^3$) at the monitoring site for different percentiles is shown in Figure 3.25.

The plots for 2017 show that the contribution from the source(s) between 130° and 170° is more evident in the higher percentiles. This suggests that there is an intermittent source(s) in this wind sector that leads to elevated NO_X concentrations at the monitoring site. The plots also show that the contribution from the sources between 40° and 100° is more evident in the lower percentiles, suggesting that the sources in this wind sector are relatively continuous, but do not cause appreciably high concentrations of NO_X at the monitoring site.

Figure 3.25: NO_X percentile rose

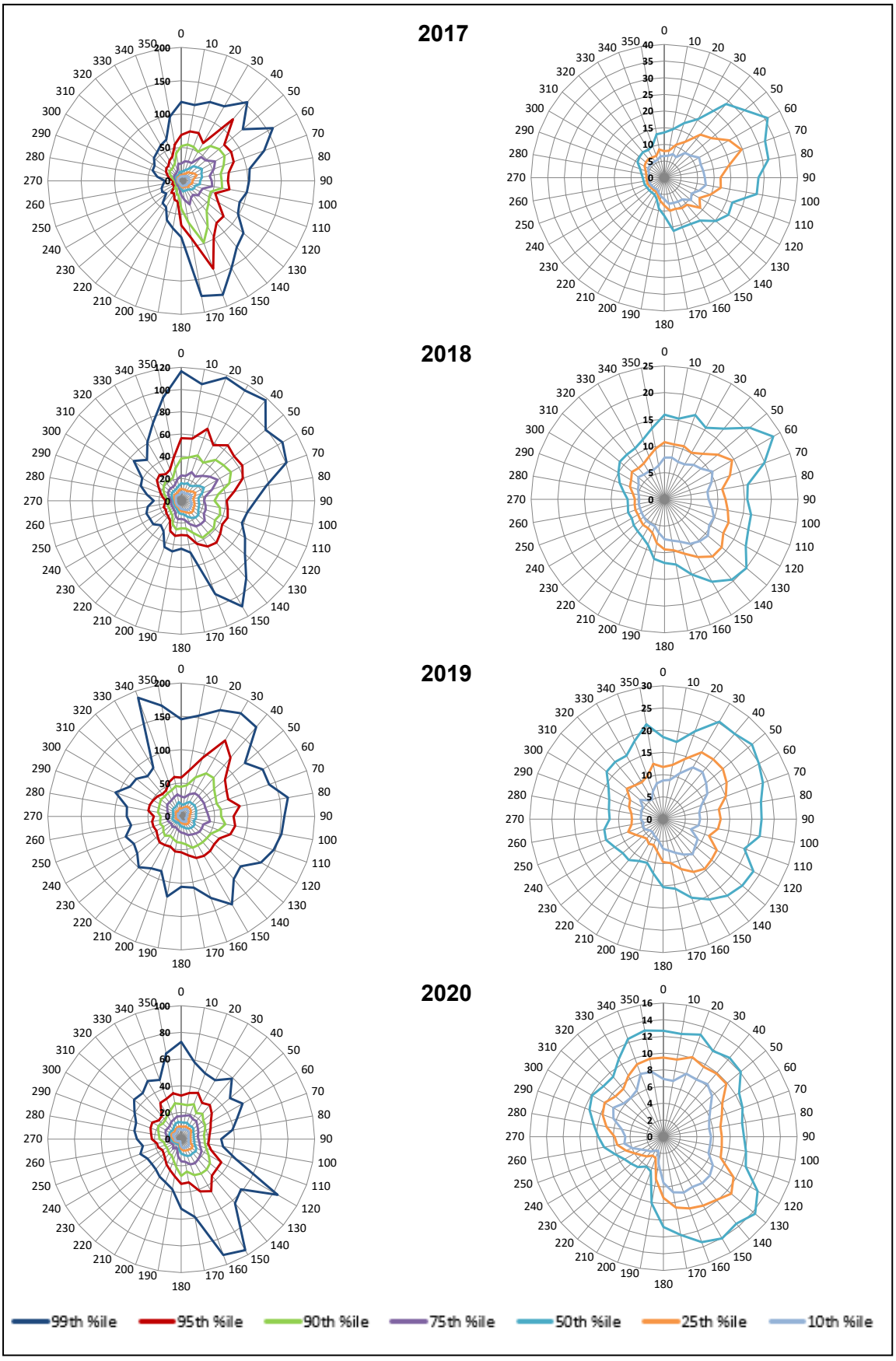

The plots for 2018 show that the contribution from the source at 60° affects all the percentiles, which indicates that the source is relatively continuous and commonly affects NO_X concentrations at the monitoring site. The plots also show that the contributions from the sources at 0° to 50° and 140° to 160° are more evident in the higher percentiles. This suggests that there are intermittent sources in these wind directions that lead to elevated NO_X concentrations at the monitoring site. The plots also show that the contribution from the sources between 130° and 140° is more evident in the lower percentiles, suggesting that the sources in this direction are relatively continuous, but do not cause appreciably high concentrations of NO_X at the monitoring site.

The plots for 2019 show that the contribution from the source(s) between 30° and 40° affects all the percentiles, which indicates that the source(s) is relatively continuous and commonly affects NO_X concentrations at the monitoring site. The plots also show that the contribution from the sources between 340° and 20° is more evident in the higher percentiles. This suggests that there are intermittent sources in these wind directions that lead to elevated NO_X concentrations at the monitoring site.

The plots for 2020 show that the contribution from the source(s) between 120° and 170° affects all the percentiles, which indicates that the source(s) is relatively continuous and commonly affects NO_X concentrations at the monitoring site. The plots also show that the contribution from the sources at 350° to 10° is more evident in the higher percentiles. This suggests that there are intermittent sources in these wind directions that lead to elevated NO_X concentrations at the monitoring site.

3.3.3.4 Conditional probability function plots

Figure 3.26 shows conditional probability function (CPF) plots for NO_X concentrations above the 90th percentile. The plot calculates the probability that NO_X concentrations would be greater than the 90th percentile value (34µg/m^{-3} over the whole ~3-year monitoring period) for a particular wind speed and wind direction. The scale of a CPF plot ranges from 0 to 1, from lowest to highest probability.

Figure 3.26: NOx conditional probability function plots

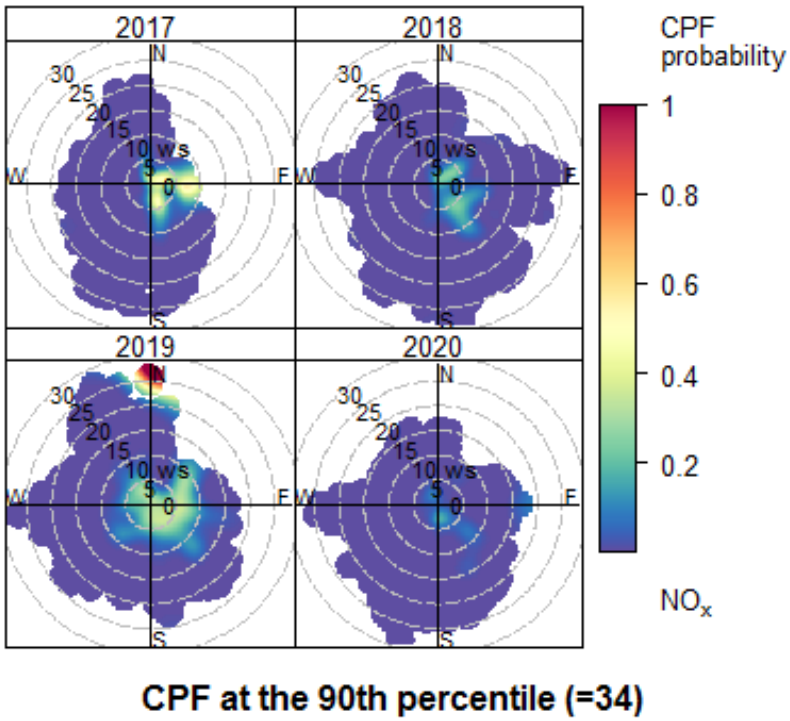

Figure 3.26 shows that high concentrations of NO_X (greater than the 90th percentile of all observations) are most probable at wind speeds above 25m/s for the wind sector 355° to 5° in 2019. There is evidence of an increased probability of higher concentrations of NOx from ~40° to 180° in 2017, ~40° to 150° in 2018, and ~40° to 145° degrees in 2019. There are lower probabilities for all directions in 2020, most likely due to reductions in emissions activity (most noticeably in road traffic emissions) associated with the Covid-19 lockdown.

3.3.4 Wind speed variation

Figure 3.27 shows an Openair polar (wind speed dependency) plot for NO_X.

Figure 3.27: NO_X polar plot

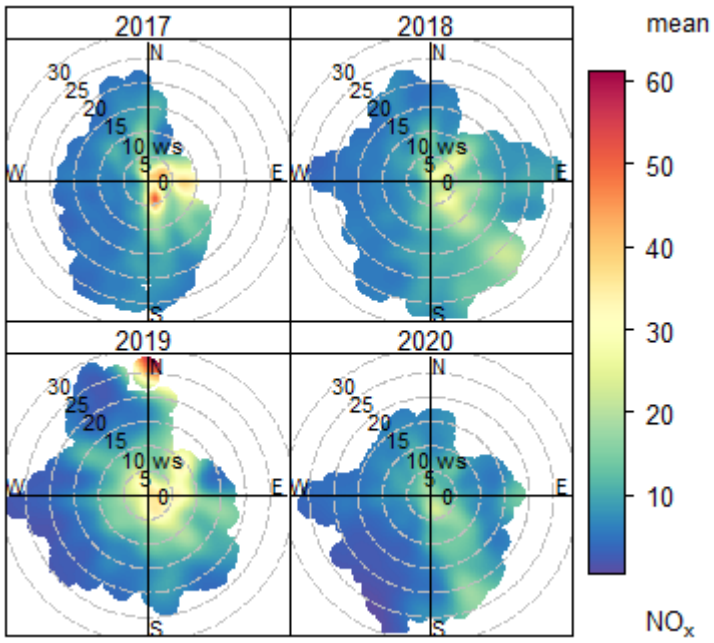

Figure 3.27 shows that the highest mean concentrations of NO_X are seen from the wind sector 355° to 5° at wind speeds greater than 25m/s in 2019. Relatively high mean concentrations of NOx are also seen from the wind sector 40° to 175° at wind speeds less than 10m/s in 2017.

3.3.5 Diurnal analysis

Diurnal Openair plots for NO_X are shown for the monitoring site in Figure 3.28.

Figure 3.28: NO_X diurnal annulus plot

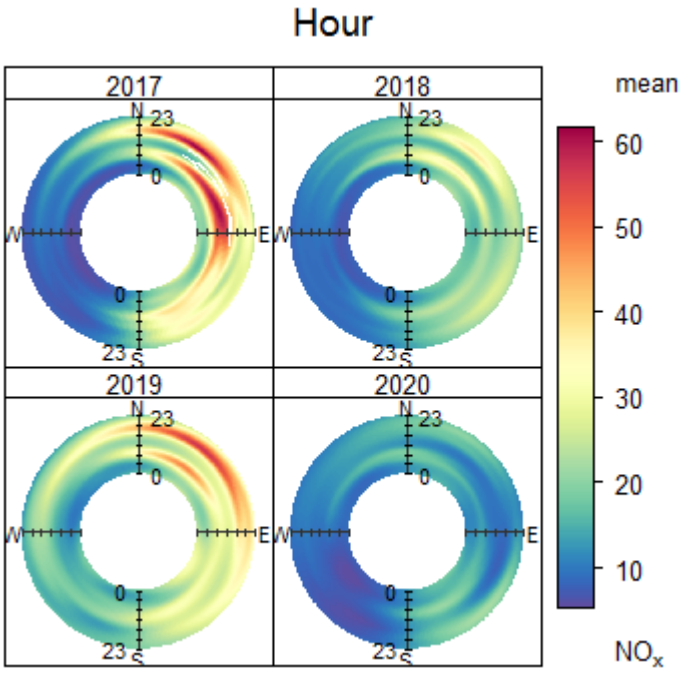

Figure 3.28 suggests that in 2017, the highest mean NO_X concentrations were seen from the wind direction range 15° to 170° during the morning, and from the wind direction ranges 355° to 90° and 135° to160° in the evening.

In 2018, the highest mean NO_X concentrations were seen from the wind direction range 25° to 55° during the morning and the evening.

In 2019, the highest mean NO_X concentrations were seen from the wind directions range 0° to 70° during the morning, and from the wind direction range 335° to 120° in the evening.

In 2020, the highest mean NO_X concentrations were lower than in previous years, most likely due to reductions in emissions activity (most noticeably in road traffic emissions) associated with the Covid-19 lockdown.

The results across the 4 years suggest a distinct contribution to measured NO_X levels from morning and evening peak traffic emissions.

3.3.6 Conclusions

Time series plots

Based on visual inspection of time series plots, there is no evidence of particularly elevated levels of NOx occurring during the hydraulic fracturing periods, although it should be noted that the wind direction was rarely blowing from the shale well pad to the monitoring site.

Comparison with standards

Comparison of the NO_2 data with the AQS objective for the 1-hour mean indicated that it was not exceeded at the monitoring site during the monitoring period.

During the monitoring period, the annual NO_2 objective was not exceeded at the monitoring site, with the highest annual concentration being 16.6µg/m^3 measured in 2019.

Comparison of the NOx data with the AQS annual mean objective applicable to vegetation indicated that this objective was not exceeded at the monitoring site, with the highest annual concentration being 23.3µg/m^3 measured in 2019.

Comparison with air quality index

The NO_2 1-hour concentrations were all in the low band of the air quality index during the monitoring period.

Directional analysis

Based on visual inspection of time series plots for 45^o sectors, there is no evidence of notably elevated concentrations coming from the (NE) 45° sector that contained the well pad during periods of hydraulic fracturing.

Pollution rose analysis indicates that the highest average NO_X concentrations were measured at the monitoring site when the wind was coming from between 350° and 160°. This changed slightly during 2020 due to the lower levels seen during the Covid-19 lockdown.

Percentile rose analysis suggests that the monitoring site was affected by both relatively continuous and intermittent sources of NO_X.

Conditional probability function (CPF) plots suggested that high concentrations of NOx (greater than the 90th percentile of all observations) were most likely to occur in 2019, at wind speeds above 25m/s for the wind sector 355° to 5°. There was also an increased probability of higher NOx concentrations for the wind sector 50° to 180° in 2017, 50° to 150° in 2019, and 50° to 150° in 2019. These wind sectors include the well pad and the A583 road.

Wind speed variation

Polar wind speed dependency plots showed that the highest concentrations of NO_X were in 2019, from the wind sector 355° to 5° at wind speeds greather than 25m/s. Relatively high mean concentrations of NOx are also seen in 2017, which came from the wind sector 40° to 175° at wind speeds less than 10m/s.

Diurnal analysis

Diurnal analysis suggest that the monitoring site is being mainly influenced by NO_X levels arising from low level sources, such as traffic emissions. Elevated concentrations of NOx were generally observed during the morning and evening periods, consistent with diurnal profiles typically associated with traffic emissions during morning and evening rush hours.

Summary

Overall, there was no evidence of notably elevated concentrations of nitrogen oxides (NOx or NO_2) when the wind came from the direction of the well pad, although winds rarely blew from the well pad to the monitor.

3.4 Methane (CH_4)

Between 23 August 2017 and 11 September 2020 (1,116 days) airborne CH_4 concentrations were measured at a height of 2m above ground. Details of the instrumentation and methodology are given in Appendix E. Successful data collection over the monitoring period was 98%.

The time series plot of 1-hour mean CH_4 concentrations (mg/m^3) over the period is shown in Figure 3.29. Two periods with hydraulic fracturing at the well pad are marked on Figure 3.29, using green and orange lines to show dates of 'start' and 'suspension' respectively. The levels of CH_4 during these periods are not notably elevated; however, it should be noted that, in general the wind rarely blew from the well pad to the monitoring site (as discussed in section 3.1).

Figure 3.29: CH_4 1-hour mean concentrations at the monitoring site

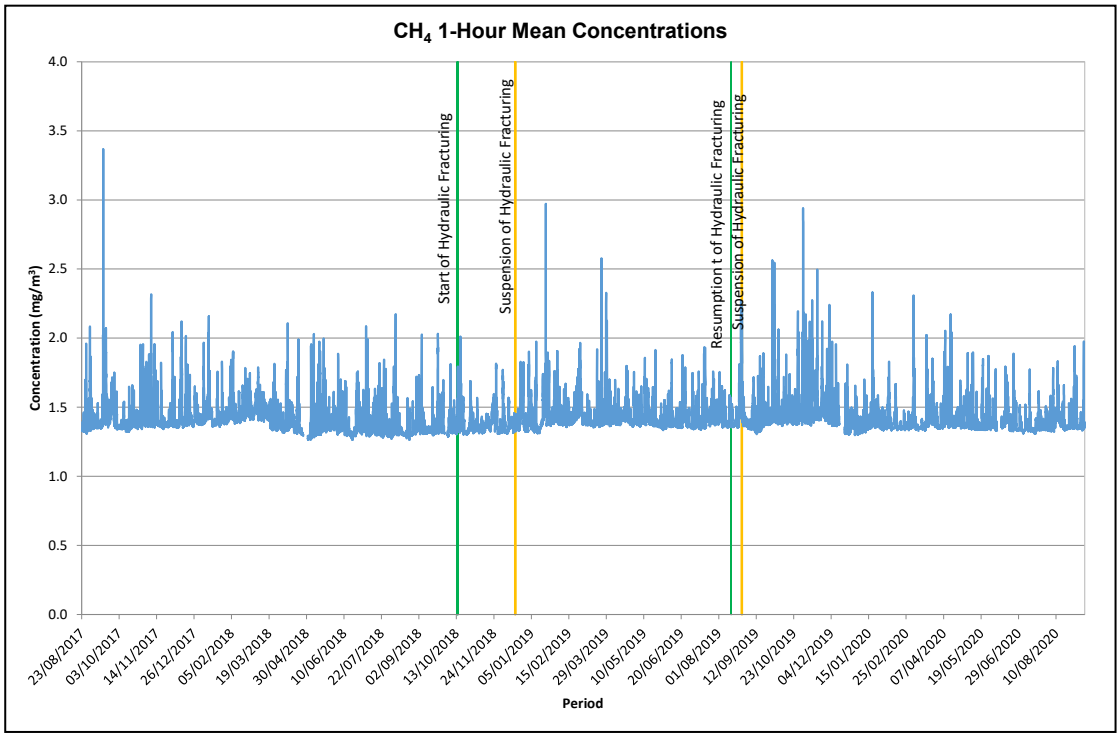

The average concentration over the period was $1.41 mg/m^3$, which is slightly higher than the average Northern Hemisphere background concentration of around $1.21 mg/m^3$.

3.4.1 Directional analysis

3.4.1.1 Time series plots for 45° sectors

Figure 3.30 presents 5-minute mean CH_4 concentrations for all wind directions, grouped into 45° sectors, for each of the years.

The plots show that the highest 5-minute mean CH_4 concentrations were seen in 2019, from the south and south-west of the monitoring site. The levels of CH_4 in the NE sector

(direction of the well pad) during the hydraulic fracturing periods were not particularly elevated; however, in general the wind rarely blew from the well pad to the monitoring site.

Figure 3.30: CH_4 5-minute mean time series for each 45° wind sector (mg/m^3)

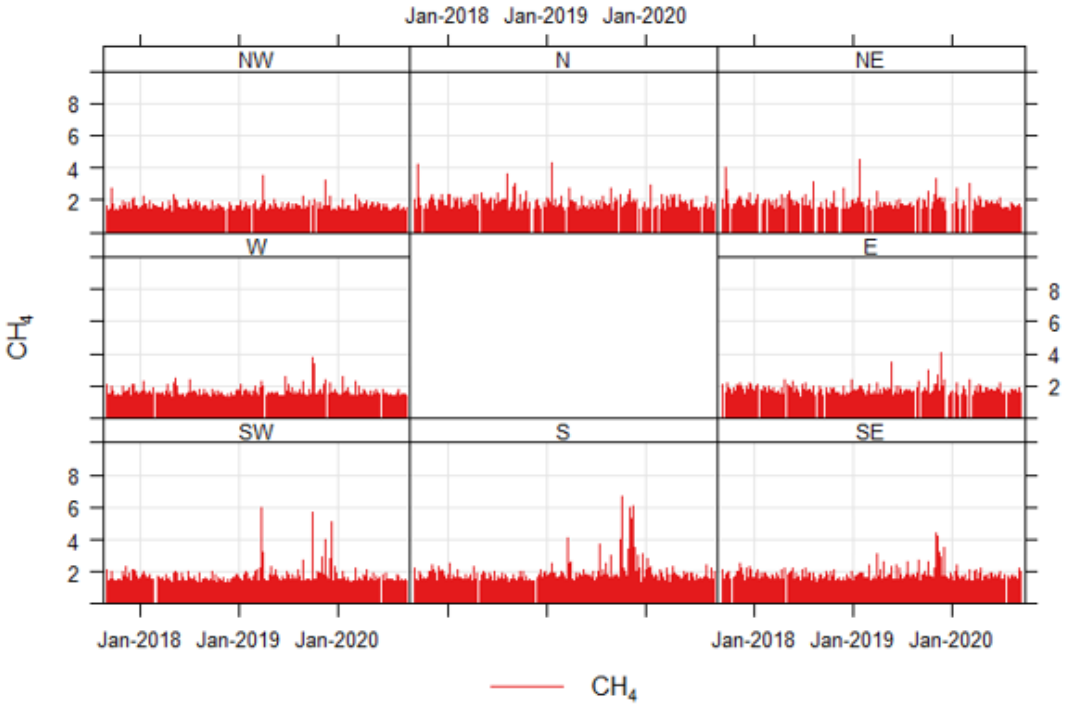

3.4.1.2 Radial plots

Radial plots of mean CH_4 concentrations against wind direction are shown for each year in Figure 3.31.

The highest average CH_4 concentrations over the monitoring period are seen in 2017 for the 10° wind sectors centred on 40° to 90°, with average concentrations >1.6mg/m^3. These wind sectors encompass the direction of the well pad (although there was no hydraulic fracturing in 2017) and the A583 road.

The highest concentrations in 2018 are seen in the 10° sectors centred on 0° to 60°, which cover part of the well pad, and 130° to 150°, with average concentrations greater than 1.45mg/m^3.

The highest concentrations in 2019 are seen in the 10° sectors centred on 30° to 60° (which cover part of the well pad), 130° to 140° and 180° to 190°, with average concentrations greater than 1.50mg/m^3.

The highest concentrations in 2020 are seen in the 10° sectors centred on 0° to 50° (which cover part of the well pad) and 120° to 150°, with average concentrations greater than 1.45mg/m^3.

The highest mean CH_4 concentrations in each year come from the 10° sectors centred on 20° or 40°, and so do not align with winds from the 3 10° sectors containing the well pad, that is, those centred on 50°, 60° and 70°.

Figure 3.31: CH_4 pollution rose

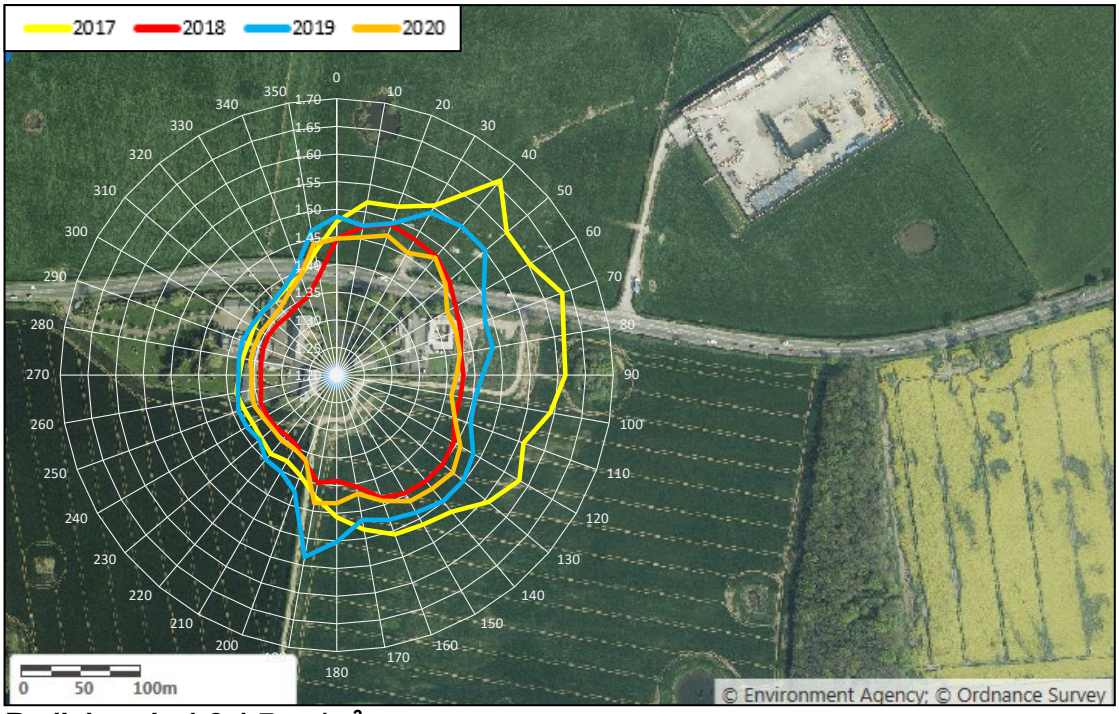

Radial scale 1.2-1.7mg/m^3

The average concentration for each 10° wind sector can also be tabulated and colour coded from the lowest (dark green) to the highest (red) average concentration (Table 3.8). This highlights the wind directions with the highest averages for CH_4. The bearing of the well pad is highlighted in blue. The table demonstrates that the main source(s) of CH_4 in the area is in the wind direction range 350° to 190°. This range includes 3 10° sectors that are partly or wholly covered by the well pad (that is, the sectors centred on 50°, 60° and 70°), but there is no distinctly elevated concentration of methane from those 3 sectors.

Table 3.8: Comparison of mean methane concentrations for each 10° wind sector

Wind direction	2017	2018	2019	2020
0				
10				
20				
30				
40				
50				
60				
70				
80				
90				
100				
110				
120				
130				
140				
150				
160				
170				
180				
190				
200				
210				
220				
230				
240				
250				
260				
270				
280				
290				
300				
310				
320				
330				
340				
350				

3.4.1.3 Percentile rose plots

An array of plots showing the contribution to CH_4 concentrations at the monitoring site for different percentiles are shown in Figure 3.32.

The plots for 2017 show that the contribution from source(s) between 10° and 30° is more evident in the higher percentiles. This suggests that there are intermittent source(s) in these wind directions that lead to elevated CH_4 concentrations at the monitoring site. The plots also show that the contribution from source(s) between 50° and 130° is more evident in the lower percentiles, suggesting that the source(s) in this wind direction range are relatively continuous, but do not cause appreciably high concentrations of CH_4 at the monitoring site. The contribution from the source(s) at 40° affects all the percentiles, which indicates that the source(s) is relatively continuous and commonly affects CH_4 concentrations at the monitoring site.

Figure 3.32: CH_4 percentile rose (mg/m^3)

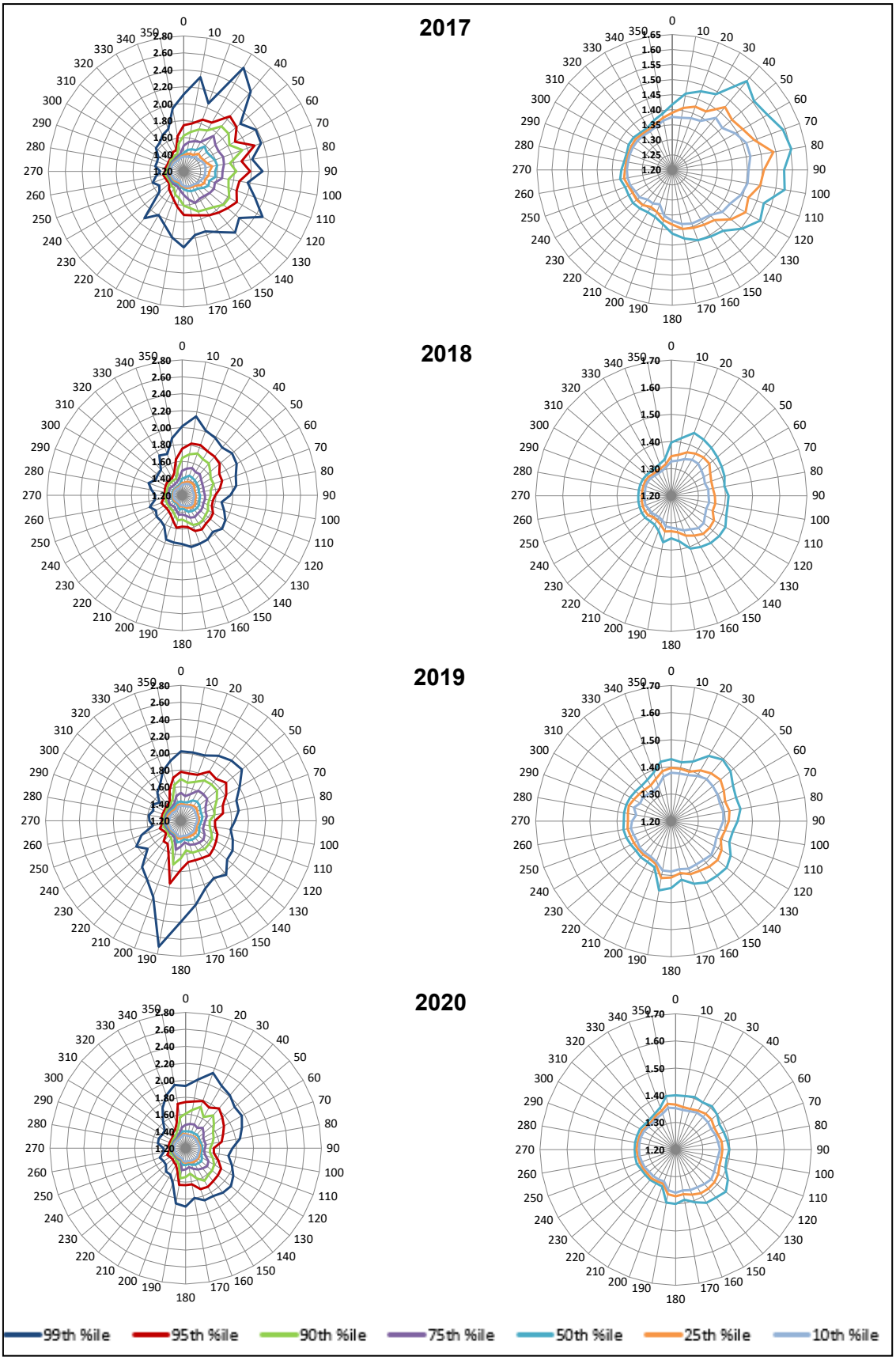

The plots for 2018 show that the contribution from the source(s) at 40° affects all the percentiles, which indicates that the source(s) is relatively continuous and commonly affects CH_4 concentrations at the monitoring site.

The plots for 2019 show that the contribution from the source(s) at 190° affects all the percentiles, which indicates that the source(s) is relatively continuous and commonly affects CH_4 concentrations at the monitoring site.

The plots for 2020 show that the contributions from the source(s) between 180° and 190° and between 120° and 160° affect all the percentiles, which indicates that the source(s) are relatively continuous and commonly affect CH_4 concentrations at the monitoring site. The plots also show that the contribution from the source(s) at 350° to 60° is more evident in the higher percentiles. This suggests that there are intermittent source(s) in these wind directions that lead to elevated CH_4 concentrations at the monitoring site.

3.4.1.4 Conditional probability function plots

Figure 3.33 shows conditional probability function (CPF) plots for CH_4 concentrations above the 90th percentile. The plot calculates the probability that CH_4 concentrations would be greater than their 90th percentile value (1.5µg/m^{-3}) for a particular wind speed and wind direction. The scale of a CPF plot ranges from 0 to 1, from lowest to highest probability. Figure 3.33 shows that high concentrations of CH_4 (greater than the 90th percentile of all observations) are most likely to occur at very low wind speeds. This is the pattern that would be expected for a pollutant which is widespread throughout the environment, and does not have a dominant or significant local source.

Figure 3.33: CH_4 conditional probability function plots

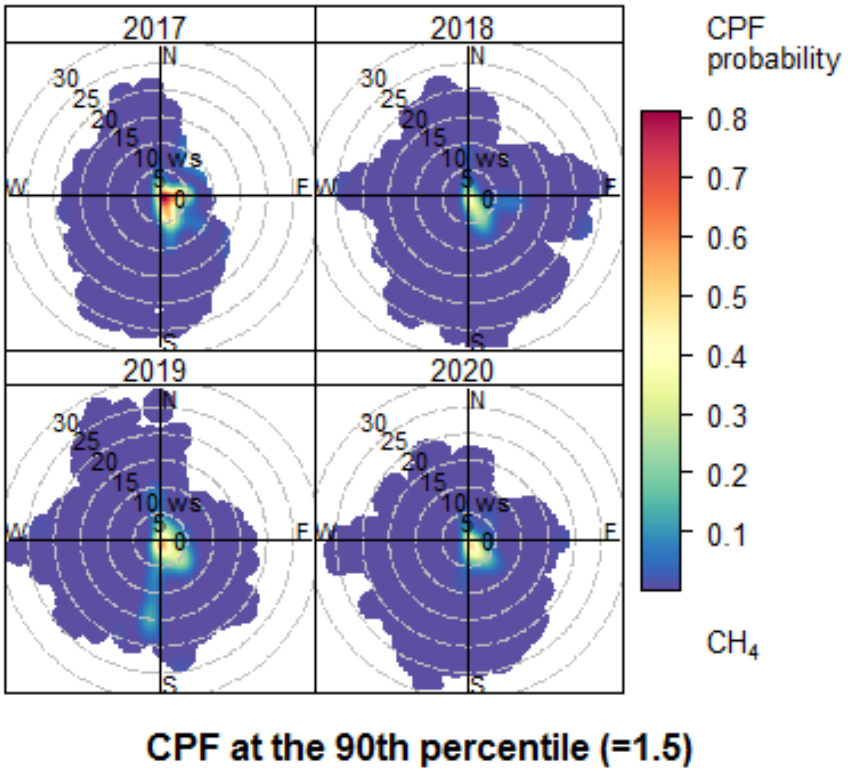

3.4.2 Wind speed variation

Figure 3.34 shows Openair polar (wind speed dependency) plots for CH_4. The plots show that the highest concentrations of CH_4 are seen in all plots at very low wind speed. Again, this pattern would be expected for a widespread pollutant with no dominant or significant local source. The fact that higher concentrations occur at low wind speeds suggests that CH_4 is coming from a near-ground level source, rather than from an elevated source, for example, from a ground-level fugitive source rather than from a chimney stack.

Figure 3.34: CH_4 Openair wind speed dependency plot (mg/m^3)

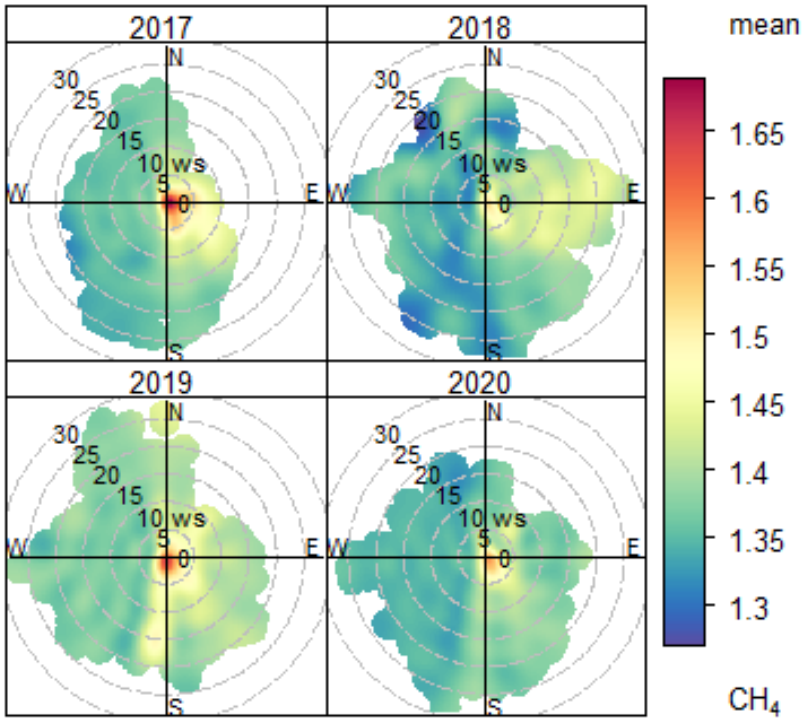

3.4.3 Diurnal analysis

Diurnal Openair plots for CH_4 are shown for the monitoring site in Figure 3.35.

The plots show that the highest mean CH_4 concentrations were seen in 2017 from the wind sector 20° to 90° during the early hours of the morning and late at night. This is likely to be the result of poor dispersion resulting from stable conditions accompanied by boundary layer lowering or nocturnal inversion layers trapping fugitive emissions close to the ground.

Figure 3.35: CH_4 Openair diurnal annulus plots (mg/m^3)

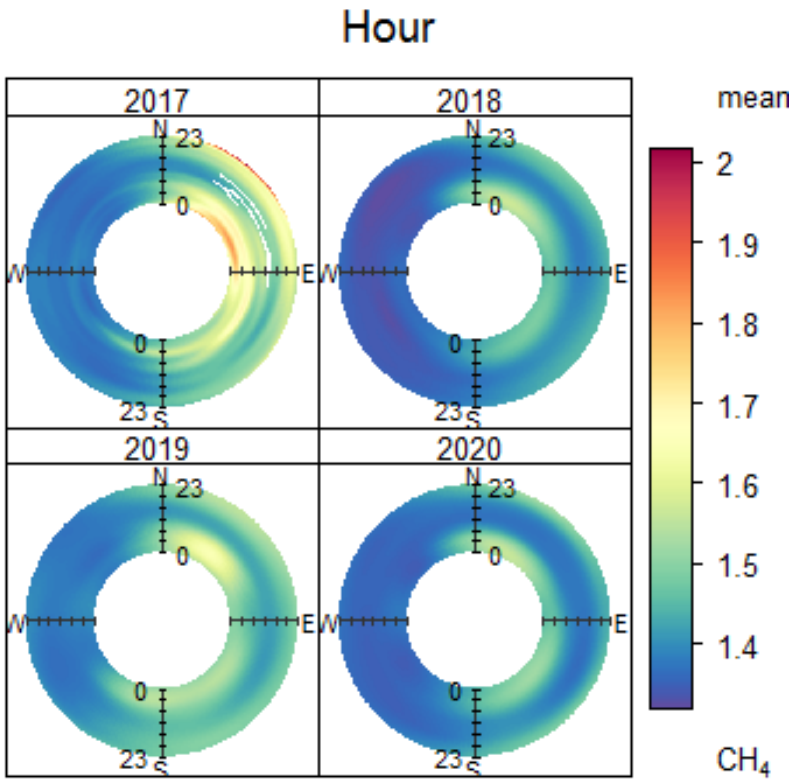

3.4.4 Conclusions

Time series plots

Based on visual inspection of time series plots, there is no evidence of particularly elevated levels of CH_4 occurring during the hydraulic fracturing periods, although it should be noted that the wind direction was rarely blowing from the shale well pad to the monitoring site.

The mean CH_4 concentration over the monitoring period was $1.41 mg/m^3$.

Directional analysis

Based on visual inspection of time series plots for 45° sectors, there is no evidence of notably elevated concentrations of CH_4 coming from the (NE) 45° sector that contained the well pad during periods of hydraulic fracturing.

Pollution rose analysis indicates that the highest average CH_4 concentrations were measured at the monitoring site when the wind was coming from between 350° and 190°.

Percentile analysis suggested that there are both relatively continuous and intermittent sources affecting the monitoring site.

Conditional probability function (CPF) plots suggested that high concentrations of CH_4 (greater than the 90^{th} percentile of all observations) were most likely to occur at very low

wind speeds. This is the pattern to be expected for a pollutant which is widespread throughout the environment and does not have a dominant or significant local source.

Wind speed variation

Wind speed analysis suggests that the monitoring site is affected by CH_4 emissions from a low-level source, such as fugitive emissions from near ground level.

Diurnal analysis

Diurnal analysis suggests that the monitoring site is being influenced by CH_4 levels arising from fugitive emissions that are trapped close to the ground during times of poor dispersion, such as boundary layer lowering and nocturnal temperature inversions.

Nitrogen Lift impact at BGS monitor

BGS operated an air-quality monitor at another position, ~0.4km East of the well pad, as explained in Section 1. This monitor recorded elevated concentrations of methane, of up to ~5 ppm (~3 mg/m^3) as a 30-minute average during 11-16 January 2019, on which days the wind was generally westerly i.e. from the well pad to that monitor. Shaw et al (2020) have attributed the elevated concentrations to a “nitrogen lift” activity at the well pad. Such elevated concentrations were not observed at the Environment Agency monitor on those days, because the wind did not blow from the well pad to that monitor.

Summary

There was no evidence of notably elevated concentrations of CH_4 when the wind came from the direction of the well pad, although winds rarely blew from the well pad to the monitor.

3.5 BTEX

Between 5 September 2017 and 1 April 2020 (940 days) airborne volatile organic compound (VOC) concentrations were measured at a height of 2m above ground. The VOCs monitored were benzene, toluene, ethylbenzene, and m&p-xylene (BTEX). The BTEX data is reported from 9 September 2017 due to technical problems with the instrument prior to this date. The decision was made during the Covid-19 lockdown to stop monitoring BTEX due to the inability to safely acquire and install the necessary gases to run the gas chromatograph. Details of the instrumentation and methodology are given in Appendix G. The successful data collection over the monitoring period was 88%.

The hourly mean BTEX concentrations are shown in Figure 3.36. Two periods with hydraulic fracturing at the well pad are marked on Figure 3.36, using green and orange lines to show dates of 'start' and 'suspension' respectively. The levels of BTEX during these periods are not notably elevated; however, it should be noted that, in general the wind rarely blew from the well pad to the monitoring site (as discussed in section 3.1).

Figure 3.36: BTEX 1-hour mean concentrations

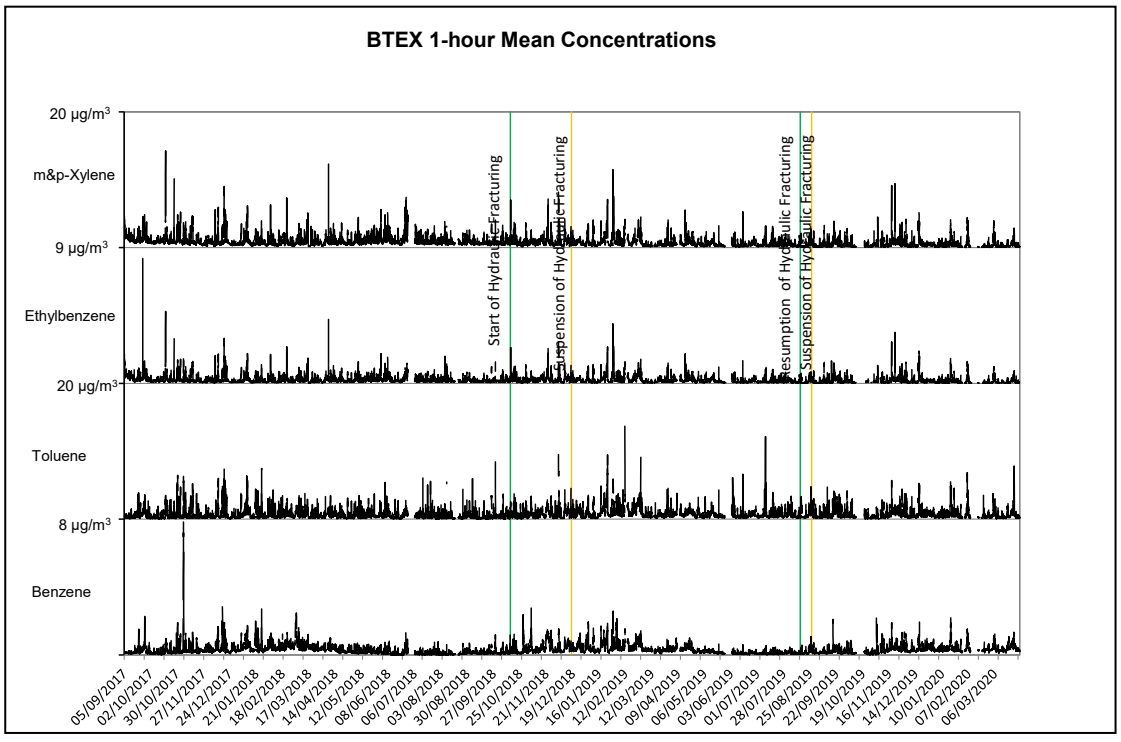

3.5.1 Comparison with standards

3.5.1.1 Comparison with Air Quality Strategy (AQS) objectives

Benzene was the only pollutant from the measured BTEX suite recorded at the monitoring site that has an AQS objective. The AQS objective for benzene is expressed as an annual mean over a calendar year and is currently set at 5ug/m^3 (1.5ppb). Table 3.9 compares the annual average concentrations of the BTEX for each year of the monitoring study. The figures for 2017 and 2020 are derived from less than a full year of monitoring data (for

example, 3 months in 2017 and 4 months in 2020). It is assumed that the concentrations during these months were representative of the whole calendar year.

The highest mean benzene concentration over the monitoring period was seen in 2020, the average being 0.38µg/m^3, which is 8% of the AQS annual mean objective. Therefore, levels of benzene did not exceed the annual benzene AQS objective at the monitoring site during the study.

Table 3.9: Benzene annual average concentrations for each year during study

	Benzene average (µg/m^3)
2017	0.31*
2018	0.31
2019	0.28
2020	0.38*

* Extrapolated from effective monitoring period

3.5.1.2 Comparison with other relevant guidelines

Toluene has 2 World Health Organisation (WHO) guidelines. The guideline for human health is 0.26mg/m^3 as a weekly average. The maximum weekly average occurred in 2019 and was 1.8µg/m^3 (0.0018mg/m^3), well within the human health guideline. The other guideline is for odour annoyance and is set at 1mg/m^3 over a 30-minute mean. The highest 30-minute mean occurred in 2019 and was 16.0µg/m^3 (0.016mg/m^3). Therefore, toluene should not have caused odour annoyance in the vicinity of the monitoring site, during the monitoring period. Table 3.10 compares the weekly average and 30-minute mean concentrations of the BTEX for each year of the monitoring study.

Table 3.10: Toluene weekly and 30-minute mean concentrations for each year during study

	Toluene maximum weekly average (µg/m^3)	Toluene highest 30-minute mean (µg/m^3)
2017	1.43*	7.6*
2018	1.51	11.0
2019	1.81	16.0
2020	1.06*	10.3*

* Extrapolated from effective monitoring period

3.5.2 Directional analysis

3.5.2.1 Time series plots for 45° sectors

Figure 3.37 shows the 30-minute mean concentrations of BTEX for all wind directions, grouped into 45° sectors.

The plots show that the highest 30-minute mean benzene concentrations came from the east, south-east and south of the monitoring site.

The plots show that the highest 30-minute mean toluene concentrations came from the west and south-east of the monitoring site.

The plots show that the highest 30-minute mean ethylbenzene concentrations came from the east and south-east of the monitoring site.

The plots show that the highest 30-minute mean m&p-xylene concentrations came from the north-east, east and south-east of the monitoring site.

Figure 3.37: BTEX 30-minute mean time series for each 45° wind sector

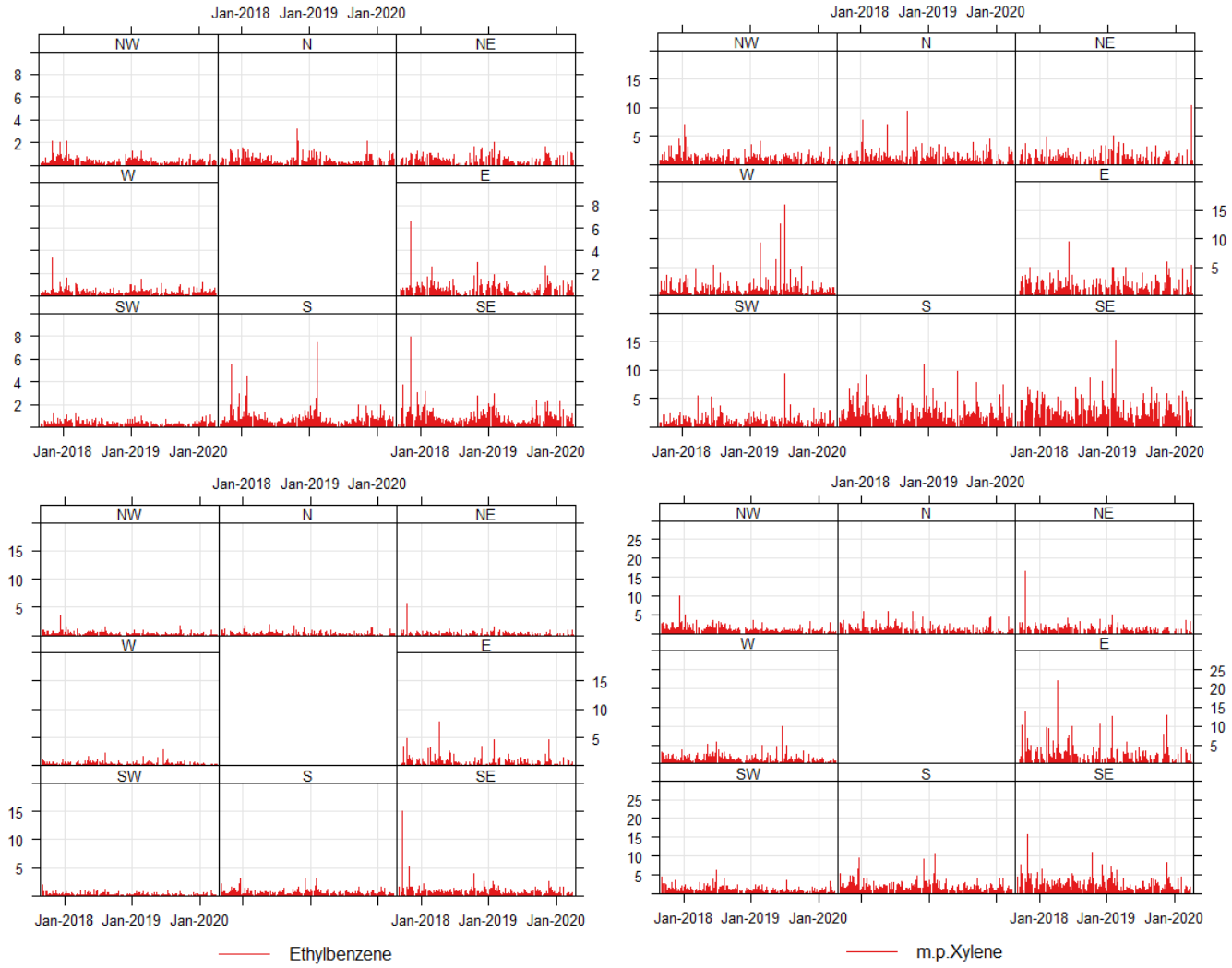

The levels of BTEX in the NE sector (direction of the well pad, which includes the A583 road) during the hydraulic fracturing periods were not particularly elevated; however, in general the wind rarely blew from the well pad to the monitoring site.

3.5.2.2 Radial plots

Radial plots of mean BTEX concentrations (µg/m^3) against wind direction are shown in Figure 3.38 to Figure 3.41.

The highest average benzene concentrations are seen between 120° and 160° during 2017 to 2019. The pollution rose for 2020 looks slightly different when compared to the other years, as it shows an increase in benzene concentration in directions to the west where levels have been consistently lower during previous years.

The highest average toluene concentrations are seen between 120° and 170° during 2018 to 2020. The pollution rose for 2017 has a broader bias, with the highest concentrations of toluene seen in the wind sector 70° to 170°.

The highest average ethylbenzene concentrations are seen between 70° and 80° during 2017. However, generally ethylbenzene was highest in the wind sector 100° to 160°.

The highest average m&p-xylene concentrations are seen between 70° and 80º during 2017. However, generally m&p-xylene was highest in the wind sector 100° to 160°.

In overall terms, the pollution roses indicate somewhat higher concentrations when the wind is from the east or south-east. There is no clear indication of a distinct contribution from the direction of the hydraulic fracturing site.

Figure 3.38: Benzene pollution roses

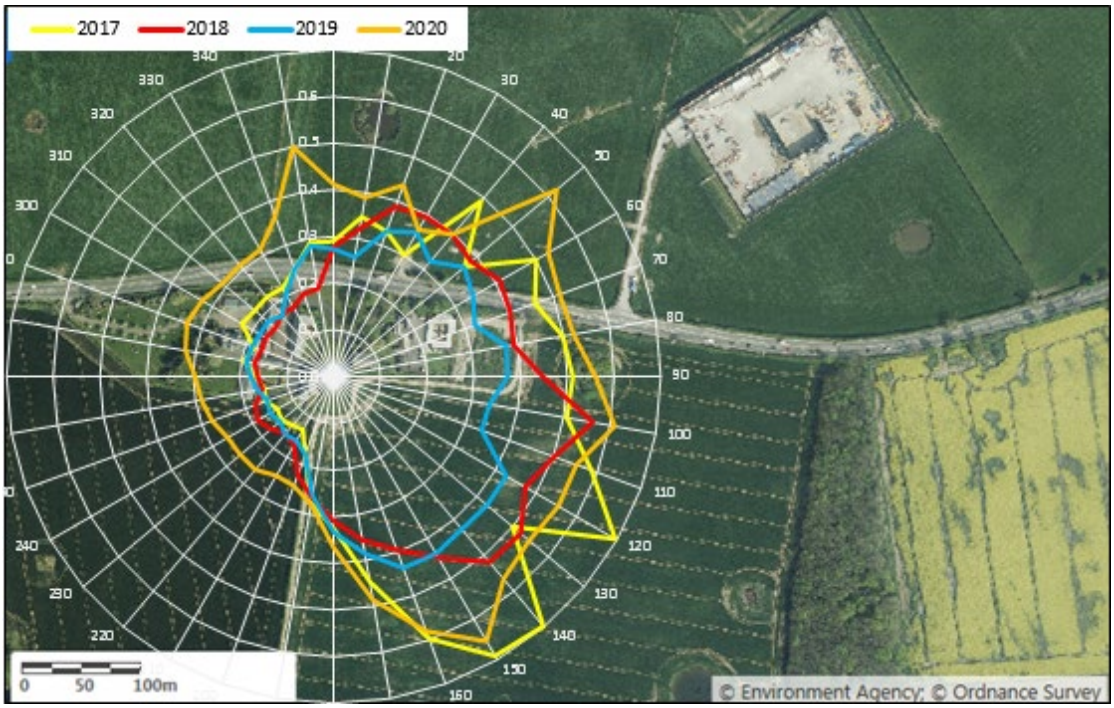

Radial scale 0-0.7µg/m^3

Figure 3.39: Toluene pollution roses

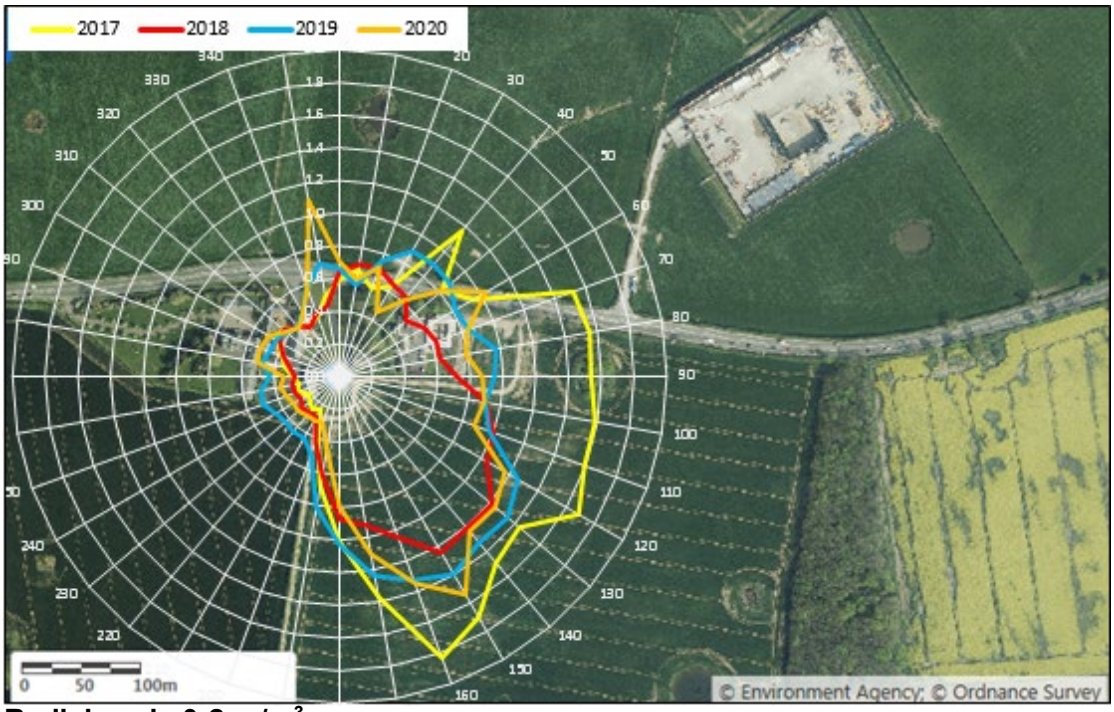

Radial scale 0-2µg/m^3

Figure 3.40: Ethylbenzene pollution roses

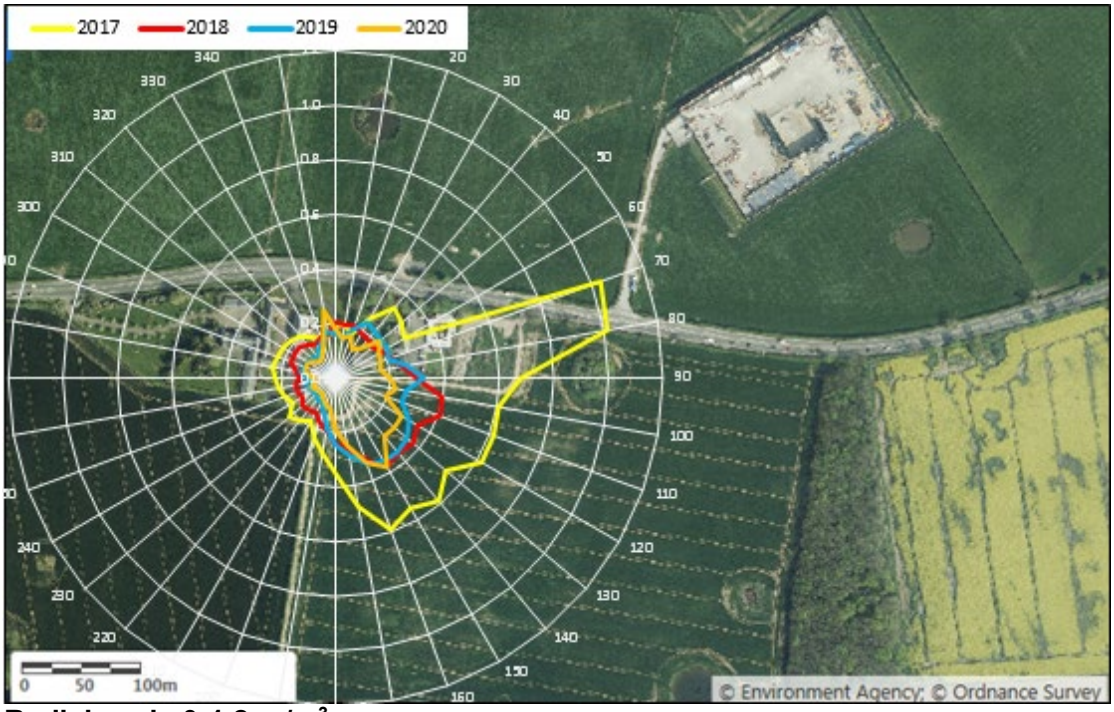

Radial scale 0-1.2µg/m^3

Figure 3.41: m&p-xylene pollution roses

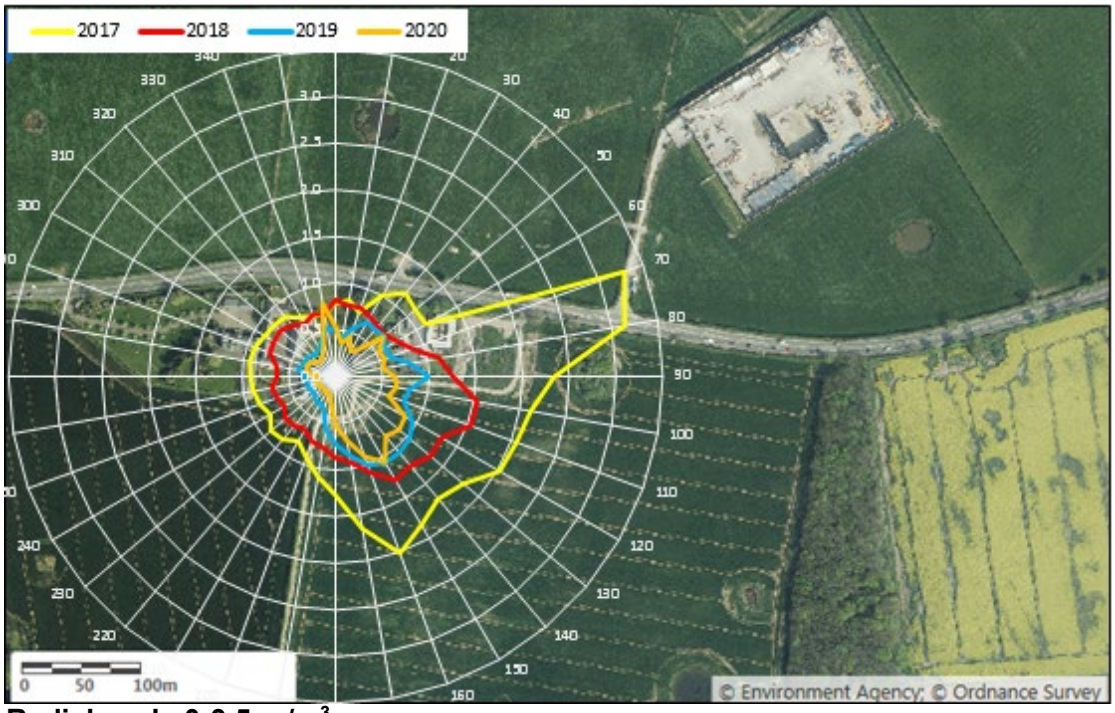

Radial scale 0-3.5µg/m^3

The average concentration for each 10° wind sector can also be tabulated and colour coded from the lowest (dark green) to the highest (red) average concentration (Table 3.11). This highlights the wind directions with the highest averages for each BTEX, but also emphasises correlations between the individual BTEX showing the wind directions of common sources. The table demonstrates that the main source(s) of BTEX in the area is in the wind direction range 350° to 190° and this does not vary over the monitoring period. The bearing of the well pad is highlighted in blue. The sectors that are partly or wholly covered by the well pad (that is, those centred on 50°, 60°, 70°) do not have notably elevated concentrations of BTEX, suggesting that the well pad was not a prominent source of BTEX.

3.5.2.3 Percentile rose plots

An array of plots showing the contribution to BTEX concentrations at the monitoring site for different percentiles is shown in Figure 3.42 to Figure 3.45.

Table 3.11: Comparison of the mean concentrations for each 10° wind sector

	2017				2018				2019				2020			
Wind direction	**Benzene**	**Toluene**	**M&p-xylenes**	**Ethylbenzene**	**Benzene**	**Toluene**	**M&p-xylenes**	**Ethylbenzene**	**Benzene**	**Toluene**	**Ethylbenzene**	**M&p-xylenes**	**Benzene**	**Toluene**	**Ethylbenzene**	**M&p-xylenes**
0																
10																
20																
30																
40																
50																
60																
70																
80																
90																
100																
110																
120																
130																
140																
150																
160																
170																
180																
190																
200																
210																
220																
230																
240																
250																
260																
270																
280																
290																
300																
310																
320																
330																
340																
350																

Figure 3.42: Benzene percentile rose

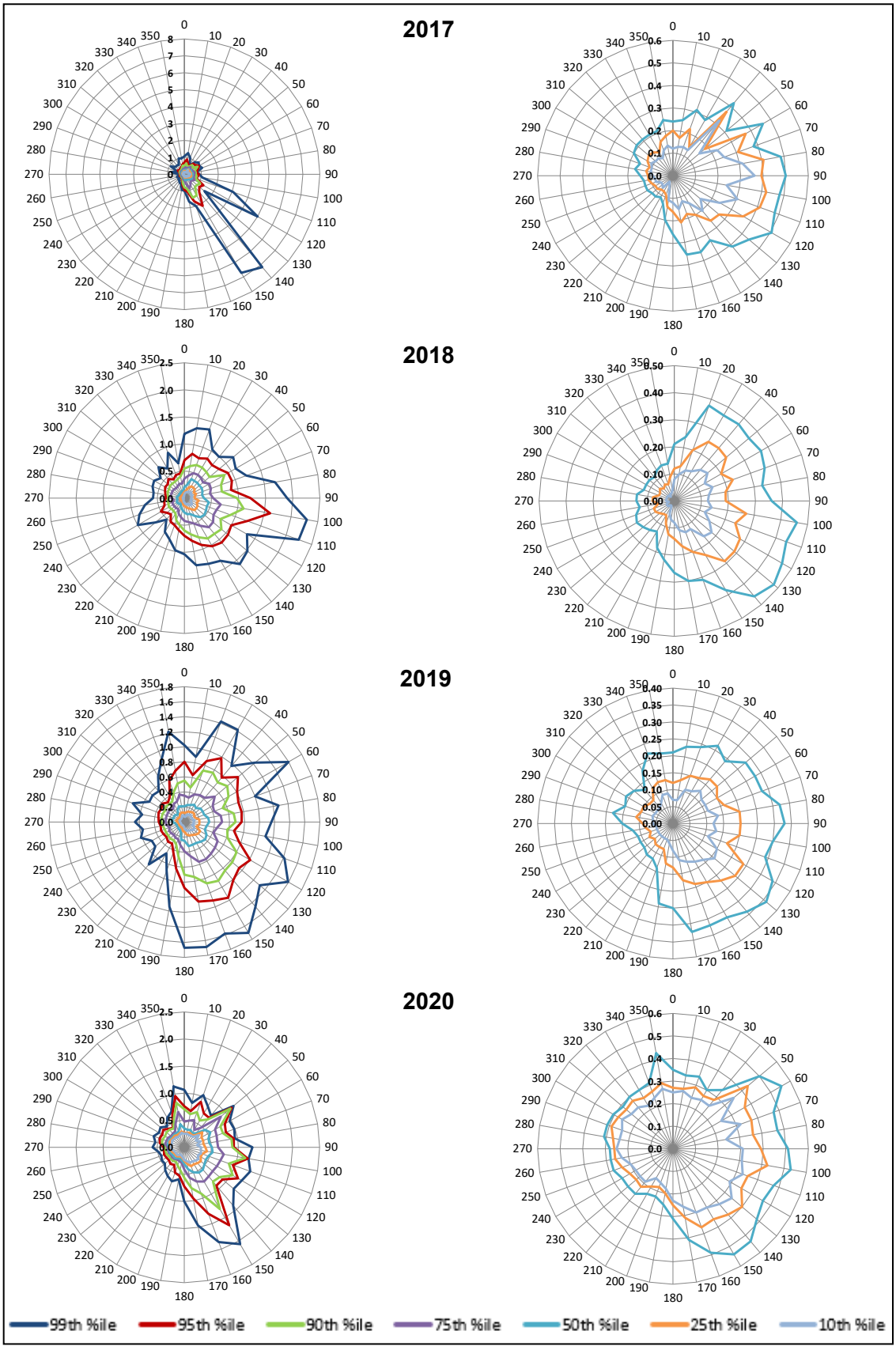

The plots for 2017 show that the contribution from the source(s) between 110° and 160° affects all the percentiles, which indicates that the source(s) are relatively continuous and commonly affect benzene concentrations at the monitoring site. The peak at 140° in the 99^{th} percentile for benzene coincides with similarly distinct peaks of PM_{10} and $PM_{2.5}$. This is not seen in the other years. The contributions from the source(s) between 40° and 100° and at 170° are more evident in the lower percentiles, suggesting that the source(s) in these wind directions are relatively continuous, but do not cause appreciably high concentrations of benzene at the monitoring site.

The plots for 2018 show that the contribution from the source(s) between 100 and 110° affects all the percentiles, which indicates that the source(s) is relatively continuous and commonly affects benzene concentrations at the monitoring site. The contributions from the source(s) between 20° and 90° and 120° and 170° are more evident in the lower percentiles, suggesting that the source(s) in these wind directions are relatively continuous, but do not cause appreciably high concentrations of benzene at the monitoring site.

The plots for 2019 show that the contribution from the source(s) between 340 and 190° affects all the percentiles, which indicates that the source(s) is relatively continuous and commonly affects benzene concentrations at the monitoring site.

The plots for 2020 show that the contribution from the source(s) between 50° and 170° affects all the percentiles, which indicates that the source(s) are relatively continuous and commonly affect benzene concentrations at the monitoring site. The plots also show that the contribution from the source(s) at 350° is more evident in the higher percentiles. This suggests that there is an intermittent source(s) in this wind direction that leads to elevated benzene concentrations at the monitoring site.

Figure 3.43: Toluene percentile rose

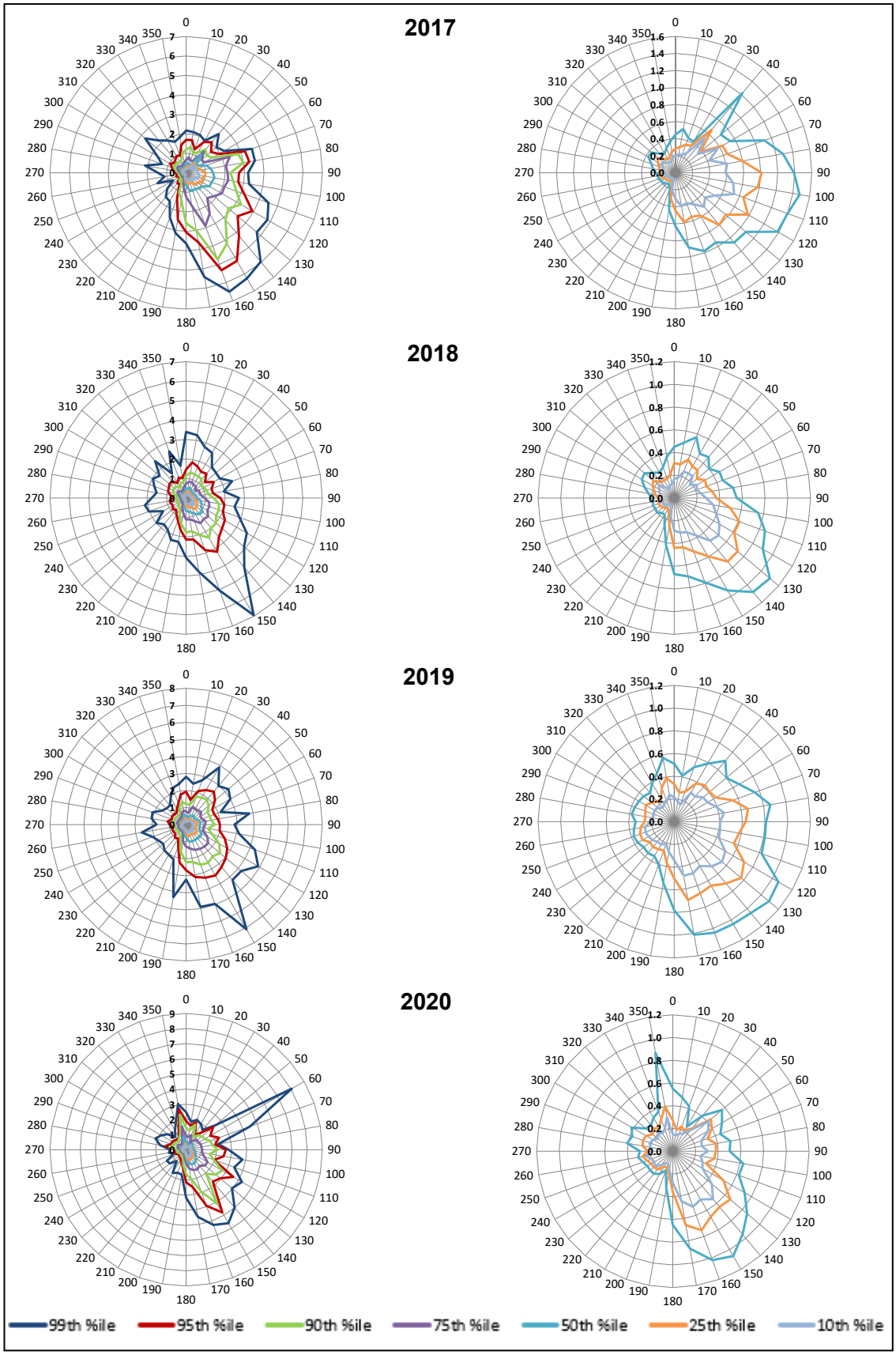

The plots for 2017 show that the contribution from the source(s) between 70° and 170° affects all the percentiles, which indicates that the source(s) are relatively continuous and commonly affect toluene concentrations at the monitoring site. The contribution from the source(s) between 40° and 60° is more evident in the lower percentiles, suggesting that the source(s) in this wind direction range is relatively continuous, but does not cause appreciably high concentrations of toluene at the monitoring site.

The plots for 2018 show that the contribution from the source(s) between 100° and 180° affects all the percentiles, which indicates that the source(s) are relatively continuous and commonly affect toluene concentrations at the monitoring site.

The plots for 2019 show that the contribution from the source(s) between 120° and 170° affects all the percentiles, which indicates that the source(s) are relatively continuous and commonly affect toluene concentrations at the monitoring site. The contributions from the source(s) between 30° and 110° are more evident in the lower percentiles, suggesting that the source(s) in this wind direction range are relatively continuous, but do not cause appreciably high concentrations of toluene at the monitoring site.

The plots for 2020 show that the contribution from the source(s) between 130° and 170° affects all the percentiles, which indicates that the source(s) are relatively continuous and commonly affect toluene concentrations at the monitoring site. The plots also show that the contribution from the source(s) at 60° to 70° is more evident in the higher percentiles; this direction corresponds to winds from the well pad, although there were no periods of hydraulic fracturing in 2020. This suggests that there is an intermittent source in this wind direction that leads to elevated toluene concentrations at the monitoring site. The contribution from the source at 350° is more evident in the lower percentiles, suggesting that the source in this wind direction is relatively continuous, but does not cause appreciably high concentrations of toluene at the monitoring site.

Figure 3.44: Ethylbenzene percentile rose

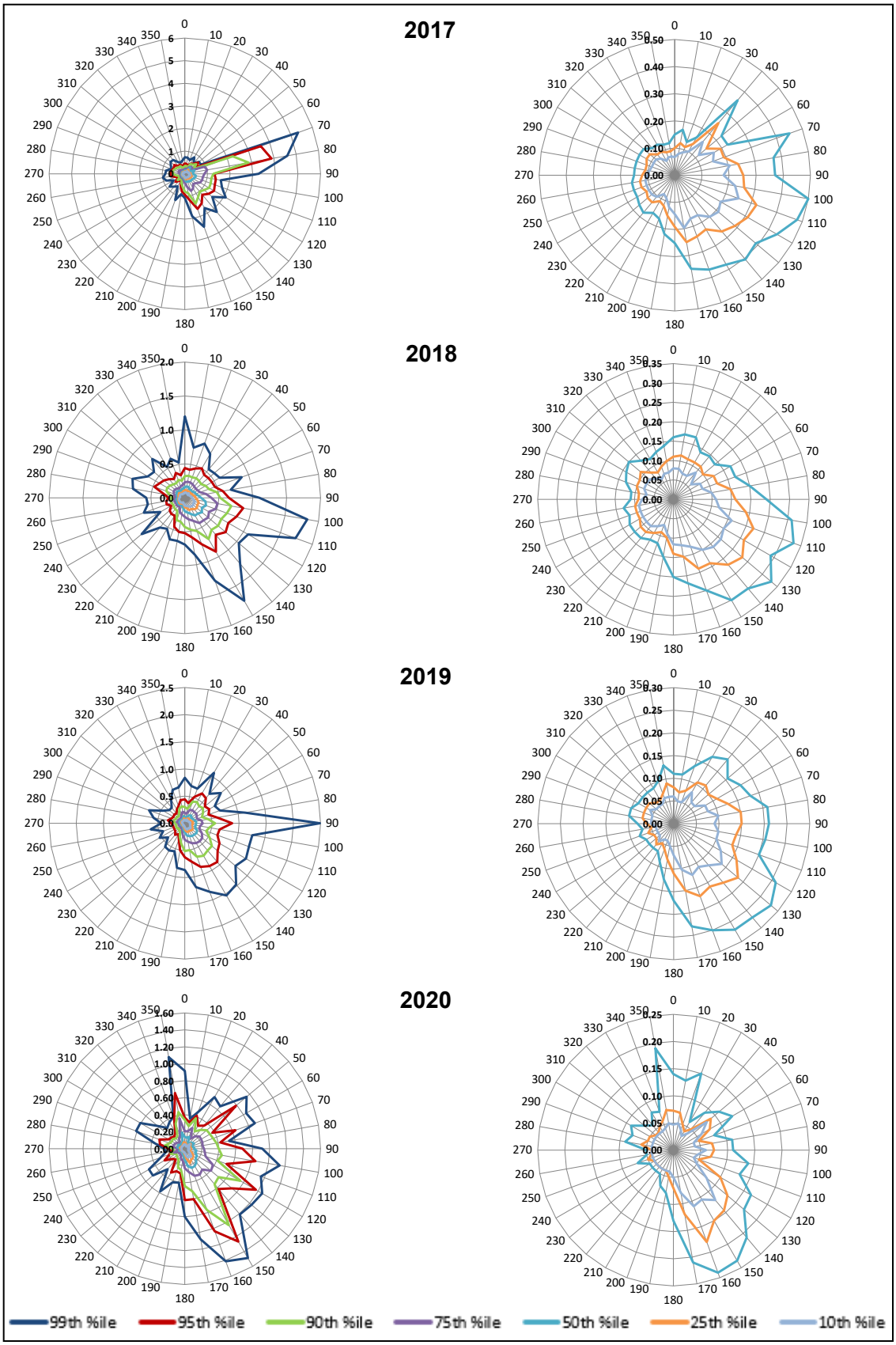

The plots for 2017 show that the contribution from the source(s) between 70° and 170° affects all the percentiles, which indicates that the source(s) are relatively continuous and commonly affect ethylbenzene concentrations at the monitoring site. The contribution from the source(s) between 40° and 60° is more evident in the lower percentiles, suggesting that the source(s) in this wind direction range is relatively continuous, but does not cause appreciably high concentrations of ethylbenzene at the monitoring site.

The plots for 2018 show that the contribution from the source(s) between 100° and 160° affects all the percentiles, which indicates that the source(s) are relatively continuous and commonly affect ethylbenzene concentrations at the monitoring site. The contribution from the source(s) between 170° and 180° is more evident in the lower percentiles, suggesting that the source(s) in this wind direction range is relatively continuous, but does not cause appreciably high concentrations of ethylbenzene at the monitoring site.

The plots for 2019 show that the contribution from the source(s) between 90° and 170° affects all the percentiles, which indicates that the source(s) are relatively continuous and commonly affect ethylbenzene concentrations at the monitoring site. The contribution from the source(s) between 30° and 80° is more evident in the lower percentiles, suggesting that the source(s) in this wind direction range are relatively continuous, but do not cause appreciably high concentrations of ethylbenzene at the monitoring site.

The plots for 2020 show that the contribution from the source(s) between 130° and 170° affects all the percentiles, which indicates that the source(s) are relatively continuous and commonly affect ethylbenzene concentrations at the monitoring site. The plots also show that the contributions from the source(s) between 50° and 70°, 90° and 120° and 350° and 360° are more evident in the higher percentiles. This suggests that there are intermittent source(s) in these wind direction ranges that lead to elevated ethylbenzene concentrations at the monitoring site.

Figure 3.45: M&p-xylene percentile rose

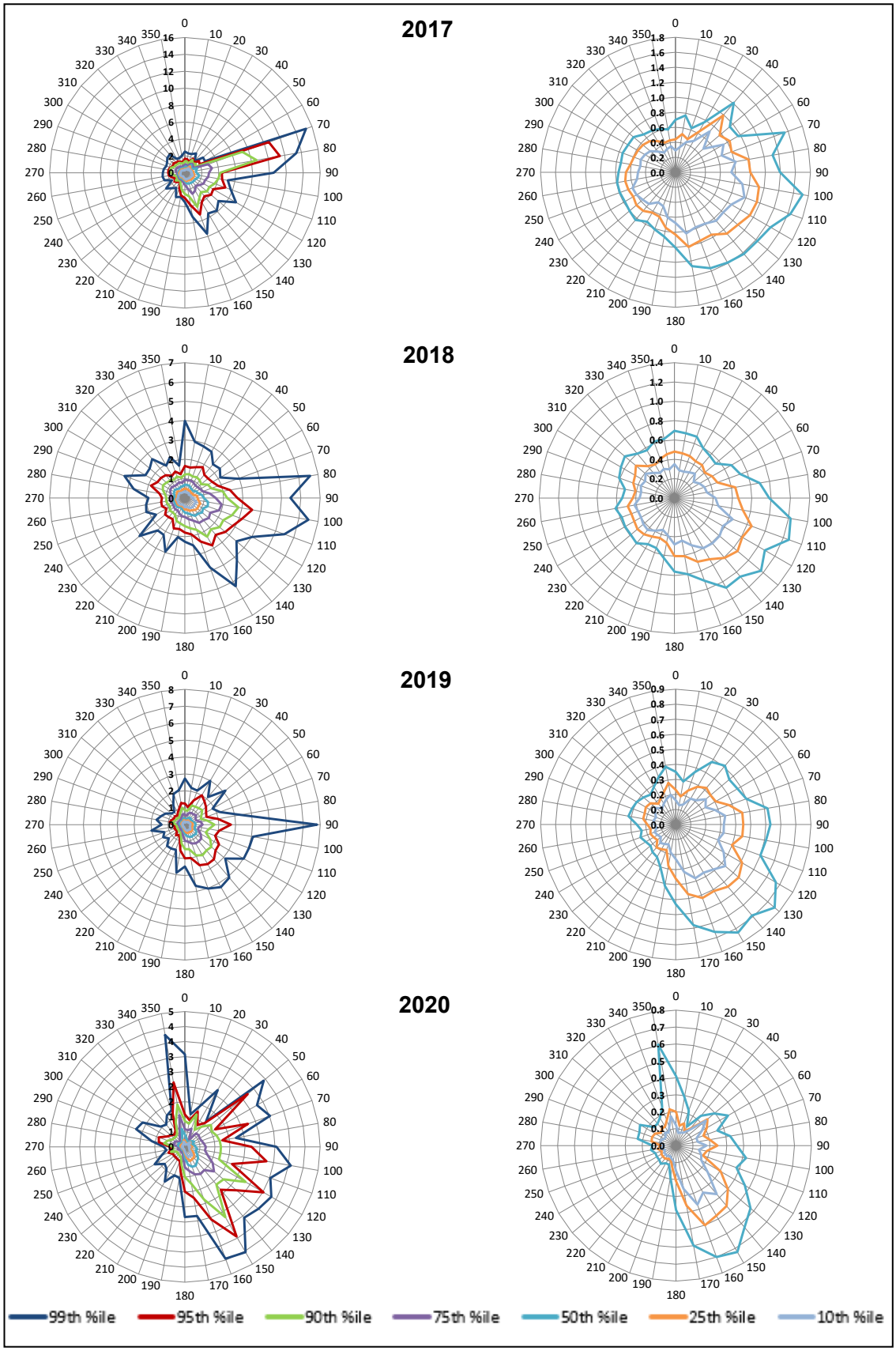

The plots for 2017 show that the contribution from the source(s) between 70° and 170° affects all the percentiles, which indicates that the source(s) are relatively continuous and commonly affect m&p-xylene concentrations at the monitoring site. The contribution from the source(s) between 40° and 60° is more evident in the lower percentiles, suggesting that the source in this wind direction range is relatively continuous, but does not cause appreciably high concentrations of m&p-xylene at the monitoring site.

The plots for 2018 show that the contribution from the source(s) between 90° and 180° affects all the percentiles, which indicates that the source(s) are relatively continuous and commonly affect m&p-xylene concentrations at the monitoring site. The plots also show that the contributions from the source(s) at 80° and 360° are more evident in the higher percentiles. This suggests that there are intermittent source(s) in these wind directions that lead to elevated m&p-xylene concentrations at the monitoring site.

The plots for 2019 show that the contribution from the source(s) between 90° and 170° affects all the percentiles, which indicates that the source(s) are relatively continuous and commonly affect m&p-xylene concentrations at the monitoring site. The contributions from the source(s) between 30° and 80° are more evident in the lower percentiles, suggesting that the source(s) in this wind direction range are relatively continuous, but do not cause appreciably high concentrations of m&p-xylene at the monitoring site.

The plots for 2020 show that the contribution from the source(s) between 130° and 170° affects all the percentiles, which indicates that the source(s) are relatively continuous and commonly affect m&p-xylene concentrations at the monitoring site. The plots also show that the contributions from the source(s) between 50° and 70°, 90° and 120° and 350° and 360° are more evident in the higher percentiles. This suggests that there are intermittent sources in these wind direction ranges that lead to elevated m&p-xylene concentrations at the monitoring site.

In overall terms, the directional analysis indicates somewhat higher concentrations of BTEX when the wind is from the east or south-east. There is no clear indication of a distinct contribution of BTEX from the direction of the hydraulic fracturing site.

3.5.2.4 Conditional probability function plots

Figure 3.46 shows conditional probability function (CPF) plots for BTEX concentrations above the 90th percentile. The plot calculates the probability that BTEX concentrations would be greater than their 90th percentile value (0.6, 1.5, 0.45 and 1.5µg/m^{-3} respectively) for a particular wind speed and wind direction. The scale of a CPF plot ranges from 0 to 1, from lowest to highest probability.

The CPF plots show that the highest concentrations of benzene (greater than the 90th percentile of all observations) occurred in the wind direction range 125° to 145° at wind speeds >15m/s in 2018.

The highest concentrations of toluene (greater than the 90th percentile of all observations) occurred in the wind direction range 90° to 180° at wind speeds of <5m/s in 2017.

The highest concentrations of ethylbenzene (greater than the 90th percentile of all observations) occurred in 2017, for winds from 80° to 115° at speeds of 5 to 10m/s, and for winds from 125° to 180° at speeds of ≤5m/s.

The highest concentrations of m&p-xylene (greater than the 90th percentile of all observations) occurred in 2017, for winds from 80° to 115° at speeds of 5 to 10m/s, and for winds from 125° to 180° at speeds of ≤5m/s.

The plots show that the highest probability of exceeding the 90th percentiles of BTEX pollutants tended to occur when winds came from the SE quadrant. By contrast, the probabilities were lower when the wind came from 10° sectors that contained the well pad, that is, 50° to 70˚. This suggests that the well pad was not a prominent source of high BTEX concentrations.

Figure 3.46: BTEX conditional probability function plots

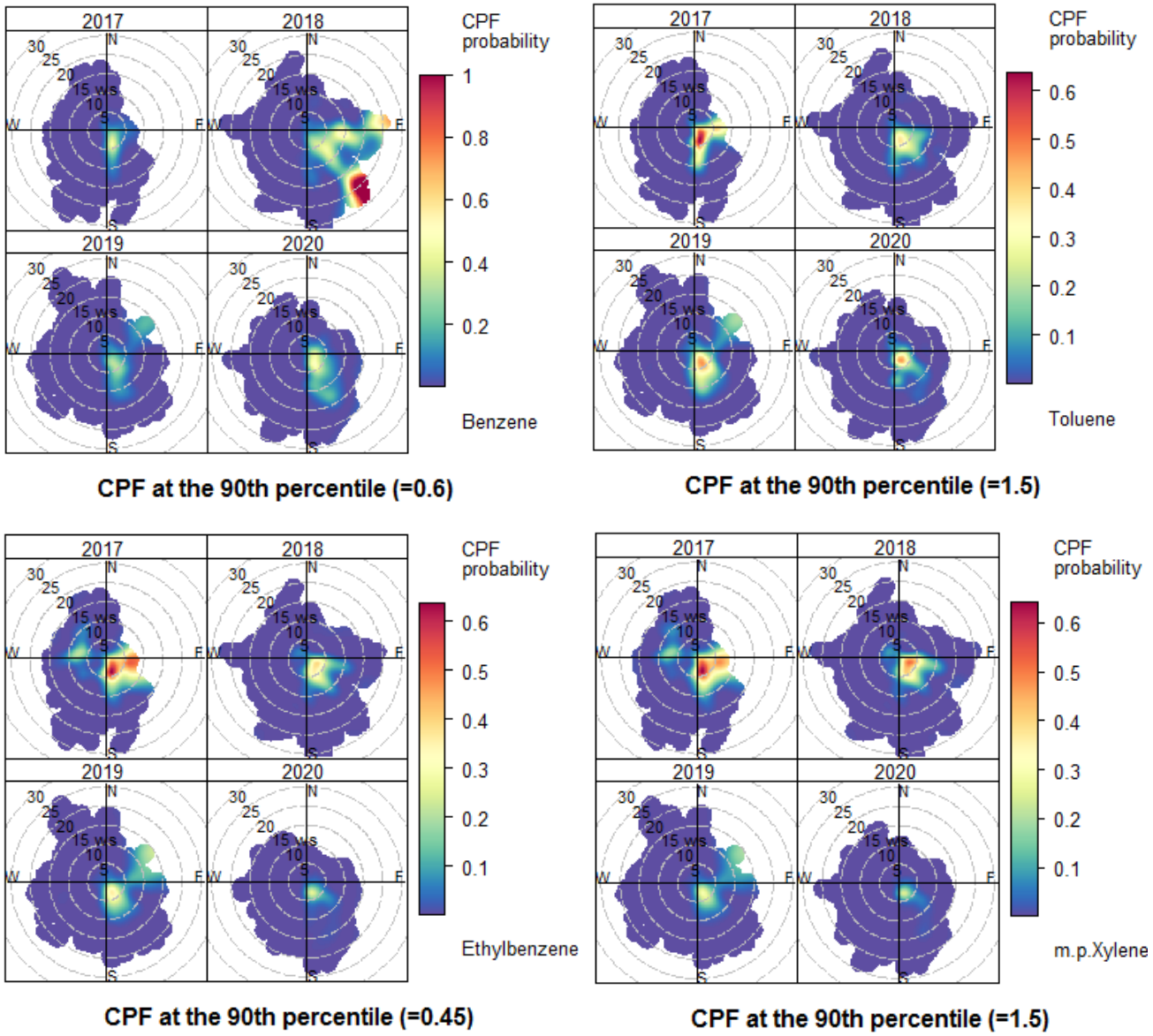

3.5.3 Wind speed variation

Figure 3.47 shows Openair polar (wind speed dependency) plots for BTEX.

Figure 3.47: BTEX Openair wind speed dependency plot (µg/m^3)

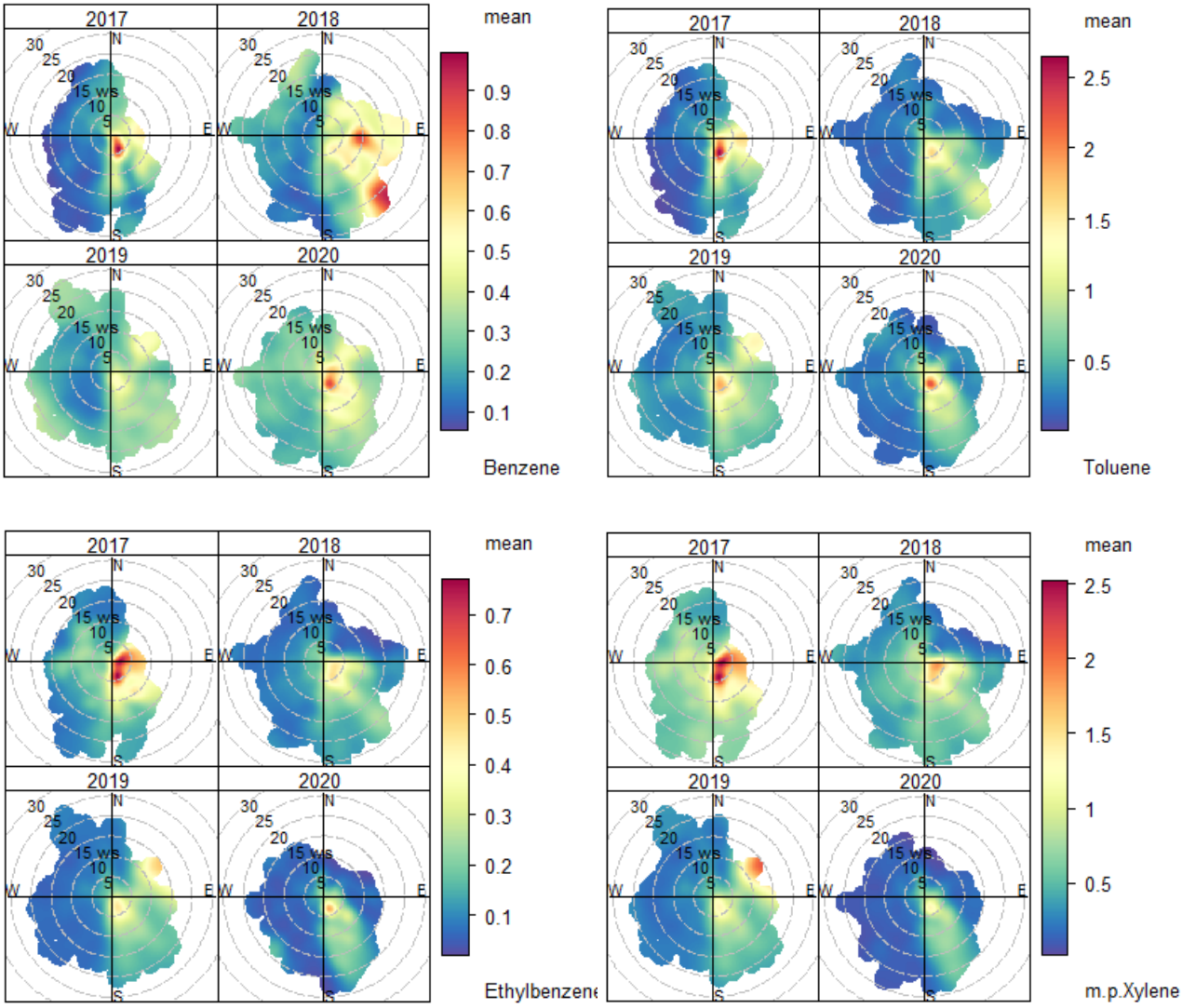

The highest levels of benzene are seen in: (i) the 2017 plot for winds from 140° to 180° at speeds of ≤5m/s; (ii) the 2018 plot for winds from 80° to 100° at speeds of 5 to 15m/s and for winds from 125° to 145° at speeds of > 15m/s; and (iii) in the 2020 plot for winds from 135° to 180° at speeds of ≤5m/s.

The highest levels of toluene are seen in the 2017 plot for winds from 140° to 180° at speeds of ≤6m/s, and in the 2020 plot for winds from 135° to 180° at speeds of ≤5m/s.

The highest levels of ethylbenzene are seen in the 2017 plot for winds from 45° to 180° for speeds of <10m/s.

The highest levels of m&p-xylene are seen in: (i) the 2017 plot for winds from 45° to 180° at speeds of <10m/s; (ii) in the 2018 plot for winds from 90° to 180° at speeds of ≤5m/s; and (iii) in the 2019 plot for winds from 45° to 65° at speeds of 10 to 15m/s.

Higher levels of BTEX are mostly seen at relatively low wind speeds, suggesting that low level sources such as traffic emissions are responsible. Background sources are also likely to be important. In cases when relatively high levels of BTEX were seen at higher wind speeds, this suggests a possible contribution from an elevated source, such as a stack emission, for example, in 2019 in the direction of the well pad.

3.5.4 Diurnal analysis

Diurnal Openair plots for BTEX are shown for the monitoring site in Figure 3.48.

Figure 3.48: BTEX Openair diurnal annulus plots (µg/m^3)

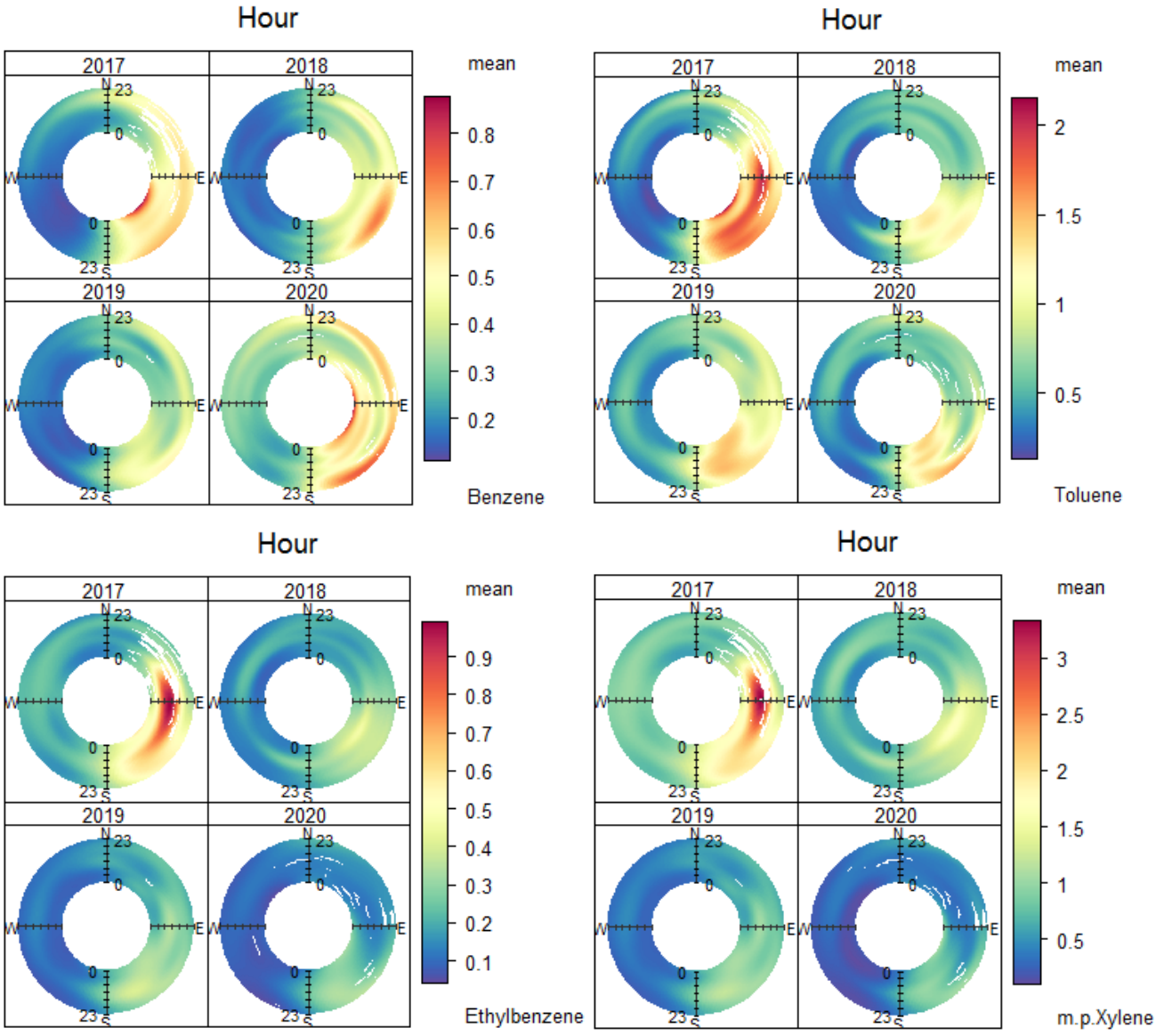

The plots show that the highest mean benzene concentrations were seen in: (i) 2017 in the wind direction range 90° to 165° during the early hours of the morning; (ii) in 2018 in the wind direction range 90° to 150° in the evening; and (iii) in 2020 in the wind direction range 55° to 150° in the morning and in the wind direction range 0° to 170° in the late evening.

The highest mean toluene concentrations were seen in 2017 in the wind direction range 65° to 180° during most of the day.

The highest mean ethylbenzene concentrations were seen in 2017 in the wind direction range 65° to 135° during the middle of the day.

The highest mean m&p-xylene concentrations were seen in 2017 in the wind direction range 60° to 125° during the middle of the day.

There was no clear evidence of increased concentrations during the morning or evening rush hours, suggesting that there was no significant contribution from road traffic.

3.5.5 Conclusion

Time series plots

Based on visual inspection of time series plots, there is no evidence of particularly elevated levels of BTEX occurring during the hydraulic fracturing periods, although it should be noted that the wind direction was rarely blowing from the shale well pad to the monitoring site.

Comparison with standards

Comparison of the benzene data with the AQS annual mean objective indicated that it was not exceeded at the monitoring site during the monitoring period.

Toluene has WHO guidelines for both human health and odour annoyance, and neither was exceeded at the monitoring site during the monitoring period.

Directional analysis

Based on visual inspection of time series plots for 45° sectors, there is no evidence of notably elevated concentrations of BTEX coming from the (NE) 45° sector that contained the well pad.

Pollution rose analysis indicates that the highest average BTEX concentrations were measured at the monitoring site when the wind was coming from between 350° and 190°.

Percentile analysis suggested that there are both relatively continuous and intermittent sources of BTEX affecting the monitoring site.

Wind speed variation

Wind speed analysis suggested that the monitoring site is being impacted by: (i) regional background levels, (ii) low-level sources such as traffic emissions, and (ii) occasionally by elevated sources (for example, stack emissions).

Diurnal analysis

There was no clear evidence of increased BTEX concentrations during the morning or evening rush hours, suggesting that there was not a significant contribution from road traffic emissions.

Summary

Concentrations of BTEX at the monitoring site were well below air quality standards throughout the monitoring period. Overall, the analysis suggested that the monitoring site was affected by regional background levels, low-level sources such as traffic emissions and occasionally by elevated sources (for example, stack emissions). Directional analysis of annual mean BTEX concentrations (based on time series plots for 45° sectors, CPF plots and polar wind speed dependency plots) showed that the maximum BTEX concentrations did not come from the direction of the well pad, suggesting that the well pad was not a prominent source of BTEX.

4 Conclusions

This report provides the results from the study of ambient air quality near the vicinity of the Cuadrilla exploratory well site at Preston New Road (PNR) in Little Plumpton.

The position of the monitoring location was useful for informing residents about ambient air quality during the period of well pad operations. However, it was not possible to carry out a detailed statistical analysis of any well pad impacts here for 2 reasons. Firstly, because winds from the well pad were very infrequent. Secondly, because the A583 lay in the same direction so that any impacts from the well pad were combined with traffic-derived impacts and were generally too small to be distinguishable from those impacts.

Comparing the collected data from the monitoring at PNR with the AQS objectives showed that the monitoring location was subject to concentrations of PM_{10}, $PM_{2.5}$, NO_2 and benzene that met their respective AQS objectives in 2018 and 2019. There were strong indications that the objectives were also met in 2017 and 2020 – based on data for parts of these years.

Comparing the data with the daily air quality index showed that levels during the study remained in the low band of the index for NO_2. PM_{10} and $PM_{2.5}$ remained primarily in the low band of the index, with just 4 days in the moderate band for PM_{10} and 9 days in the moderate band for $PM_{2.5}$.

Toluene data was compared with the World Health Organisation (WHO) guidelines and was found to be within the specified health and odour limits.

Although the data did not allow a detailed assessment of well pad impacts, pollutant time series and directional plots were inspected visually for any prominent signals from the direction of the well pad. These inspections indicated that there were no substantially elevated levels of air pollution during periods of hydraulic fracturing or from the direction of the well pad.

References

2. Department for Environment, Food and Rural Affairs. (July 2007) The Air Quality Strategy for England, Scotland, Wales, and Northern Ireland, (HMSO).

3. Department for Environment, Food and Rural Affairs. UK AIR - Air Information Resource, Daily Air Quality Index (DAQI) Daily Air Quality Index - Defra, UK.

4. WORLD HEALTH ORGANISATION, 2000. WHO Air Quality Guidelines for Europe.

5. CARSLAW, D.C. AND ROPKINS, K., 2012. Openair --- an R package for air quality data analysis. Environmental Modelling & Software. Volume 27-28, 52-61.

6. SHAW J. T. et al., Methane flux from flowback operations at a shale site, Journal of the Air & Waste Management Association, 2020, Vol. 70, No. 12, 1324-1339.

Appendix A: Mobile monitoring facility

National Monitoring Services carries out ambient air monitoring on behalf of Environment Agency regions using mobile monitoring facilities (MMFs). These facilities allow us to carry out flexible, short-term studies examining the impact of specific Environmental Permitting Regulations (EPR) permitted installations on local communities. The facilities contain a number of analysers designed to sample the atmosphere for a selection of pollutants commonly associated with industrial emissions. The equipment is contained within a trailer that can conveniently be towed. This allows it to be strategically sited at temporary locations with the intention of quantifying pollution loadings and determining sources. The MMFs used in the Preston New Road study were MMF1 and MMF2. The pollutants that can be measured using these MMFs are:

- particulate matter (PM_{10} & $PM_{2.5}$)
- methane
- oxides of nitrogen (NO_X)
- BTEX (benzene, toluene, ethylbenzene, and m&p-xylene)

Meteorological instruments

In addition to analysers measuring the concentration of pollutants in the air, the facility contains equipment that can measure meteorological conditions. This provides the opportunity to consider measured pollutant levels relative to the prevailing meteorological situation. This can supply important information, allowing a more detailed understanding of the pollutants' dispersion in the atmosphere and consequently a more accurate assessment of their origins. The meteorological parameters that can be measured are:

- wind direction
- wind speed
- ambient air temperature
- relative humidity

All meteorological measurements are taken at an elevation of 8m above the ground and from positions where the wind approach was unobstructed. The temporal resolution of all logged meteorological data is 5 minutes.

Wind direction is an important consideration as it provides direct information about the orientation of any source relative to the monitoring site. It must be noted, however, that pollutants will be carried along a wind's trajectory that may, over distances of several kilometres, be curved, so that in these cases the wind direction will not simply 'point' to the source's direction. Wind speed and temperature both have a significant influence on the amount of mixing within the atmosphere, having profound effects on the vertical distribution of pollutants through the atmospheric boundary layer. Relative humidity is important because the level of moisture within the air affects the rates of reaction and removal of some air pollutants.

Appendix B: Quality assurance and quality control

Quality assurance (QA) covers practices that are carried out before data collection to ensure that the sampling arrangements and analysers can provide reliable measurements. Quality control (QC) covers practices applied after data collection in order to ensure that the measurements obtained are repeatable and traceable.

In order to ensure that data from the MMF are representative of pollutant concentrations and meet appropriate standards of quality, a number of QA and QC procedures are routinely implemented when the monitoring facility is operating.

Quality assurance included:

Training	- all personnel involved in running the facility have received appropriate training in carrying out the tasks they are expected to do. This training has been recorded in the personal training log of the individuals concerned.
Procedures	- all routine activities undertaken in the operation of the facility are clearly and unambiguously laid out in a documented set of procedures.
Analyser selection	- careful consideration has been given to the choice of analysers, ensuring that they meet the required standards of accuracy and precision. Also, that they can be relied on to be robust and flexible enough to present the data in a suitable format.
Trailer location	- attention is given to how representative the location of the facility is when compared against the objectives of the study.

Quality control included:

Routine calibration	- calibrations are performed every 2 weeks, using traceable gas standards and documenting any adjustments made to the analysers.
Routine maintenance	- carrying out stipulated checks and changing filters.
Periodic maintenance	- employing a qualified engineer to service the analysers twice a year.
Instrument history	- all invasive work carried out on analysers is documented and recorded.

Data review	- all data is checked to ensure correct scaling, rejecting negative or out-of-range readings, questioning rapid excursions, generally considering the integrity of recorded levels.
Data handling	- following recognised procedures to ensure that data capture is maximised. The data is analysed frequently so that measurements affected by instrument faults are recognised quickly.
Data comparison	- comparing the collected data sets with data sets from other monitoring studies that are carried out in close enough proximity to be relevant. Considering the relationship between different pollutants, as some pollutant levels will be expected to rise and fall together.
Data rectification	- the adjustment of data to minimise the effects of analyser drift.

Appendix C: Particulate matter (PM_{10} and $PM_{2.5}$)

Airborne particulate matter can be found in a wide range of particle sizes (nm-µm) and chemical constituents. PM_{10} and $PM_{2.5}$ levels have been monitored in this study. PM_{10} is defined as particulate matter with an aerodynamic diameter less than 10µm. $PM_{2.5}$ is defined as particulate matter with an aerodynamic diameter less than 2.5µm. The description of PM_{10} and $PM_{2.5}$ is restricted to its physical characteristic and no particular chemical composition is implied. The size-selective samplers used to collect small particles preferentially are designed to collect 50% of 10µm aerodynamic diameter particles, more than 95% of 5µm particles, and less than 5% of 20µm particles. The size is important because it is this that determines where in the human respiratory tract a particle deposits when inhaled. Most concern is given to particles small enough to penetrate into the lungs reaching the alveoli where the delicate tissues involved in the exchange of oxygen and carbon dioxide are found. When inhaled, almost all particles larger than 7µm are deposited in the nose and throat, and only 20 to 30% of particles between 1 and 7µm are deposited in the alveoli. However, up to 60% of particles below 0.1µm are deposited in the alveoli. The size of the particles also determines how long they spend in the atmosphere; smaller particles remain in suspension for longer and can be transported over long distances. Measuring PM_{10} and $PM_{2.5}$ relies on using a size-selective instrument, which collects small particles preferentially.

Sources

There are a number of important natural sources of particulate in the air, with forest fires and volcanic eruptions being 2 sources that can cause extreme pollution and can be very adverse to human health. Sea spray and the erosion of soil and rocks by wind are important sources in many localities. There are also many biological sources, with considerable numbers of pollen grains, fungal spores and their fragments contributing to the total loading of airborne particles. Man-made airborne particles result mainly from combustion processes, from the working of soil and rock, from industrial processes and from the attrition of road surfaces by motor vehicles.

The major PM components are sulphate, nitrates, ammonia, sodium chloride, carbon, mineral dust, and water. Particles can be classified as being either primary or secondary: the former are released directly into the air, while the latter are formed in the atmosphere by the chemical reaction of gases, first combining to form fewer volatile compounds, which, in turn, condense into particles. Primary particles have an immediate effect on the particulate loading in the vicinity of the source. The main sources of primary PM_{10} and $PM_{2.5}$ in the UK in 2019 were [(1)]:

- road transport; nationally, road transport contributed around 12% of primary PM_{10} and 12% of primary $PM_{2.5}$ emissions, however, the contribution can be much higher in urban areas

- industrial processes; including a range of different industrial processes leading to the release of dust as well as construction, mining, and quarrying activities. Nationally, it is estimated that these processes accounted for around 31% of primary PM_{10} emissions and 13% of primary $PM_{2.5}$ emissions

- combustion in industry, commercial and residential settings; traditionally coal burning was a major source of airborne particles, but now wood is increasingly being used as a domestic fuel. Nationally, it is estimated that combustion of various types of fuel accounted for approximately 42% of primary PM_{10} emissions and 63% of primary $PM_{2.5}$ emissions

- public electricity and heat production; is estimated to have been responsible for 1.0% of primary PM_{10} emissions and 1.3% of primary $PM_{2.5}$ emissions

Secondary particles are less easy to ascribe to their original sources. They comprise mainly ammonium sulphate and nitrate, originating from the oxidation of gaseous sulphur and nitrogen oxides to acids, which are then neutralised by atmospheric ammonia, derived from agricultural sources. The chemical processes involved in the formation of these secondary particles are relatively slow (in the order of days) and their persistence in the atmosphere is similarly prolonged. Therefore, while road traffic may be the main source of the original oxides of nitrogen, and coal and oil burning the main sources of sulphur oxides, the secondary particles are distributed more evenly throughout the air, with less difference between urban and rural areas. They may also drift for considerable distances. This can result in pollution being transported across national boundaries.

Particulate analyser

TEOM

The analyser used to measure PM_{10} & $PM_{2.5}$ concentration at the start of the study was a Rupprecht and Patashnick (R&P) tapered element oscillating microbalance (TEOM). It provides measurements in real time and stores them as 15-minute averages. PM_{10} and $PM_{2.5}$ fractions were measured using 2 separate TEOM systems with specific PM_{10} and $PM_{2.5}$ filter inlets. The system measures PM concentration by continuously determining the particle mass deposited on a filter. The filter is attached to a hollow tapered element that vibrates at its natural frequency of oscillation (f). As particles collect on the filter, the frequency changes by an amount inversely proportional to the square root of the mass deposited (**m**).

$$\mathbf{m} = \mathbf{k}/f^2$$

Where k is a constant determined during calibration of the instrument.

The flow rate through the system is controlled using thermal mass flow controllers and automatically measured so that the mass concentration can be calculated. The analyser consists of a sample inlet head that has an airflow of 16.67 litres per minute. The action of the air through the head selects particles of aerodynamic diameter less than 10μm. After

the air has passed through the head, the flow is divided using a flow splitter to direct 3 litres per minute through the filter cartridge.

It is a requirement of the TEOM instrument that the filter is kept at a constant temperature of 50°C. This can lead to a difference between mass concentrations determined using a TEOM and co-located gravimetric filter samplers, for which the collection filters are unheated and therefore at ambient temperature. The effect of this difference is variable depending on the nature of the particulate being measured. It is considered most probable that the discrepancy is a consequence of evaporation of semi-volatile secondary particles such as ammonium nitrate and some organic compounds. Therefore, care must be taken when predicting the secondary particle contribution to the total mass concentration.

The Airborne Particles Expert Group (APEG - now the Air Quality Expert Group) has published a report which concluded that at concentrations around 50$\mu m/m^3$ compared with a gravimetric sampler the TEOM tends to under-read by between 15 and 30%. However, this effect is not constant, and varies depending on the mass concentration, the distance from a specific source, and the environmental conditions. Further studies have been commissioned by the Department of the Environment, Transport, and the Regions (DETR) to investigate these effects, and to provide a more robust relationship between the TEOM and the European transfer gravimetric reference method.

The air quality objectives are based on measurements carried out using the European transfer reference method or equivalent. Therefore, there is a potential inconsistency between measurements of PM_{10} concentrations made using a TEOM analyser and the objectives. For example, a daily mean concentration of $45\mu g/m^3$ measured using a TEOM analyser could be underestimating the gravimetric concentration by $15\mu g/m^3$ or more. It is therefore necessary to apply a correction factor when assessing TEOM measured concentrations against the objectives.

Recent findings have suggested that the correction factor of 1.3 originally recommended by the National Air Quality Strategy (NAQS) guidance for use with PM_{10} and $PM_{2.5}$ data is not equivalent to the reference method for particulate matter and therefore not strictly comparable to the European Daughter Directive Limit Values.

Kings College London (KCL), on behalf of Defra, has developed a volatile correction model (VCM) which can be used to correct PM_{10} TEOM measurements for the loss of volatile components caused by the high sampling temperature, with corrected measurements being comparable to the gravimetric reference equivalent. The VCM works by using volatile particulate measurements from nearby Filter dynamics measurement system (FDMS) within a radius of 130km. This allows for the loss of volatiles from the TEOM measurements to be calculated and added to the measurements obtained from the TEOM.

Reference equivalent PM_{10} = TEOM – 1.87 FDMS purge

FDMS purge is usually a negative value due to the loss of volatiles. It can be measured at a remote site, allowing for the possibility of using one FDMS to correct many TEOM instruments within suitable distance.

The model provides adequate coverage for the whole of the UK, except Scotland and Northern Ireland.

KCL has developed a VCM for $PM_{2.5}$ that goes some way toward estimating the volatile fraction of the particulate lost on the TEOM. Although not strictly equivalent to the reference method, it does give a better estimation of total particulate $PM_{2.5}$ than uncorrected TEOM data and therefore has been used in this study.

The manufacturer's specification states that the TEOM is accurate to within 4$\mu g/m^3$.

This instrument is used extensively in the UK automatic monitoring networks and has been designated by the US Environmental Protection Agency (EPA) as an equivalent method for determining 24-hour average PM_{10} concentrations.

Fidas®

The analyser used to measure PM concentration from January 2019 was a Palas Fidas® 200 optical measuring system. It provides measurements in real time and stores them as 15-minute averages.

The Fidas® measures PM using an optical light scattering technique and uses an algorithm to calculate concentrations based on the number and size distribution of particles.

The Fidas® has a flow volume of 0.3m^3/h (flow rate of 4.8l/m). The inlet is fitted with a Sigma-2 (TSP) sampling head, which allows the full range of particle sizes to reach the Intelligent Aerosol Drying System (IADS). The IADS conditions the sampled air, which helps prevent possible measurement inaccuracies due to condensation during periods of high ambient air humidity.

Once the sample has been conditioned, the particle size is determined using the Lorenz-Mie scattered light analysis of single particles by an optical aerosol spectrometer. The spectrometer measures the scattered light impulse generated by each particle as it is illuminated by a white LED light at an angle of 90°. The number of scattered light impulses allows the determination of the particle number and the height of the impulse is related to particle size. The scattered light signal is allocated to a particle size diameter bin using a calibration curve and measurement of the signal number. The bins are then used to form a histogram of the measured particle sizes.

A number of computational steps are required to convert the measured particle sizes into a mass concentration. The measured size distribution is altered to a distribution based on a representative index for environmental aerosol. To account for the variability in the shape of each particle, the distribution is altered from optical diameter (spherical shape) to reflect the aerodynamic diameter (variable shape) of the particles. Once the distribution

has been altered to account for the refractive index and diameter the particle distribution line is used to apply the cut curves for each of the PM fractions.

The data is then converted from particle size to particle mass using a size dependent density algorithm. This system allows for a lower detection limit of 180nm with a sampling range of 0.18 to 18µm.

References

1. National Atmospheric Emissions Inventory (NAEI), Pollutant Information pages for PM_{10} and $PM_{2.5}$, © Crown 2022 copyright Defra & BEIS via naei.beis.gov.uk, licenced under the Open Government Licence (OGL).

2. DETR – May 2000 - Pollutant Specific Guidance.

3. Palas, Fidas® 200 operating manual.

Appendix D: Oxides of nitrogen (NO_X)

Nitrogen dioxide is a gas produced by the reaction of nitrogen and oxygen in combustion processes. The nitrogen is most commonly atmospheric nitrogen, although nitrogen atoms in the combustion fuel can also be involved. The reaction usually takes place in 2 stages. The first reaction, at high temperature, is between one nitrogen atom and one oxygen atom to form a nitric oxide (NO) molecule. This molecule will then be oxidised by the addition of a further oxygen atom to form nitrogen dioxide (NO_2); this may occur sometime later at ambient temperatures. As nitric oxide is a precursor in the formation of nitrogen dioxide its levels are often of interest. These 2 oxides of nitrogen are, for local air quality purposes, collectively known as NO_X. Typically, 90 to 95% percent of NO_X at the time of emission from an industrial combustion source is in the form of NO.

Once formed, nitrogen dioxide takes part in chemical reactions in the atmosphere that convert it to nitric acid and nitrates, both of which can be removed by rain. However, nitrates can also remain in the air as very small particles, for example, as ammonium nitrate, which can be dispersed widely in the atmosphere, contributing to the airborne concentrations of PM_{10}.

Sources

There are several natural sources of oxides of nitrogen in the atmosphere, including lightning and forest fires. However, by far the largest amount is formed from the combustion of fossil fuels - petrol, oil, coal, and gas. In the UK in 2019, road transport emissions accounted for 33% of total NOx emissions, with other forms of transport accounting for 21%, power stations and other energy producers accounting for 9%, and other industrial combustion processes accounting for 10%. [(1)]

As mentioned, once nitric oxide is emitted it combines further with atmospheric oxygen to form nitrogen dioxide. The source of this oxygen atom is sometimes by reaction with atmospheric oxygen; however, this mechanism is relatively slow and is thought only to be significant during stagnant, cold weather conditions that sometimes occur in wintertime. The main way in which nitrogen dioxide is produced is through oxidation by ozone, where action between atmospheric ozone and nitric oxide result in the formation of nitrogen dioxide, described by the equation:

$$NO + O_3 \rightarrow NO_2 + O_2$$

This reaction is fast and approaches completion in approximately one minute. However, within pollution plumes and close to sources of nitric oxide the ozone supply may be depleted, resulting in a slower rate of conversion.

Nitrogen dioxide in the atmosphere can photodissociate to reform nitric oxide. In this reaction, an oxygen radical ($O^{\bullet}$) is produced, which, in turn, reacts with oxygen molecules to form ozone:

$NO_2 + h\nu \rightarrow O^{\bullet} + NO$
$O^{\bullet} + O_2 + M \rightarrow O_3 + M$
$O_3 + NO \rightarrow O_2 + NO_2$

It can be seen from these reactions that concentrations of ambient nitrogen dioxide are dependent on the amount of solar radiation present. It should be expected, therefore, that concentration levels will vary through the day as the sunlight changes in intensity.

The analyser used to measure oxides of nitrogen is a ML 9841B. This instrument is designed to measure the concentration of nitric oxide (NO), total oxides of nitrogen (NO_X) and (by calculation) nitrogen dioxide (NO_2). NO in the sample air stream reacts with ozone (O_3) in an evacuated chamber to produce activated NO_2, which, in turn, produces chemiluminescent radiation:

$$\mathbf{NO + O_3 \rightarrow NO_2^* + O_2 \rightarrow NO_2 + O_2 + h\nu}$$

The intensity of the chemiluminescent radiation is measured using a photo-multiplier tube (PMT), with the PMT tube output voltage being proportional to the NO concentration. The ambient air sample is divided into 2 streams. From one, levels of NO are obtained. In the other, NO_2 is reduced to NO using a heated molybdenum catalyst before reaction allowing measurement of total oxides of nitrogen NO_X (= NO + NO_2). The NO_2 concentration is calculated from the difference (NO_2 = NO_X - NO).

Assessment of compliance for NO_2 chemiluminescence analyser according to ISO 14956			
MonitorLabs ML 9841B nitrogen dioxide analyser			
2000 NAQS for NO_2 concentrations		1 hour limit value 105ppb	
Measurement performance related to dynamic conditions			
Performance characteristic	**Value**	**Distribution Type**	**Standard uncertainty at 100ppb**
Linearity	1% of reading	Rectangular	0.6ppb
Precision	0.5ppb or 1% of reading	Normal	1ppb
Zero drift	2ppb	Rectangular	0.6ppb
Span drift	0.5% of reading	Rectangular	0.3ppb
Noise	0.25ppb	Rectangular	0.15ppb
Losses in collection system (sample lines, filters)	10%	Rectangular	6ppb
Standard uncertainty of calibration gas	10%	Rectangular	6ppb
Total standard uncertainty			8.5ppb
Total uncertainty for NO_2 (95% confidence)			**14ppb**

The total uncertainty calculation is made for the NO_2 1-hour 2000 NAQS limit value of 105ppb.

Data for the uncertainty analysis was taken from the specifications reported by both the instrument and calibration gas manufacturer's manual and from the report: 'Quality Assessment of Ambient NO, NO_2 and SO_2 Measurements in European Monitoring Networks', Payrissat M, Gerboles M, Sieja B and De Saeger E (1997).

These instruments are used extensively in the UK automatic monitoring network and have been designated as reference methods for the determination of oxides of nitrogen by the USEPA.

References

1. National Atmospheric Emissions Inventory (NAEI), Pollutant Information page for Nitrogen oxides, © Crown 2022 copyright Defra & BEIS via naei.beis.gov.uk, licenced under the Open Government Licence (OGL).

Appendix E: Methane (CH_4)

Methane, commonly known as marsh gas, is a colourless, odourless gas with a melting point of -184°C and boiling point -164°C. Its main environmental impact is from its relatively high potential for global warming. It affects the radiation balance of the Earth by absorbing infrared radiation and converting it to heat; therefore, increased methane concentrations lead to increased surface temperatures.

Sources

Methane is produced by anaerobic bacterial fermentation processes in water that contains substantial organic matter, such as swamps, marshes, rice fields, lakes, and landfills. This microbial degradation of organic matter may be written as:

$$CO_2 + 4H_2 \rightarrow CH_4 + 2H_2O$$

Methane is also produced by enteric fermentation in mammals and other species.

Until the late 1970s, it was accepted that the background concentration of methane was in the range of 1.4 to 1.6ppm. Since then, ambient levels have risen to a background norm of approximately 1.8ppm. The increase in methane background concentrations is mainly due to an increase in the emissions from primary sources. However, the reduction in environmental levels of the hydroxide radical [OH] brought about by the increased levels of carbon monoxide (CO) also plays a part.

CH_4 analysers

The analyser used was a Los Gatos Research (LGR) CH_4 analyser, which uses Off Axis Integrated Cavity Output Spectroscopy (OA-ICOS).

Until recently, high-sensitivity trace-gas measurements have been possible only by using expensive lasers (for example, lead-salt or quantum-cascade) or broadband lamps that operate in the mid-infrared region where absorption features are strong. LGR's advances in cavity-enhanced absorption-spectroscopy techniques provide dramatic increases in the optical path length and, as a result, enable ultrasensitive trace-gas measurements using robust, reliable, room temperature diode lasers that operate in the near infrared.

Off-Axis ICOS uses a high-finesse optical cavity as an absorption cell as shown in Figure 1. Unlike conventional multi-pass arrangements, which are typically limited to path lengths less than two-hundred metres, an Off-Axis ICOS absorption cell effectively traps the laser photons so that, on average, they make thousands of passes before leaving the cell. As a result, the effective optical path length may be several thousands of metres using high-reflectivity mirrors. Therefore, the measured absorption of light after it passes through the optical cavity is significantly enhanced. For example, for a cell composed of 2 99.99% reflectivity mirrors spaced by 25cm, the effective optical path length is 2,500 metres.

Figure 1: Schematic diagram of an Off-Axis ICOS Instrument

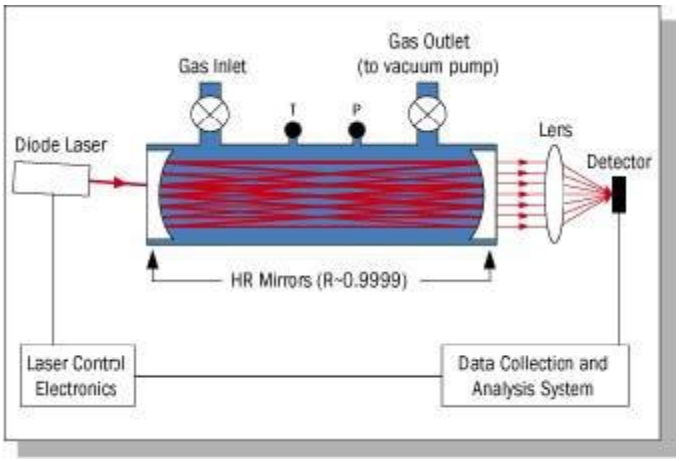

Because the path length depends only on optical losses in the cavity and not on a unique beam trajectory (like conventional multipass cells or cavity-ring-down systems), the optical alignment is very robust, allowing for reliable operation in the field. The effective optical path length is determined routinely by simply switching the laser off and measuring the necessary time for light to leave the cavity (typically tens of microseconds).

As with conventional tuneable-laser absorption-spectroscopy methods, the wavelength of the laser is tuned over a selected absorption feature of the target species. The measured absorption spectra are recorded and combined with measured gas temperature and pressure in the cell, effective path length, and known line strength, then used to determine a quantitative measurement of mixing ratio directly and without external calibration.

References

1. Los Gatos Economical Ammonia Analyser User Manual.

Appendix F: Volatile organic compounds (VOCs)

Volatile organic compounds (VOCs) are an important class of air pollutant commonly found in the atmosphere at ground level in urban and industrial areas. The strict definition of a VOC is an organic compound present in the atmosphere as a gas, but which under normal conditions of temperature and pressure would be a liquid or solid. However, a more general description VOC includes all carbon-containing compounds found in the atmosphere, excluding elemental carbon, carbon monoxide, and carbon dioxide.

Sources

Natural biogenic processes can give rise to substantial ambient concentrations of a limited number of organic compounds, including isoprene, monoterpenes, and methane. Natural sources include emissions from plants, trees, wild animals, natural fires and anaerobic processes in bogs and marshes. However, the contributions resulting from human activities are considerably greater. The main sources of non-methane VOC (NMVOC) emissions in the UK in 2019 were industrial processes and product use (55%), extraction and distribution of fossil fuels (15%), agriculture (14%), stationary combustion plants (8%) and transport and other mobile sources (7%). [(1)]

Environmental considerations

The presence of VOCs in the atmosphere is of concern because of their role in a number of environmental issues. These include:

- ground level photochemical ozone formation
- toxic or carcinogenic human health effects
- accumulation and persistence in the environment
- enhancing the global greenhouse effect
- stratospheric ozone depletion

Ground level ozone formation

Ozone is formed by the reaction of atomic oxygen with molecular oxygen. In the troposphere the only significant source of atomic oxygen is photodissociation of NO_2, which also results in the formation of NO. In the atmosphere, NO reacts with ozone, forming molecular oxygen and NO_2. This series of reactions establishes a dynamic equilibrium, with the amount of ozone formed by reaction between molecular and atomic oxygen equal to that removed by reaction with NO. The equilibrium depends on the amount of prevailing sunlight. The ‘background’ concentration of ozone in the atmosphere in the UK is 20 to 30ppb depending on the season.

The primary removal process for VOCs in the troposphere is reaction with OH radicals, where the OH radical removes a hydrogen atom from the VOC to leave a VOC radical. The products of the reaction of VOCs with OH radicals can result in the conversion of NO to NO_2, but with no corresponding removal of ozone. As a consequence, the set of

reactions result in a net production of ozone, with the concentration of ozone being limited by the available VOCs, photochemical dissociation, and dry deposition. Maximum hourly concentrations of ozone observed in the UK over recent years have been around 100ppb.

Table G2.1 VOC POCPs

Measured VOC	POCP[$]
t-2-butene	*
c-2-butene	*
i-Pentane	12
n-Pentane	9
t-2-pentene	*
2-methylpentane	19
3-methylpentane	11
n-hexane	10
cyclohexane	*
n-heptane	13
benzene	13
toluene	41
ethylbenzene	35
(m+p)-xylene	77
o-xylene	31
1,3-butadiene	*
Isoprene	*
Styrene	*
1,2,4-trimethylbenzene	86
1,3,5-trimethylbenzene	74

[$] Data from 'Editor's: R.E. Hester and R. M. Harrison, Issues in Environmental Science and Technology 4 – Volatile Organic Compounds in the atmosphere, The Royal Society of Chemistry, 1995'.

[*] Data not supplied

N.B.

1) The ozone depletion potential of all the listed VOCs is zero because they do not contain any halogen atoms and will all undergo reaction in the troposphere.

2) The global warming potential has not been calculated for any of the listed VOCs in Table G2.1.

However, each VOC can contribute differently to the formation of ozone and other secondary oxidants in the troposphere, both in terms of quantity and timescale. Concern resulting from the generation of elevated levels of ozone in regions of high population has led to greater priority being placed on controlling those compounds that are oxidised rapidly. The concept of photochemical ozone producing potential (POCP) has been introduced to allow the different compounds to be ranked. The POCP scale indicates the relative abilities of VOCs to produce ozone over short timescales (up to 5 days). Ethene (C_2H_4) is the reference compound, for which a POCP value of 100.0 is assigned. A POCP value is defined per unit mass emission. Currently, calculated POCP values range from zero for unreactive fully halogenated compounds to about 130 for reactive substituted aromatic compounds.

POCP is a calculated quantity that depends on the use of models and their underlying assumptions. When POCPs are calculated using different atmospheric models, the ratio of POCPs for any given compound may differ appreciably.

Toxic and carcinogenic health effects

Organic compounds may have important impacts on human health through direct mechanisms in addition to their indirect impacts. Some organic compounds affect the human senses through their odour, some others exert a narcotic effect and certain species are toxic. There is particular concern about those organic compounds that could cause cancer in the human population: the human genotoxic carcinogens. A wide range of other chemicals are also coming under scrutiny in this context. The most prominent organic compounds that belong to the air toxic category, and are widely distributed in the ambient atmosphere, are benzene and 1,3-butadiene.

Accumulation and persistence

There is an important class of organic compounds, the semi-volatile VOCs, which, because of their molecular size and complexity, tend to become adsorbed onto the surface of suspended particulate matter. In this form, they undergo long-range transport and may be removed in rain remote from their point of original emission. Once deposited in rain, they may re-evaporate back into the atmosphere and begin the cycle all over again. Ultimately, this material may be recycled through the atmosphere before reaching its more permanent sink in the colder aquatic environments in polar regions. Biological accumulation in these sensitive environments can lead to toxic levels in human foodstuffs in areas exceedingly remote from the point of original emission. Compounds associated with biological accumulation include polychlorinated biphenyls (PCB), phthalic acid and its derivatives.

Global greenhouse effect

Some of the longer-lived organic compounds accumulate in the troposphere or may have the potential to do so. If any of these compounds can absorb solar or terrestrial infrared radiation, then they may contribute to the enhanced greenhouse effect. Such compounds would be classed as radiatively active gases and their relative effectiveness can be

expressed through their global warming potential (GWP). The GWP of a substance is a measure of the extra amount of heat that is trapped in the atmosphere when 1kg of the substance is released instantaneously into it, relative to the case when 1kg of carbon dioxide is released.

Many organic compounds are not themselves radiatively active gases, but they do have the property of potentially being able to perturb the global distributions of other radiatively active gases. If they exhibit this property, then they can be classed as secondary greenhouse gases and indirect GWPs may be defined for them. Organic compounds can behave as secondary greenhouse gases by reacting to produce ozone in the troposphere (ozone is an important greenhouse gas) or increasing or decreasing the concentration of hydroxyl (OH) radicals in the troposphere and so perturbating the distribution of methane.

GWPs are calculated using computer models which incorporate the radiative heat balance of the atmosphere and the chemical kinetics of the substance. GWP values are published by the World Meteorological Organisation (1995).

Stratospheric ozone depletion

Some organic compounds do not react with OH in the troposphere due to the lack of available hydrogen atoms in the molecules. As a result, they are relatively unreactive in the troposphere and can enter the stratosphere. The organic compounds may be fully substituted halogenated compounds. The primary reaction the compounds undergo is photolysis which releases the halogens into the stratosphere. The halogen atoms become involved in an ozone-destroying reaction where the halogen acts as a catalyst for the destruction of ozone. A large number of ozone molecules can be destroyed by each halogen atom before the halogen atom is removed from the stratosphere. An example of the result of the destruction of stratospheric ozone is the formation of the Antarctic ‘ozone hole’. Many chlorinated solvents and refrigerants, and bromine-containing fire retardants and fire extinguishers have been identified as containing organic compounds that may lead to stratospheric ozone layer depletion.

The extent to which VOCs can contribute to depletion of ozone in the stratosphere is usually expressed in terms of ozone depletion potentials (ODPs). An ODP is a calculated quantity. To find the ODP for a particular compound, properties of that compound are put into a mathematical model. The model calculates the rate and height at which the compound interacts with other atmospheric constituents in the presence of sunlight, to initiate chains of reactions that destroy stratospheric ozone. The ozone depletion arising from an instantaneous release of the compound is calculated for the whole of the life of the compound in the atmosphere. The depletion of stratospheric ozone calculated for the compound is then expressed as a fraction of the depletion calculated for CFC-11 (trichlorofluoromethane) which is given an ODP of 1.0.

ODP is only associated with compounds containing the halogens fluorine, chlorine, bromine, and iodine; consequently, the majority of VOCs are ascribed a zero ODP.

ODP values are published by the World Meteorological Organisation (1994).

Monitoring methodology

The VOCs were monitored using a Chromatotech BTEX analyser.

C_6-C_{10}:

Carrier Gas - Nitrogen

Column - EPA 624 equivalent

Detector - PID (10.6eV)

The BTEX analyser was calibrated daily with a benzene standard to account for drift. The analyser was also calibrated on occasion with a gas standard supplied by National Physical Laboratory (NPL). These calibrations were used for comparison against the internal calibration system of the analyser.

References

1. National Atmospheric Emissions Inventory (NAEI), Pollutant Information page for Non methane VOC, © Crown 2022 copyright Defra & BEIS via naei.beis.gov.uk, licensed under the Open Government Licence (OGL).

Appendix G: Percentile analysis

Percentile analysis provides a method of looking at the distribution of concentrations within a data set.

Excel calculates percentiles by first sorting the concentrations into ascending order and then ranking each concentration. It then uses the following formulas:

$$r = 1 + \left[\frac{P(n-1)}{100}\right] I + D$$

P = the percentile you want
n = the total number of values
I = the integer part of the ranking
D = the decimal part of the ranking
r = rank

$$p = Y_I + D(Y_{I+1} - Y_I)$$

Y_I = value corresponding to the rank I
p = Value of the required percentile

BetterSolutions.com

to interpolate the value of a particular percentile from the calculated ranking. In other words, it calculates the concentration below which a certain percentage of concentrations fall. For example, at the 95th percentile, 95% of the data will lie below this value and 5% of the data will lie above it.

In order to produce radial percentile roses, the data is first divided into the required wind sectors and then the data in each sector undergoes separate percentile analysis. By calculating the concentration of a pollutant at different percentiles for different wind sectors, you are able to visually examine the distribution of pollutant concentrations at a particular monitoring site. This, in turn, will provide information on the source that may be influencing levels at the monitoring site.

By separating the data into various wind sectors, it allows you to assess which wind directions are having the greatest influence on pollutant concentrations at the monitoring site. By calculating the average concentration for every wind sector, you can produce a ‘mean pollution rose’, where the influence on pollutant concentrations from a particular wind sector is seen as a bias on a radial plot. This type of analysis is very effective at visually highlighting the wind sectors where there are significant sources of a given pollutant. By breaking each wind sector down into a number of different percentiles, it can be seen whether biases are present in all of the percentiles or just certain ones. This can tell you whether a source is affecting the monitoring site relatively continuously or just intermittently. For example, a bias that is observed in all of the percentiles (Figure 1)

suggests that the source in that particular wind sector is emitting relatively continuously as it is influencing a large percentage of the data. While a bias that is only observed in the higher percentiles (Figure 2) suggests that the source is intermittent as it only affects a small percentage of the data, that is, it doesn't affect concentrations at the monitoring site every time the wind is coming from this direction. Occasionally, a bias is observed in the lower percentiles that is not evident in the higher percentiles (Figure 3). This suggests that the source is relatively continuous, as it is affecting a large percentage of the data, but it also tells you that the source is not causing appreciably high concentrations at the monitoring site.

Figure 1 - shows a bias between 280° and 300° that is evident in all of the percentiles.

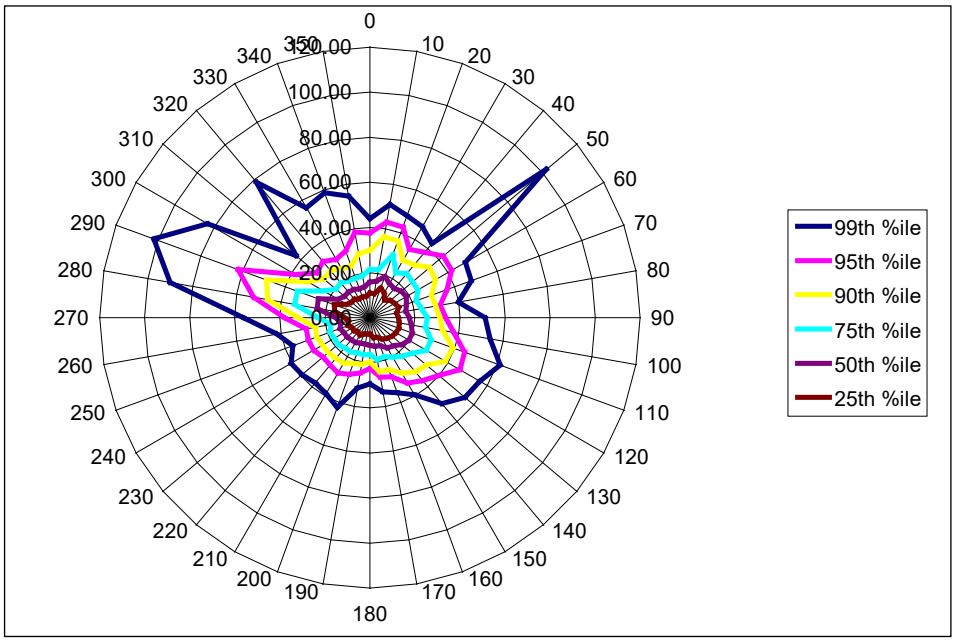

Figure 2 - shows a bias at 260° that is only evident in the 99th percentile.

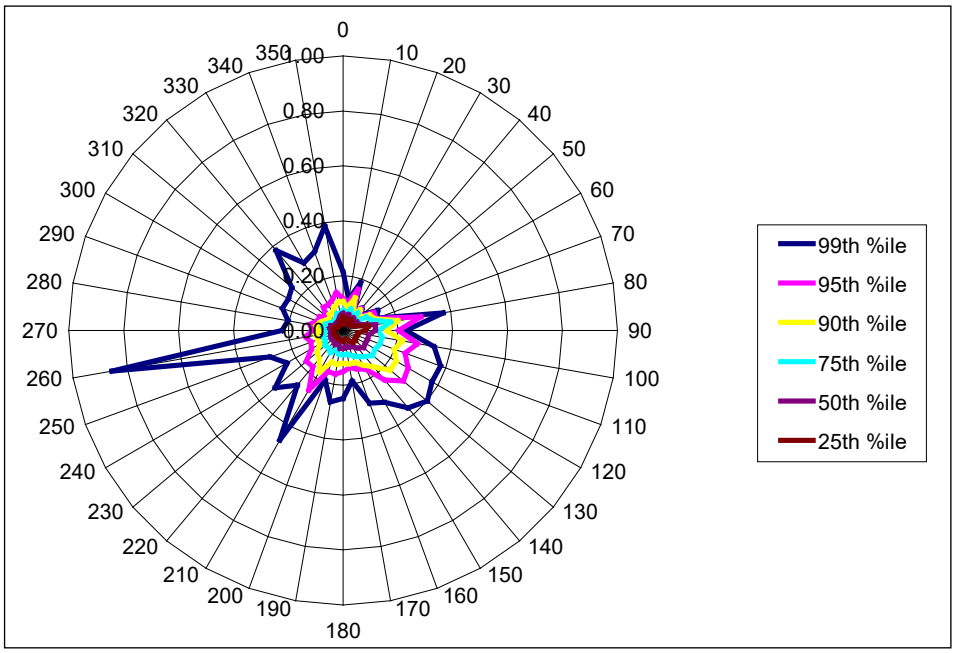

Figure 3 - shows a bias between 20° and 50° that is only evident in the lower percentiles.

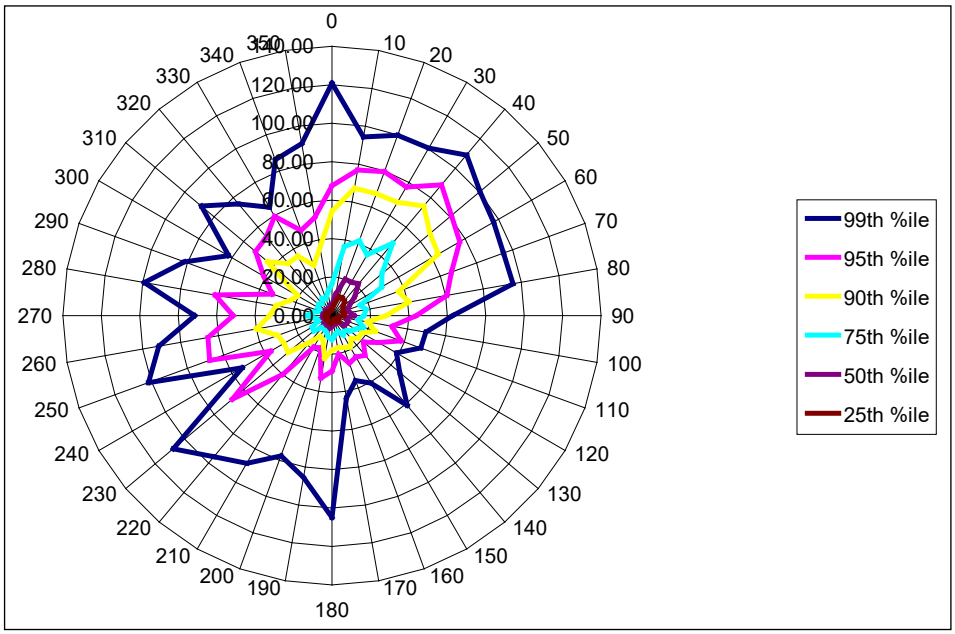

Appendix H: Conditional probability function (CPF) plots in Openair

Conditional probability function (CPF) plots have been used in this report, using the Openair software package in R, to help identify the wind direction and wind speeds from which the most prominent pollutant sources are likely to occur.

The conditional probability function calculates the probability that in a particular wind sector the concentration of a species is greater than some specified value. The value specified is usually expressed as a high percentile of the species of interest, for example, the 75th or 90th percentile. CPF analysis is very useful for showing which wind directions are dominated by high concentrations and give the probability of doing so (example in Figure 1).

The CPF is defined as:

$CPF\Delta\theta = m\Delta\theta \mid C>x / n\Delta\theta$

where $m\Delta\theta$ is the number of samples in the wind sector θ having concentration C is greater than or equal to a threshold value x, and $n\Delta\theta$ is the total number of samples from wind sector $\Delta\theta$. Therefore, CPF indicates the potential for a source region to contribute to high air pollution concentrations. Conventionally, x represents a high percentile of concentration, for example, the 75th or 90th percentile.

Therefore, where a high number of data points with values greater than your chosen threshold value have been measured for a particular wind direction, there will also be a higher probability value for that wind direction.

Figure 1: CPF plot of SO2 concentrations at Marylebone Road

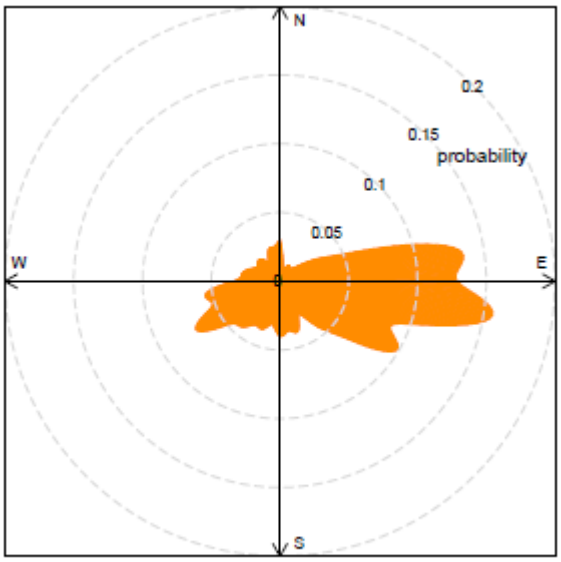

CPF at the 95th percentile (=11.3)

The conditional bivariate probability function (CBPF) couples ordinary CPF with wind speed as a third variable, allocating the observed pollutant concentration to cells defined by ranges of wind direction and wind speed rather than to only wind direction sectors (example in Figure 2).

It can be defined as:

$$CBPF\Delta\theta, \Delta u = m\Delta\theta,\Delta u \mid C \geq x / n\Delta\theta,\Delta u$$

where $m\Delta\theta,\Delta u$ is the number of samples in the wind sector $\Delta\theta$ with wind speed interval Δu having concentration C greater than a threshold value x, $n\Delta\theta,\Delta u$ is the total number of samples in that wind direction-speed interval.

Figure 2: Polar plot of SO2 concentrations at Marylebone Road based on the CPF function

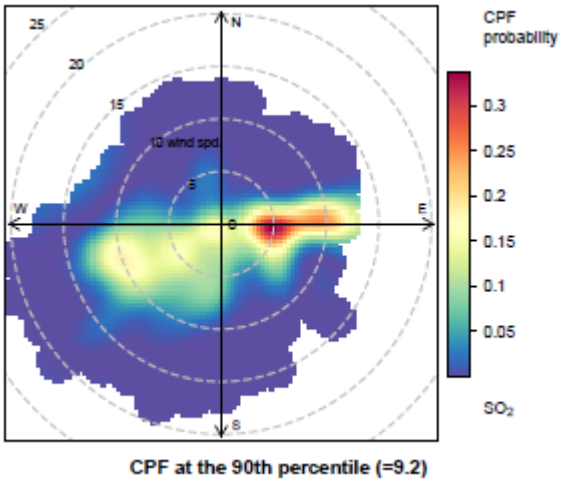

Therefore, where there are a high number of data points with values greater than the chosen threshold value, for a particular wind direction and wind speed, there will be a higher probability value for that wind direction and speed.

The extension to the bivariate case provides more information on the nature of the sources because different source types can have different wind speed dependencies. The use of a third variable can therefore provide more information on the type of source in question. The third variable plotted on the radial axis does not need to be wind speed, it could, for example, be temperature. The main issue is that the third variable allows some sort of discrimination between source types due to the way they disperse.

The scale of a CPF plots ranges from 0 to 1, from lowest to highest probability.

References

1. CARSLAW, D.C., 2015. The Openair manual — open-source tools for analysing air pollution data. Manual for version 1.1-4, King's College London.

2. URIA-TELLAETXE, I. AND CARSLAW, D.C., 2014. Conditional bivariate probability function for source identification. In: Environmental Modelling & Software 59, pp. 1–9. DOI: 10.1016/j.envsoft.2014.05.002 (cit. on pp. 125, 135, 136).

Would you like to find out more about us or your environment?

Then call us on

03708 506 506 (Monday to Friday, 8am to 6pm)

Email: enquiries@environment-agency.gov.uk

Or visit our website

www.gov.uk/environment-agency

incident hotline

0800 807060 **(24 hours)**

floodline

0345 988 1188 **(24 hours)**

Find out about call charges (https://www.gov.uk/call-charges)

Environment first

Are you viewing this onscreen? Please consider the environment and only print if absolutely necessary. If you are reading a paper copy, please don’t forget to reuse and recycle.